Universidad de Concepción
Dirección de Postgrado
Facultad de Ingeniería Agrícola - Doctorado en Ingeniería Agrícola con mención en Recursos Hídricos en la Agricultura

# PREDICCIÓN DE HELADAS RADIATIVAS EN SUELOS PLANOS SIN CUBIERTA VEGETAL

PABLO ALBERTO VENEGAS FUENTES
CHILLÁN - CHILE
2013

Profesor Guía: Jorge Jara Ramírez
Dpto. de Recursos Hídricos, Facultad de Ingeniería Agrícola
Universidad de Concepción

# PREDICCIÓN DE HELADAS RADIATIVAS EN SUELOS PLANOS SIN CUBIERTA VEGETAL

Aprobado por:

Jorge Jara Ramírez
Ingeniero Agrónomo, PhD.

Profesor guía

Jerónimo Paredes Cáceres
Licenciado en Matemáticas, M.Sc. Doctor.

Profesor co-tutor

Octavio Lagos Roa
Ingeniero Civil Agrícola, PhD.

Evaluador interno

Aldo Montecinos Gula
Oceanógrafo, MSc. Doctor.

Evaluador externo

Diego Rivera Salazar
Ingeniero Civil, Doctor.

Director de programa

## AGRADECIMIENTOS

*Quiero agradecer a todas las personas que me apoyaron en mi titulación y especialmente a:*

*A mis padres por brindarme apoyo incondicional desde las lejanas tierras de Magallanes.*

*A mi Gabrielita que la quiero y me quiere incondicionalmente.*

*A Angélica que siempre estuvo conmigo, entregándome todo su afecto en aquellos momentos de debilidad espiritual, y apoyándome permanentemente en todos los pasos que involucra la obtención de la tesis.*

*Al profesor Jorge Jara por brindarme todo su apoyo académico, en cualquier horario y en cualquier día, sacrificando incluso el tiempo que le corresponde a su familia, como también por entregarme sabios consejos.*

*Al profesor Jerónimo Paredes por entregarme su apoyo en el proceso de elaboración de tesis, y estoy consciente que sacrificó tiempo que tenía destinado a otras actividades para dedicarlo a mi persona.*

*A Carlos Cea por ayudarme en la instalación de mi ensayo y que producto del trabajo conjunto y permanente se creó una linda amistad.*

*A Clara Castro por apoyarme permanentemente en todo lo relativo a los procesos administrativos del Programa de Doctorado, y que producto de esa ayuda otorgada surgió una sincera amistad.*

*Al profesor Rick Snyder por su dedicación y esfuerzo en hacerme sentir a gusto en mi estadía en la Universidad de California - Davis, y por brindarme su apoyo dentro de sus posibilidades.*

*A Javier Bello por apoyarme en la traducción de los trabajos publicados y enviados.*

*A don Fernando Acosta, Marcelo Jelvez, Paola Sobarzo, Elías Contreras, Rodolfo Garrido, Magdalena Zambrano, Lissette Grandón y Richard Silva, por brindarme en su momento apoyo y facilidades, dentro del ámbito laboral de INDAP, para culminar esta etapa.*

**INDICE**

**RESUMEN**

La helada radiativa es un fenómeno climático que causa serios daños a la agricultura durante la primavera. La severidad del daño depende de la resistencia del cultivo a este evento, de su estado fenológico, de la intensidad de la helada y de su prevención oportuna a través de métodos activos de control. Por lo tanto, es de importancia predecir no solo las heladas, sino el momento en que estas se producirán. Es por esto que los modelos predictivos juegan un rol sustancial para evitar daños productivos y económicos en la actividad agrícola. Hoy en día existe una diversidad de modelos que predicen las heladas radiativas. Sin embargo, algunos requieren información ambiental histórica para su desarrollo y se caracterizan por ser sitios específicos. Otros, pueden ser extrapolables a diferentes condiciones ambientales, pero para su desarrollo requieren gran cantidad de mediciones en el suelo y en la atmósfera, razón que impide que sean de uso masivo. Es por ello, que el objetivo de este estudio es desarrollar dos modelos, uno numérico y otro mecanístico, de predicción de heladas que requieran información fácil de obtener o de estimar. Para cumplir con este fin, se realizaron diversas mediciones de variables biofísicas, tanto en el aire como en el suelo, en la Estación Agro Meteorológica de la Facultad de Ingeniería Agrícola, de la Universidad de Concepción, sede Chillán, desde septiembre de 2010 hasta diciembre de 2011. Estas se realizaron bajo condiciones de suelo desnudo. Se midió la temperatura del suelo a diferentes profundidades, la densidad de flujo de calor del suelo a 0,05 m de profundidad, contenido de humedad del suelo a tres profundidades y radiación neta a 1,5 m sobre el nivel del suelo. Además, se usó información proporcionada por la Estación Agro Meteorológica de la Universidad, correspondiente a radiación solar, velocidad de viento, temperatura del aire a tres alturas y humedad relativa. Los resultados obtenidos indican que los modelos desarrollados presentan un buen comportamiento en la predicción de la temperatura de la superficie del suelo en eventos de heladas radiativas. Sin embargo, la complejidad del modelo numérico desarrollado limita su uso masivo, no así el modelo mecanístico desarrollado, el que es fácil de aplicar a inicios de primavera. Por otra parte, se calibró y evaluó modelos desarrollados por diversos autores. De ellos, el de mejor comportamiento fue el de Allen (1957) para estimar la temperatura superficial del suelo, y el de Gandia *et al.* (1985) para estimar la temperatura del aire a 2 m de altura.

## I. INTRODUCCIÓN

### I.1 Definición y tipos de helada

Técnicamente, la palabra "helada" se refiere a la formación de cristales de hielo sobre una superficie, ya sea por congelación del rocío o por la fase de cambio de vapor a hielo (Blanc *et al.*, 1963; Bettencourt, 1980; Mota, 1981; Cunha, 1982). Sin embargo, la palabra es ampliamente utilizada por el público para describir un fenómeno meteorológico cuando los cultivos y otras plantas experimentan daño por congelamiento (Snyder *et al.*, 2010). También puede ser definida como la aparición de temperaturas inferiores o iguales a 0 ° C medida a una altura entre 1.25 y 2.0 m (Hogg 1971, Lawrence 1952).

Snyder *et al.* (1987) y Kalma *et al.* (1992) han clasificado las heladas en dos categorías: "advectivas" y "radiativas". Las heladas advectivas se asocian con incursiones a gran

escala de masas de aire frío, que se desarrollan en condiciones calmas o ventosas donde la temperatura a menudo alcanza 0 ºC, incluso durante el día. Las heladas radiativas están asociadas con el enfriamiento debido a la pérdida de radiación infraroja durante noches claras y calmas y con formación de inversiones de temperatura del aire. En algunos casos, se produce una combinación de ambos tipos de heladas (Snyder *et al.*, 2010).

**I.2 Descripción del proceso de formación de heladas radiativas**

Lo regular es que bajo condiciones ideales de heladas, es decir, noches despejadas y sin viento (para no perturbar la estratificación de las capas bajas de la atmósfera), la temperatura disminuya por la influencia de la liberación de radiación desde el suelo, pudiendo llegar bajo el punto de congelación al amanecer (Ellison, 1928).

Sin embargo, bajo condiciones de nubosidad o neblina, la radiación infraroja desde la atmósfera hacia el suelo se incrementa, dependiendo de la temperatura de las nubes o de la neblina; por lo tanto, la pérdida neta de energía es pequeña (Snyder *et al.*, 2010).

La inversión térmica es un fenómeno que se presenta donde sea que ocurran heladas, debido a que la conductividad termal del aire que se encuentra próximo a la superficie del suelo es menor que el de las estratas superiores. En la noche, bajo condiciones ideales de heladas, la superficie del suelo se enfría por la liberación de radiación hacia la atmósfera. Al enfriarse el suelo, comienza a enfriar la capa de aire inmediatamente adyacente. Al enfriarse esta capa, la densidad del aire se incrementa, lo que provoca que éste se mueva o drene a sectores de terreno más bajos (Ellison, 1928).

Para una superficie de suelo desnudo, el proceso de formación de heladas radiativas implica un proceso de balance de energía cuyos componentes son: la densidad del flujo de radiación neta de onda larga ( $Rn$ ); la densidad de flujo de calor sensible ( $H$ ); la densidad de flujo de calor latente ( $LE$ ); y la densidad de flujo de calor del suelo ( $G$ ). Durante las heladas radiativas, hay una pérdida de la radiación desde la superficie del suelo a la atmósfera y una ganancia de radiación de la atmósfera al suelo, así como una ganancia de energía por conducción de calor en el suelo y por flujo turbulento de calor en el aire. Sin embargo, más calor se pierde que el que se gana en este proceso (Snyder *et al.*, 2010). De manera similar, Figuerola y Mazzeo (1997) indicaron que la evolución de la temperatura de la noche sobre una superficie horizontal y homogénea se ve afectada por la pérdida de radiación desde la superficie, que es parcialmente sustituida por la conducción de calor desde el suelo, pero también por el aporte de calor sensible desde el aire.

De los componentes de la ecuación de balance de energía que aportan energía al sistema, el de mayor importancia es $G$, pues éste se incrementa con el tiempo, porque el gradiente de temperatura comienza a aumentar próximo a la superficie y el calor comienza a transferirse desde el suelo hacia la superficie (Snyder *et al.*, 2010).

La cantidad de energía que recibe la superficie de la tierra desde la atmósfera depende de la distribución vertical de la temperatura y de la humedad de la capa inferior de la atmósfera. Así, la radiación neta que se pierde durante la noche depende sólo de las condiciones atmosféricas y de la temperatura sobre la superficie del suelo (Brunt, 1941).

## I.3 Importancia de las heladas

La importancia de las heladas como factor medioambiental que afecta el desarrollo de los cultivos es bien conocido. Esto puede causar una parcial o total destrucción de los cultivos, como también un retardo en su desarrollo (Bagdonas *et al.*, 1978).

Algunas plantas tropicales y subtropicales padecen daños por efecto de las bajas temperaturas aún por encima de 0ºC. En cambio, las de regiones templadas sufren daños severos y hasta la muerte cuando la temperatura desciende por debajo de 0ºC. Los efectos varían marcadamente durante la vida de las plantas y es diferente según el estado de su crecimiento y desarrollo (Snyder *et al.*, 2010).

En Estados Unidos de América, las pérdidas económicas son mayores por heladas que por cualquier otro fenómeno agroclimático. Por lo tanto, el impacto de este fenómeno puede afectar sustancialmente la economía de los agricultores (Snyder *et al.*, 2010).

Las etapas de mayor riesgo, en muchos cultivos, son el estado de emergencia, floración y el de formación del fruto. Por lo tanto, los agricultores requieren la predicción de la temperatura mínima o del comportamiento de la temperatura nocturna, con el fin de decidir la implementación de alguna técnica de protección de los cultivos, ya sea con métodos de protección activos o pasivos (Bagdonas *et al.*, 1978; Cellier 1992; Figerola y Mazzeo, 1997; Lhomme y Guilioni, 2004). Por lo tanto, una predicción confiable de heladas radiativas es una problemática importante en muchas áreas de la agricultura.

## I.4 Evolución de modelos predictivos

Existe una diversidad de modelos predictivos de temperaturas nocturnas. Los primeros modelos desarrollados (Smith, 1917; Nichols, 1920; Angström, 1920) predicen las temperaturas mínimas en base a información medioambiental previa a la helada. Tales expresiones fueron desarrolladas ocupando registros históricos obtenidos de estaciones agroclimáticas, por lo que son de utilidad para las zonas donde fueron desarrolladas, pero no pueden ser extrapoladas a otras localidades.

Otra forma de enfrentar el problema de predicción de las heladas es a través de ecuaciones de regresión que modelan el comportamiento de la temperatura del aire durante la noche. En este sentido, Allen (1957) desarrolló un modelo para predecir las heladas a través del uso de una tasa constante de disminución de la temperatura durante el transcurso de la noche, asociada a la raíz cuadrada del tiempo. Para la calibración de su modelo utilizó registros históricos de la temperatura del aire y del punto de rocío, y también las temperaturas del aire mínimas observadas durante noches claras y tranquilas y con ocurrencia de eventos de heladas. Más tarde, Gandia *et al.*, (1985) usaron una técnica exponencial para predecir la temperatura mínima del aire, durante una noche de cielo despejado, con velocidades de viento bajas sobre el área que está siendo investigada. De manera similar, Emmanouil *et al.*, (2006) propusieron un modelo polinomial de tercer grado, en el que sus coeficientes se obtuvieron mediante ajuste de curva. Al igual que los primeros modelos, estos son sitios específicos y no pueden ser extrapolados a otras localidades.

Otros modelos de predicción del comportamiento de las temperaturas nocturnas se basaron en la solución analítica de la ecuación de conducción de calor, aplicada sobre

suelo desnudo. La primera aproximación la realizó Brunt (1941), luego lo siguieron Jaeger (1945), Gröen (1947) y Reuter (1951), entre otros. La principal idea de Brunt y de autores de fórmulas asociadas es que el suelo juega un rol importante en limitar el decrecimiento de la temperatura superficial del suelo, en condición de heladas radiativas. La fácil operación es una de las principales ventajas de estas expresiones y es por esta razón que ellas son ampliamente usadas (Cellier, 1993).

Últimamente han aparecido modelos más sofisticados, ya sea porque se ha incrementado el conocimiento de transferencia de calor en la capa límite de la atmósfera, o porque ha habido un rápido desarrollo computacional que facilita la determinación de cálculos complejos. Generalmente, estos modelos simulan la evolución de la temperatura del aire y del suelo próximos a la superficie del suelo, usando soluciones numéricas de ecuaciones de balance de energía más o menos complejas (Cellier, 1993).

## II. HIPÓTESIS

Es posible modelar la evolución de la temperatura superficial del suelo sin cobertura vegetal durante heladas radiativas, a partir de información meteorológica disponible, considerando el rol desempeñado por la conducción de calor en el suelo y/o la radiación neta nocturna.

## III. OBJETIVO GENERAL

Desarrollar modelos predictivos de temperaturas mínimas nocturnas en condiciones de heladas radiativas para sectores llanos, sobre suelo sin cubierta vegetal

### III.1 Objetivos específicos:

- Analizar y modelar la densidad de flujo de calor en el suelo, como principal variable que limita el descenso de la temperatura superficial del suelo durante eventos de helada radiativas.
- Desarrollar un modelo numérico que permita determinar la evolución de la temperatura nocturna en la superficie del suelo desnudo.
- Contrastar el uso de este modelo numérico con los principales modelos predictivos de heladas radiativas descritos en la literatura.
- Desarrollar un modelo mecanístico simple de predicción de la temperatura superficial del suelo, bajo condiciones de heladas radiativas, para suelo sin cubierta vegetal.

## IV. DESARROLLO

## IV. 1 Hourly estimation of soil heat flux density at the soil surface with three models and two field methods


### Abstract

Heat flux density at the soil surface ($G_0$) was evaluated hourly on a vegetal cover 0.08 m high, with a leaf area index of 1.07 $m^2$ $m^{-2}$ and positive net radiation (Rn>0), during daylight hours, using Choudhury et al. (1987) ($G_0^{rn}$), Santanello and Friedl (2003) ($G_0^{s}$) and Force-restore ($G_0^{fr}$) models, and the plate calorimetry methodology ($G_0^{pco}$), where the gradient calorimetry methodology ($G_{0R}$) served as a reference for determining $G_0$. This study was carried out at the Agrometeorological Station of the Faculty of Agricultural Engineering, University of Concepción in Chillán – Chile, during spring. It was found that the peak of $G_{0R}$ was at 1 p.m., with values that ranged between 60 and 100 W $m^{-2}$, depending on whether the day was cloudy or sunny, and that the $G_0/Rn$ relation varied during the day with values close to zero in the early hours of the morning and close to 0.25 in the last hours of daylight. The $G_0^s$ model presented the best performance in estimating $G_0$, with a root mean square error (RMSE) and a mean absolute error (MAE) of 22.2 W $m^{-2}$ and 17.9 W $m^{-2}$, respectively, followed by the $G_0^{rn}$ model, and the poorest performance was that of the $G_0^{fr}$ model. The plate calorimetry methodology showed a similar behavior to that of the gradient calorimetry referential methodology, with RMSE and MAE of 16.2 W $m^{-2}$ and 12.6 W $m^{-2}$, respectively.


*Keywords:* soil heat flux, thermal conductivity, gradient calorimetry, plate calorimetry, soil heat storage

### IV.1.1. Introduction

The estimation of evapotranspiration in vegetal covers is a helpful tool for decision-making in irrigation programming and management in agriculture. The energy balance or combination equation can be used to determine it:

$$Rn - G_0 - H - LE = 0 \qquad (1)$$

where its component is the net radiation ($Rn$), which is partitioned into sensible heat flux density ($H$), latent heat flux density ($LE$) and heat flux density at the soil surface ($G_0$). In contrast to what happens to the other components, the determination of $G_0$ is generally overlooked and has remained the least measured variable (Liebethal et al., 2005). In this regard, some studies show that the soil heat flux can be little to insignificant when integrated over 24 hour cycles. However, it can be an important fraction of the net radiation partition for short periods of time (minutes to hours) (Howell et al., 1990), as well as under conditions of bare dry soil during the night and before dawn (Liebethal et al., 2005).

Many studies have developed a wide range of methods and models in order to estimate $G_0$ for short periods of time. Among them are 1) the $G_0/Rn$ relation; 2) the Santanello's model; 3) the Force-restore model; as well as direct measurement through 4) soil heat flux plates and 5) temperature measurement in the soil profile.

**IV.1.2. Background**

One of the most commonly used approximations is the $G_0/Rn$ ratio. Some studies relate this ratio to crop height or vegetation indices (Kustas and Daughtry, 1990). In this respect, several studies have shown that this ratio fluctuates between 0.05 and 0.1 at noon for a dense and uniform cover, and between 0.2 a 0.4 for a partial canopy (Kustas et al., 2000). Coincidentally, Clothier et al. (1986) found that, in alfalfa, this relation decreases from 0.25 to 0.1 as the crop height increases from 0.05 m, after being cut, until it reaches a height of 0.4. For heights over 0.4 m, the $G_0/Rn$ relation stays at 0.1 with a variation of $\pm 0.01$. Oke (1979), cited in Choudhury et al. (1987), found that this ratio varies between 0.1 and 0.2 for natural pastures and, that in the cases of wheat, maize, sorghum and soybeans, the $G_0/Rn$ relation is 0.07 (Choudhury et al., 1987).

Choudhury et al. (1987) found a strong correlation between $Rn$ and $G_0$ for bare soil; however, the proportion between them has been variable. When relating the $G_0/Rn$ ratio to moisture content, discrepancies appear. Fuchs and Hadas (1973) found that there is no linear relationship between this ratio and the moisture content in the soil, where $G_0/Rn$ for wet and dry soil was 0.34 and 0.22, respectively. On the other hand, Idso and Jackson (1975) point out that moisture content is an important factor in the $G_0/Rn$ ratio. Thus, variations in this relation are caused by evaporation from the soil after rains or irrigations, which take place during the first four days following these events. The same authors found that the $G_0/Rn$ relation increases from 0.22 to 0.51, as the soil dries. Fuchs and Hadas' $G_0/Rn$ measurements for wet soils were carried out nearly two weeks after a rain or irrigation, when the $G_0/Rn$ relation was already stabilized (Fuchs and Hadas, 1973). Clothier et al. (1986) agree with Idso and Jackson (1975) that there is a significant variation in the highest values of the $G_0/Rn$ relationship, from 0.05 to 0.5, depending on the soil moisture content.

On the other hand, Idso and Jackson (1975) found that in bare soils the difference between $Rn$ and $G_0$, normalized by the energy absorbed, is related to moisture content in the first four centimeters of depth and the soil albedo and, in turn, the albedo is related to the moisture content. Therefore, a way to adjust the $G_0/Rn$ relation is using the normalized difference of $Rn$ and $G_0$ and the soil albedo.

Considering that the $G_0/Rn$ relation varies between bare soil and soil with a vegetal cover, Choudhury et al. (1987) expressed $G_0$ in function of $Rn$ as:

$$G_0 = \alpha\, Rn \qquad (2)$$

Therefore, for soils with a vegetal cover it can be expressed as:

$$G_0 = \alpha \tau Rn \quad (3)$$

where $\alpha$ is the fraction of the net radiation used in the heat flux density in the soil surface and $\tau$ is the fraction of $Rn$ exchanged at the soil surface, which can be expressed as an exponential relation:

$$\tau = \exp(-\beta LAI) \quad (4)$$

where $LAI$ is the leaf area index ($m^2$ $m^{-2}$) and $\beta$ is the extinction coefficient of incident radiation in the canopy. Thus, to estimate $G_0$ two constants ($\alpha$ and $\beta$) need to be determined. Choudhury et al. (1987) found that for nine days observation of wheat at different phenological stages, the expression that determines the soil heat flux density hourly, for midday, as function of IAF, is as follows:

$$G_0 = 0.4\exp(-0.5 LAI)Rn \text{ , for } Rn > 0 \quad (5)$$

The calculated value of $\alpha$=0.4 is similar to that observed by Fuchs and Hadas (1973) ($\alpha$=0.34) and Idso and Jackson (1975) ($\alpha$=0.22 to 0.51), and the $\beta = 0.5$ value lies within the range of observations from 0.45 to 0.65 for several crops (Monteith, 1973, cited in Choudhury et al., 1987). When considering a LAI of 2.77, $G_0$ equals 0.1 $Rn$, a relationship recommended for determining the referential evapotranspiration for daytime hours ($Rn$ >0), and $G_0$ = 0.5 $Rn$ for nighttime hours ($\alpha$=2, $Rn$ <0) (Allen et al., 1998; ASCE, 2005).

Even if $G_0$ is parameterized as a constant ratio of $Rn$ for the period of interest, some studies have shown that $G_0$ is not a constant ratio of $Rn$ at an hourly timescale, and that it can account for more than 50% of $Rn$ for surfaces with partial vegetal cover (Santanello and Friedl, 2003).

The Santanello and Friedl model (2003) proposes a $G_0/Rn$ relationship that includes the daily variations at the soil surface temperature, as a way to integrate the moisture and vegetation factor. It considers a variable $G_0/Rn$ relationship during the day, including the $A$ and $B$ parameters into the expression:

$$\frac{G_0}{Rn} = A\cos\left(\frac{2\pi(t+10800)}{B}\right) \quad (6)$$

where $A$ represents the variation amplitude of the $G_0/Rn$ ratio, and indicates the importance of $G_0$ in the energy balance during a cycle, and corresponds to the highest value of $G_0/Rn$. $B$ represents the period of time a cycle lasts and indicates the variation of $G_0$ during the day, which fluctuates between 60000 and 142000 s $rad^{-1}$; for this reason the period of time is long and the daily variation is little. It is determined by

curve fitting. Finally, *t* is the relative time at solar noon, which is positive before noon and negative after that period. The *A* and *B* values for a specific condition should ideally be assigned based on knowledge about type of soil, moisture regime and seasonal dynamics in the leaf area index (LAI). However, these relationships are not easy to explain because the effect of soil properties and canopy on the soil heat flux can be easily confused. As a way to solve this problem, Santanello and Friedl (2003) related the *A* and *B* values to the daily variations at the soil surface temperature, $\Delta T_s$, resulting in the following expressions:

$$A = 0.0074\left(\Delta T_s\right) + 0.088 \tag{7}$$

$$B = 1729\left(\Delta T_s\right) + 65013 \tag{8}$$

The coefficients of determination obtained from *A* and *B* with $\Delta T_s$ were 0.91 and 0.56, respectively, which suggests a strong relationship between A and $\Delta T_s$ but this is not so in the case of *B*. However, when Santanello and Friedl (2003) made a sensitivity analysis between the *A* and *B* values, with respect to RMSE, they found that if A and B varied in $\pm 0.05$ and $\pm 15000$ s rad$^{-1}$, respectively, the RMSE variation was not higher than 6 W m$^{-2}$, which could indicate that the uncertainty level of B does not cause error in the Eq. (6).

The Force-restore model, originally proposed by Bhumralkar (1975) and Blackadar (1976), and later developed by Deardorff (1978), Dickinson (1988) and Lin (1980), was used to estimate the soil surface temperature. It is based upon the assumption of two soil layers: a thermally active upper layer (where there are temporal and spatial variations of temperature) and a thermally inactive lower layer.

This method suggests that the soil moisture content is vertically uniform, and therefore the thermal properties it has, such as volumetric heat capacity, soil thermal conductivity and diffusivity are also assumed as vertically uniform (Gao et al., 2008).

The Force-restore method has been incorporated into many hydrologic and atmospheric numerical models. However, it tends to overestimate the diurnal amplitude of surface temperature, thus requiring careful evaluation (Gao et al., 2008).

Force-restore originated in De Vries' (1963) expression, assuming that conduction dominates the process of heat transfer. Then, the sub-surface heat flux at a *z* depth, $G\left(z,t\right)$, is expressed as follows:

$$G\left(z,t\right) = -k\ \partial T/\partial z \tag{9}$$

where $k$ is the thermal conductivity, $T$ is the soil temperature at a $z$ depth, and $t$ is time. On the other hand, the equation for transient heat conduction is:

$$C_v \frac{\partial T}{\partial t} = -\frac{\partial G\left(z,t\right)}{\partial z} \tag{10}$$

where $C_v$ is the volumetric heat capacity of the soil, and the rest of the variables have the same meaning given in the previous equations. If a soil layer is considered from the surface to a $z$ depth, then the temperature change rate for that layer can be expressed as (Bhumralkar, 1975):

$$C_v \frac{\partial T_s(z,t)}{\partial t} = -\left[\frac{G(z,t) - G(0,t)}{\Delta z}\right] \tag{11}$$

where $T_s(z,t)$ is the mean temperature of the soil layer having a $\Delta z$ width or a $z$ depth as measured from the surface. On the other hand, if the soil profile is assumed to be homogeneous and the heat flux to be in vertical direction only, then the equation for heat conduction can be written as follows:

$$\frac{\partial T_s}{\partial t} = K \frac{\partial^2 T}{\partial z^2} \tag{12}$$

where $T_s$ is the mean temperature of the soil layer and $K$ is the thermal diffusivity ($k/C_v$). Carslaw and Jaeger (1959) considered an initial soil temperature profile (Eq. 13) and temperature time behavior at the soil surface (Eq. 14). The expression which verifies the aforementioned conditions, for a homogeneous soil with semi-infinite thickness and a mean daily temperature of $\overline{T}$, is presented in Eq. (15):

$$T(z,0) = \overline{T} - \Delta T_0 \exp\left(-\frac{z}{d}\right)\sin\left(-\frac{z}{d}\right) \tag{13}$$

$$T(0,t) = \overline{T} + \Delta T_0 \sin(wt)\, t \geq 0 \tag{14}$$

$$T(z,t) = \overline{T} + \Delta T_0 \exp\left(-\frac{z}{d}\right)\sin\left(wt - \frac{z}{d}\right) \tag{15}$$

where $\overline{T}$ is the mean daily soil surface temperature (ºC), $\Delta To$ is the amplitude of the daily temperature fluctuations (24 hours) at the soil surface (ºC) (half of the peak-to-peak variation), $t$ is time (s), $d$ corresponds to the temperature damping depth for a given cycle (m), and $w$ is the angular speed of earth's rotation ($2\pi/86400$ rad $s^{-1}$).

From the initial condition (Eq. 13) it can be inferred that the initial temperature in the soil profile increases from $z = 0$ until it reaches its highest value at a depth that equals $0.25\pi$ times $d$, with a temperature of $\overline{T} + 0.32\,\Delta T_0$. Then it decreases until it reaches its lowest value at a depth that equals $1.25\pi$ times $d$, with a temperature of $\overline{T} - 0.014\,\Delta T_0$. From Eq. (14) it can be inferred that the soil surface temperature presents a sinusoidal pattern during the day, which is the same for day and night.

Campbell and Norman (1998) made a correction to the sine function by adding the term "$t_0$" to adjust the temporal behavior of temperature to the local time records. Thus, Eq. (15) is expressed as:

$$T(z,t) = \overline{T} + \Delta T_0 \exp\left(-\frac{z}{d}\right)\sin\left(w(t-t_0) - \frac{z}{d}\right) \quad (16)$$

where $T(z,t)$ is the soil temperature at a $z$ depth and $t$ time. The $d$ value is obtained from the thermal diffusivity ($K$) and the angular speed of earth's rotation ($w$) (Gao et al., 2008):

$$d = \sqrt{2K/w} \quad (17)$$

Applying the $G$ concept Eq. (9) in Eq. (16) and considering the following two equalities:

$$\frac{1}{w}\frac{\partial T(z,t)}{\partial t} = \Delta T_0 \exp\left(-\frac{z}{d}\right)\cos\left(w(t-t_0) - \frac{z}{d}\right) \quad (18)$$

$$T(z,t) - \overline{T} = \Delta T_0 \exp\left(-\frac{z}{d}\right)\sin\left(w(t-t_0) - \frac{z}{d}\right) \quad (19)$$

We obtain:

$$G(z,t) = \left(\frac{w k C_v}{2}\right)^{\frac{1}{2}}\left[\frac{1}{w}\frac{\partial T(z,t)}{\partial t} + T(z,t) - \overline{T}\right] \quad (20)$$

Clearing $G(0,t)$ from Eq.(11) and considering $G(z,t)$ from Eq.(20), we obtain (Bhumralkar, 1975):

$$G(0,t) = \Delta z\ C_v \frac{\partial T_s(\Delta z/2,t)}{\partial t} + \left(\frac{w\ k\ C_v}{2}\right)^{\frac{1}{2}}\left[\frac{1}{w}\frac{\partial T(z,t)}{\partial t} + T(z,t) - \overline{T}\right] \quad (21)$$

where the first term of Eq.(21) corresponds to the soil heat storage, measuring the mean temperature of the layer ($T_s$) of a width of $\Delta z$, and the second term corresponds to the heat flux density, $G$, measuring the soil temperature ($T$) at a $z$ depth, where $\overline{T}$ is the mean daily temperature at the soil surface.

As the purpose of Bhumralkar (1975) was to determine the soil surface temperature, he considered a soil layer of infinitesimal thickness ($\Delta z = 0.01m$), and assumed that the layer mean temperature is close to the soil surface temperature ($T_s \approx T_g$). Therefore, the model he proposes corresponds to Eq. (21), modified as mentioned above.

There is no a priori certainty of an appropriate $\Delta z$. Bhumralkar (1975) used $\Delta z = 0.01$m in his calculations, while Liebethal et al. (2007) used different layer thicknesses and in their calibrations found that the optimal $\Delta z$ is equivalent to 0.1 m.

Heat flux plates allow direct measuring of the soil heat flux. Although their simplicity makes them very popular, their accuracy depends on certain use considerations, especially those that have to do with errors in sensor installation. In this respect, three

potential errors have been identified: first, differences between thermal conductivity of the plate and that of the soil (Philip, 1961); second, thermal contact resistance in soil-plate inter-phase (Fuchs and Hadas, 1973); and third, the plate can indirectly alter the heat flux of the surrounding soil due to water phase changes and water vapor movement (Mayocchi and Bristow, 1995; Sauer et al., 2003).

Heat flux distortion occurs surrounding the plate because the soil thermal conductivity varies according to the static and dynamic properties of the soil, while the plate is made of a material with a thermal conductivity considered constant (Sauer et al., 2007). In order to correct the heat flux distortion measured by the plate, Philip (1961) developed a method based upon the plate dimension and the thermal conductivity in the soil-plate inter-phase. Morgensen (1970) (cited in Sauer et al., 2007) generalized Philip's equation:

$$\frac{G_z^p}{G_z^{pc}} = \frac{1}{\left[1-\gamma\, r\left(1-\frac{k}{k_p}\right)\right]} \tag{22}$$

where $G_z^p$ is the soil heat flux measured by the plate at a $z$ depth; $G_z^{pc}$ is the soil heat flux density, measured by the plate and corrected at a $z$ depth; $k$ is the soil thermal conductivity; $k_p$ is the plate thermal conductivity; $\gamma$ is the empirical factor related to the plate shape; and $r$ is a dimesionless factor equal to the plate's thickness divided by the square root of its area (on one side).

Sauer et al. (2003) found that the Morgensen's equation often improves the plate $G_z$ estimation, especially when $k > k_p$. They concluded that the $k_p$ uncertainty and other error causes, which are not considered in Philip's correction, include thermal contact resistance and can have limited effectiveness in the correction.

Thermal contact resistance refers to the formation of small air gaps on the plate's surface, which produce a significant underestimation of the $G_z$ measured and can cause distortions between 20 and 25% in dry soils (Sauer et al., 2007). According to Philip (1961), this underestimation can reach higher than 54%. Fortunately, thermal contact resistance is probably less than 10% in humid and loamy texture soils, and can be minimized by careful installation preventing the formation of air gaps. The exact error magnitude of contact resistance is very hard to manage in field conditions (Sauer et al., 2007).

Plate error in heat flux measurement, as a result of soil water shift to vapor phase and vapor movement, can be explained by the fact that the energy going in or out of the soil ($E_e$), can be used for evaporation ($LE$) and for heat flux density at the soil surface, $G_0$ (Mayocchi and Bristow, 1995):

$$E_e = LE + G_0 \tag{23}$$

On the other hand, the energy that the plate buried at a $z$ depth measures, $G_z^p$, corresponds to the energy entering the soil surface ($E_e$), minus the energy stored in the soil ($\Delta S$) and the energy used for evaporation ($LE$):

$$G_z^p = E_e - \Delta S - LE \quad (24)$$

Replacing (23) in (24) and re-organizing, we have:

$$G_0 = G_z^p + \Delta S \quad (25)$$

If thermal resistance correction in $G_z^p$ is used, according to Eq.22, we obtain:

$$G_0 = G_z^{pc} + \Delta S \quad (26)$$

That is to say, the heat flux density at the soil surface ($G_0$) corresponds to the amount of flux measured by the plate at a $z$ depth, corrected according to Eq. (22) ($G_z^{pc}$) and the heat flux stored between the plate and the surface ($\Delta S$). This happens when the plate is placed below the point where the liquid to vapor shift of water in the soil occurs.

However, when the plate is buried above the point of water phase shift (near the surface), the energy measured by the plate at a z depth ($G_z^p$) corresponds to the energy entering the soil minus the energy used for heat storing (the first millimeters of soil depth are dry, therefore, $LE = 0$):

$$G_z^p = E_e - \Delta S \quad (27)$$

That is to say:

$$E_e = G_z^p + \Delta S \quad (28)$$

Replacing Eq. (28) in Eq. (23), and reorganizing, we obtain that:

$$G_0 = G_z^p + \Delta S - LE \quad (29)$$

Which would complicate the measurement of $G_0$, since additional measurements of soil moisture content are required to determine evaporation. Therefore, in order to avoid corrections caused by evaporation, it is advisable to bury the flux plates below the point of phase shift, which could be found at three centimeters depth (Mayocchi and Bristow, 1995).

$G_0$ can be obtained through temperature measurements in the soil profile. In order to do so, it is necessary to take the soil heat flux from a given z depth ($G_z^m$) to the surface ($G_0$), which requires quantifying the increase of soil heat storage capacity ($\Delta S$). That means that the difference between the heat flux at the soil surface ($G_0$) and the one occurring at a z depth ($G_z^m$), is due to the change in heat storage inside the soil layer ($\Delta S$). The relation can be expressed as:

$$G_0 = G_z^m + \Delta S \quad (30)$$

Thus, according to Fuchs (1987), $G_z^m$ and $\Delta S$ can be expressed as follows:

$$G_z^m = -k\frac{\partial T}{\partial z} \quad (31)$$

$$\Delta S = \int_z^0 C_v \frac{\partial T}{\partial t} dz = C_v \frac{\partial T}{\partial t}\Delta z \quad (32)$$

where $C_v$ represents the volumetric heat capacity of the soil, $\partial T/\partial t$ is the soil temperature change ratio with respect to time (K $s^{-1}$), and $dz$ is the thickness of the soil layer analyzed (m). $G_0$ and $G_z^m$ are expressed in W $m^{-2}$. The volumetric heat capacity of the soil is determined by the addition of the specific heat of the soil components, which includes minerals, organic matter, water and air (De Vries, 1963):

$$C_v = \left[4.19 X_w + 2.51 X_0 + 1.93(1-\varepsilon - X_0)\right]10^6 \quad (33)$$

where $X_w$, $X_0$ and $\varepsilon$ correspond to the fraction of water volume, organic matter and soil porosity, respectively.

However, for discrete measurements of time and temperature of the soil profile, Eq. (32) can be expressed as follows:

$$\Delta S = \frac{\left[(T_i - T_{i-1})\Delta z\ C_v\right]}{\Delta t} \quad (34)$$

where $\Delta S$ corresponds to change in soil heat storage (W $m^{-2}$); $T_i$ is the temperature measured in time $t_i$; $\Delta z$ is the thickness of the layer analyzed (m); $\Delta t$ is the time interval between $t_i$ and $t_{i-1}$ (s); and $C_v$ is the volumetric heat capacity of the soil (J $m^{-3}$ $C^{-1}$).

The present study aims at evaluating, during daytime hours ($Rn > 0$), three models of hourly estimation of heat flux density at the soil surface, $G_0$, and the plate calorimetry methodology ($G_0^{pco}$) of heat flux plate measurements corrected at a z depth ($G_z^{pc}$), considering the heat stored between the plate and the soil surface ($\Delta S$), according to Eq. (26). A gradient calorimetry methodology will be used as a comparison or reference, by measuring the temperature gradient in the soil profile, where the heat flux at a $z$ depth ($G_z^m$) is corrected at the soil surface level (Eq.30), in agreement with Fuchs' expressions (1987) which will be called referential heat flux density at the soil surface ($G_{0R}$).

### IV.1.3. Methodology

IV.1.3.1 Experimental site:

This experiment was carried out at the Agrometeorological Station of the Faculty of Agricultural Engineering , University of Concepción in Chillán (36º 35' 43.4'' S, 72º 4'

47.3'' O), which is located at an altitude of 142 m.a.s.l. The soil is clay loamy, with a soil bulk density of 1.45 Mg $m^{-3}$ at a depth between 0 and 0.1 m and of 1.60 Mg $m^{-3}$ at a depth between 0.1 and 0.2 m and a fraction of clay of 33% in the first layer. It belongs to the Tres Esquinas series (member of the fine, mixed, thermic Ultic Haploxeralfs soil family), has a slightly inclined slope and rests upon a substrate of weathering solid rock, mixed, dark brown and reddish material with 5YR shades under humidity. The soil had pasture as vegetal cover, which had an average height of 0.08 m, with a leaf area index of 1.07 $m^2$ $m^{-2}$.

The measurement period went from September 03 (DOY 246) to September 25 (DOY 268) of 2010, leaving out days of the year 257, 258 and 259 due to incomplete records. There were no rains during the days of study, and they were divided into clear and cloudy days in order to determine the models behavior under those conditions, using a sunlight hour criterion where the critical value was 5.5 hours, which accounts for 50% of daylight hours during the period studied. The following direct measurements were carried out during this period:

IV.1.3.2. Soil temperature

In order to measure the soil temperature seven nickel / chrome nickel type K thermocouples, of 1 mm diameter were used. These thermocouples were made at the Water Resources Department of the Faculty of Agricultural Engineering. They were buried at depths of 0, 0.01, 0.03, 0.05, 0.09, 0.15 and 0.22 m. Monitoring readings were recorded every 1 second and averaged every 15 minutes.

IV.1.3.3. Soil moisture

In order to measure moisture, two ECHO-5 capacitive sensors (Decagon Devices) were used, placed horizontally at depths of 0.05 and 0.1 m. The sensors were calibrated with gravimetric measurements of moisture in situ at 0.05 and 0.1 m. Seven repetitions at every depth were made for every measurement. Monitoring readings were recorded every 1 second and averaged every 1 hour.

IV.1.3.4. Soil heat flux density (heat flux plates)

In order to measure the soil heat flux density, two circular heat flux plates, model HFT-3 (Campbell Scientific, Inc.), of 38 mm of diameter, 3.9 mm of width and 1.22 W $m^{-1}$ $K^{-1}$of thermal conductivity were used. They were placed at a depth of 0.05 m. The constants to transform voltage to flux density were 47.1 and 42.4 W $m^{-2}$ $mV^{-1}$, respectively. To prevent air gap formation in the soil-plate inter-phase, once buried in the soil, the soil surface under which the flux plates had been placed was moistened and compacted. Readings were recorded every 1 second and averaged every 15 minutes.

IV.1.3.5. Net radiation

The net radiation was measured with a net radiometer, model Q-7.1 (Campbell Scientific, Inc.), placed at a height of 1.55 m above the vegetal cover. The constant to transform voltage to flux density was 9.1 W $m^{-2}$ $mV^{-1}$, for millivolts greater than zero, and 11.4 W $m^{-2}$ $mV^{-1}$, for millivolts smaller than zero. Readings occurred every 1 second and were averaged every 15 minutes.

IV.1.3.6. Storage of records

The net radiation and flux plate records were stored in a 21 X micrologger (Campbell Scientific Inc.), and thermocouple records were stored in a HL20 micrologger. Soil moisture records were stored in an ECHO 5 micrologger (Decagon Device).

In order to have a better idea of how the sensors were placed, Picture 1 shows how they were arranged:

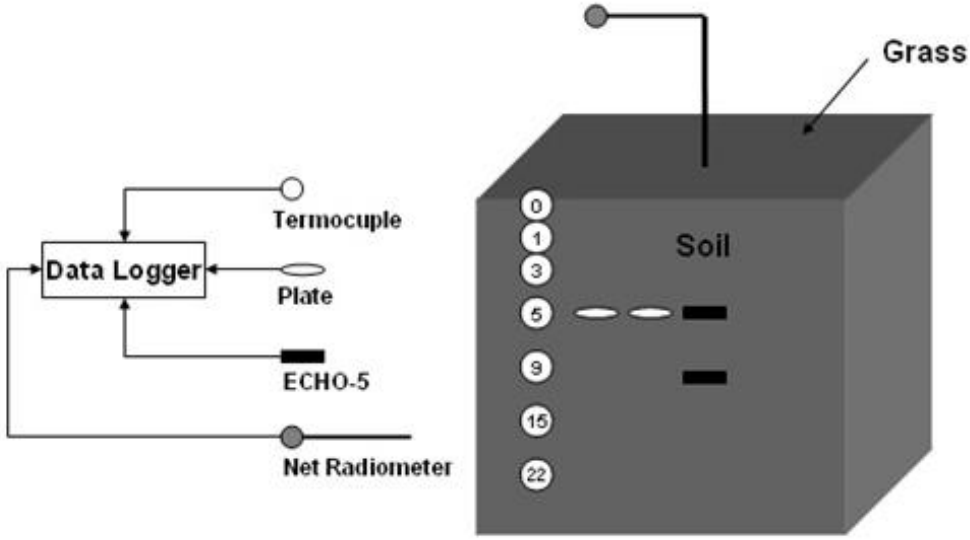


Fig. 1. Arrangement of the sensors used in the soil profile and at the soil surface during the research period. The numbers inside the thermocouples show the depth (cm) at which the sensors were buried.

IV.1.3.7. Additional information

Obtaining the heat flux density at the soil surface implies determining soil thermal conductivity ($k$), soil temperature gradient ($\partial T/\partial z$) and the change in heat storage in the soil ($\Delta S$), which were achieved in the following way:

a) Soil thermal conductivity (present in Eqs. 9, 21, 22 and 31) was estimated from the expression developed by Campbell (1985), which relates thermal conductivity to soil moisture, apparent density and the percentage of clay in the soil:

$$k = A + B\,X_w - (A - D)\exp\left[-(C\,X_w)^E\right] \quad (35)$$

$$A = 0.65 - 0.78\rho + 0.6\rho^2 \quad (36)$$

$$B = 1.06\,\rho^{X_w} \quad (37)$$

$$C = 1 + 2.6\,m^{-0.5} \quad (38)$$

$$D = 0.03 + 0.1\rho^2 \quad (38)$$

$$E = 4 \quad (40)$$

where $k$ is the soil thermal conductivity (W m$^{-1}$ K$^{-1}$), $\rho$ the soil bulk density (Mg m$^{-3}$), $X_w$ the soil volumetric moisture (m$^3$ m$^{-3}$), and $m$ the soil clay fraction.

Soil thermal conductivity was estimated at depths of 0.05 and 0.1m, which implied determining the bulk density and moisture of the soil at these depths. The fraction of clay was constant in the first 10 cm of depth, with a value of 33.

b) The change in soil temperature with depth, $\partial T/\partial z$ (Eq. 31 of $G_z^m$) was determined by the readings from the thermocouples buried at seven different depths, applying the cubic spline methodology to obtain $\partial T/\partial z$ at 0.1 m depth. These values were used to obtain the soil heat flux density at a depth of 0.1 m by multiplying it by the soil thermal conductivity.

c) The change in soil heat storage, $\Delta S$, (present in Eqs. 30 and 32) was calculated numerically from Eq. (34). In this case, $T_i$, $T_{i-1}$ and $C_v$ was obtained at a depth of 0.05 m, which is half the thickness of the analyzed layer. Such layer thickness ($\Delta z$=0.1) corresponds to the difference between the soil surface and the depth at which the heat flux density is determined (0.1 m). The time interval, $\Delta t$, corresponds to hourly measurements and it equals 3600 s.

IV.1.3.8. Determination of the referential heat flux density at the soil surface, based on the gradient-calorimetry methodology ($G_{0R}$).

$G_{0R}$ was determined based on Eq. (30) according to Fuchs' expressions (1987) (Eqs. 31 and 32), with a $\Delta z$ equivalent to 0.1 m. This implied determining the soil heat flux density (Eq. 31) at a depth of 0.1m ($G_{0.1}^m$). In order to do so, the soil thermal conductivity and the temperature gradient were determined as indicated in 3.1.6, letters a) and b), respectively. On the other hand, the increase in the soil heat storage capacity ($\Delta S$) (Eq. 32) was determined as indicated in 3.1.6, letter c).

IV.1.3.9. Estimation of the heat flux density at the soil surface ($G_0$)

IV.1.3.9.1. Based on the net radiation model by Choudhury et al. (1987) ($G_0^{rn}$).

Eq. (5) was used and, considering a measured LAI of 1.07 $m^2$ $m^{-2}$, the expression remains as follows:

$G_0^{rn} = 0.2343\,Rn$, for $Rn > 0$
(41)

IV.1.3.9.2. Based on the model by Santanello and Friedl (2003) ($G_0^s$).

In order to estimate the values of *A* and *B* of Eq. (6), the model was calibrated with information from days of the year 246, 247, 248 and 249 (clear days). Despite the authors of the model suggesting that *A* is obtained as the highest value of the $G_0/Rn$ relation and *B* is obtained by curve fitting, in this study, combinations of values of *A* (between 0.05 and 0.5) and *B* (between 50000 and 140000 s rad $^{-1}$) were made to determine $G_0$ of Eq. (6). Thus the combination of *A* and *B* that best fits $G_{0R}$ (smaller RMSE) was determined, $G_{0R}$ being the referential heat flux density at the soil surface,

estimated with Eq. (30). In Fig. (2) the combinations of the parameters *A* and *B* of Eq. (6), which estimate $G_0$, are shown. It can be observed that the combined values of *A* and *B* which cause a smaller RMSE are 0.22 and 97500 s rad $^{-1}$, respectively.

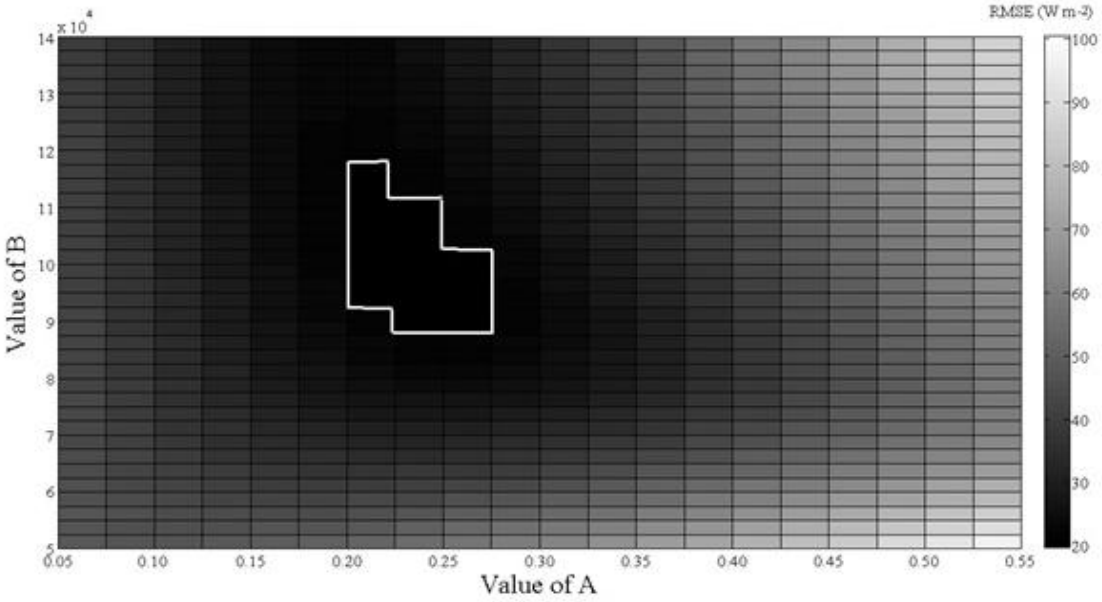


Fig. 2. RMSE response surface, in relation to the combination of values of the parameters *A* and *B* (Eq. 6) of the model for heat flux density at the soil surface ($G_0$) by Santanello and Friedl (2003), $G_0^s$, in relation to referential $G_0$ ($G_{0R}$) (Eq. 30)

IV.1.3.9.3. Based on the Force-restore model ($G_0^{fr}$)

The expression by Bhumralkar (1975) (Eq. 21) was used in order to determine $G_0^{fr}$. However, the suggestion of Liebethal et al. (2007) regarding the use of a $\Delta z$ equivalent to 0.1 m was also considered. This implied determining the soil heat storage (first term of Eq. 21) with $\partial Ts(0.05,t)/\partial t$, $C_v$ with soil moisture at a depth of 0.05 m and a $\Delta z$ of 0.1 m. The soil heat flux at 0.1 m (second term of Eq. 21) was determined with $\partial T(0.1,t)/\partial t$, $T(0.1,t)$ and the thermal conductivity, $k$, with soil moisture measured at 0.05 m. In order to do this, the records of moisture at 0.05 m were used, while for the daily thermal amplitude (24 hrs) of temperatures at the soil surface ($\Delta T_0$, Eqs. 18 and 19), the maximum and minimum records of temperature at the soil surface were used. The expressions used to determine $\partial T(z,t)/\partial t$, $T(z,t)-\overline{T}$, $C_v$ and *k* were the Eqs. (18, 19, 33 and 35), respectively.

IV.1.3.9.4. Based on the plate calorimetry methodology ($G_0^{pco}$):

In order to determine $G_0^{pco}$ Eq. (26) was used. The mean values of readings from two heat flux plates buried at a depth of 0.05 m were used, taking into account corrections for differences in thermal conductivity of the plate-soil inter-phase (Eq. 22), and the heat flux stored in the soil between the soil surface and the plate installation depth ($\Delta S$) (Eq. 32). The value of $\Delta S$ was obtained numerically from Eq. (34). In this case, $T_i$ and

$T_{i-1}$ was estimated at a depth of 0.025 m, through the cubic spline interpolation methodology, considering the temperatures recorded at the soil surface and at a depth of 0.03 m. The volumetric heat capacity of the soil, $C_v$, was determined from Eq. (33), estimating soil moisture at 0.025 m of depth ($\theta_{0.025}$) with the following expression, obtained in the experiment site for days without rain or irrigation:

$$\theta_{0.025} = \theta_{0.05} - 2\left(\theta_{0.1} - \theta_{0.05}\right) \quad (42)$$

Where $\theta_{0.05}$, and $\theta_{0.1}$ correspond to the volumetric moisture content in the soil measured at 0.05 and 0.1 m of depth, respectively. Finally, the variables $\Delta z$ and $\Delta t$, of Eq. (34) took values of 0.05 m and 3600 s, respectively.

IV.1.3.10. Validation of the models.

The validation of the models used was done through the interpretation of the following coefficients:

Graphic relation1:1. The data of the referential heat flux density at the soil surface ($G_{0R}$, Eq. 30) contrasted with the data estimated through the three models ($G_0^{rn}$, $G_0^{s}$ and $G_0^{fr}$), and the measurements of (corrected) heat flux plates ($G_0^{pco}$) were illustrated on a graph. The mean absolute error, MAE, and the root mean square error, RMSE, obtained from the expressions are:

$$MAE = \frac{1}{N}\sum_{i=1}^{N}\left|O_i - P_i\right| \quad (43)$$

$$RMSE = \sqrt{\frac{1}{N}\sum_{i=1}^{N}\left(O_i - P_i\right)^2} \quad (44)$$

where $O_i$ is the referential $G_{0R}$ value (Eq. 30) and $P_i$ is the estimated values of $G_0$ through the three models and the corrected soil heat flux plate, $N$ is the number of observations and $i$ denotes the $i$th observation.

**IV.1.4. Results and discussion**

IV.1.4.1 Referential soil heat flux density at the soil surface ($G_{0R}$)

The referential heat flux density at the soil surface, $G_{0R}$ (Eq. 30), and its components, heat flux density measured at a depth of 0.1 m ($G_{0.1}^{m}$, Eq. 31) and the change in heat storage in the soil layer ($\Delta S$, Eq. 32), show an hourly behavior with a four-hour time lag between the peaks of each flux (Fig. 3). In the case of the $G_{0.1}^{m}$ peak values are reached at 3 pm, and $\Delta S$ is reached at 11 a.m., while the peak of $G_{0R}$ (the addition of its components) occurs between 1 and 2 p.m. The peak of $G_{0R}$ reached values of 103 and 63 W m$^{-2}$ for clear and cloudy days, respectively. These values are within those indicated by Mayocchi and Bristow (1995), who reported, in the month of November, in North Queensland, that the heat flux density at the soil surface, $G_0$, determined through

plate-calorimetry methodology and heat flux plates buried at a depth of 0.1 m, peaked at 12 hrs (UTC) with a value of 80 W $m^{-2}$, in a soil covered with sugar cane 0.65 m high. However, Cobos and Baker (2003) indicate that the peak of $G_0$ occurred at 1 p.m. (UTC) with a magnitude of 80 W $m^{-2}$, on silt loam soil, covered with soybean 0.1 m high. In a study carried out during the summer of 2007 in central Chile, in a soil with a vegetal cover, Nuñez et al. (2010), found that $G_0$ peaked at 4 p.m. local time (13 UTC) with a magnitude of 55 W $m^{-2}$. Similarly, in November of 1984, in Phoenix, United States, using a plate-calorimetry methodology through measurements of heat flux plates at a depth of 0.05 m, Clothier et al. (1986), obtained a peak value at 12 hrs (MST) with a magnitude of 100 W $m^{-2}$, in a soil with a vegetal cover of just-cut alfalfa. Finally, Liebethal and Foken (2007), in the summer of 2003, in Lindenberg, Germany, found that $G_0$, obtained using a gradient-calorimetry methodology, through measurements of thermal gradient at a depth of 0.2 m, had its peak at solar noon, with a magnitude of 70 W $m^{-2}$, measured in a sand loam soil with a vegetal cover 0.2 m high. On the other hand, it can be seen that the time behavior of $G_{0R}$ and its components is similar for clear days (Fig.3a) as well as for cloudy days (Fig.3b), with a variance in magnitude only. It is worth mentioning that $G_{0R}$ is positive (flux coming in from the surface) around 10:00 hours (a.m.) (sunrise at 08:00 a.m) and becomes negative at sunset (sunset at 7:45 p.m.).

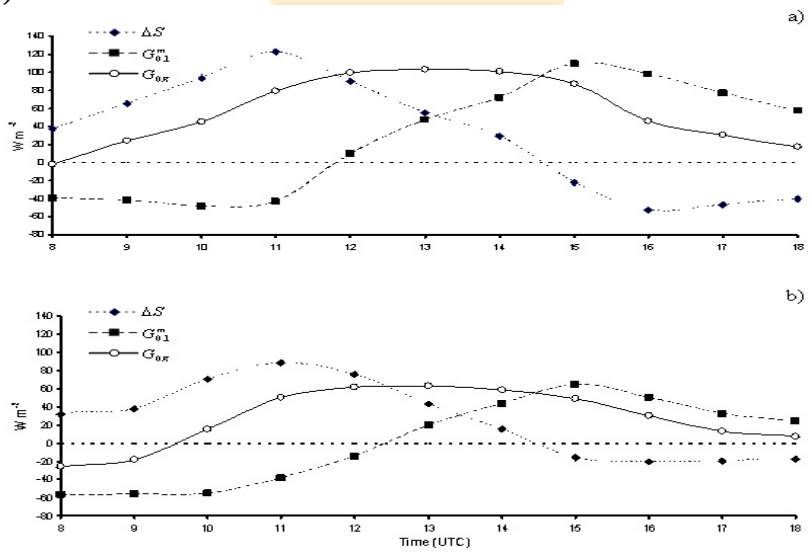


Fig. 3. Hourly behavior of referential heat flux density at the soil surface, $G_{0R}$, formed by the heat flux density measured at a depth of 0.1 m ($G^{m}_{0.1}$) and the change in heat storage in the soil layer with a thickness of 0.1 m ($\Delta S$) for a) clear day (DOY 263) and b) cloudy day (DOY 254).

IV.1.4.2. $G_0/Rn$ relation:

Unlike the model by Choudhury et al. (Eq.41), which assumes the $G_0^{rn}/Rn$ relation as constant (0.2343 in this study), the behavior of the $G_{0R}/Rn$ and $G_0^s/Rn$ relations is not constant throughout the day. This rate increases as the day goes by, and reaches a value close to 0.25 at 3 p.m, for clear as well as cloudy days (Fig.4). The time variations of the $G_0/Rn$ ratio have also been recorded by Clothier et al. (1986) and Kustas et al.

(2000), among others. However, the distribution indicated by these researchers does not agree with that found in this study. For Clothier et al. (1986), the lowest value is found at the hours of daybreak and sunset, and the highest value at 1 p.m. (MST). However, for Kustas et al. (2000), the highest and lowest values of $G_0/Rn$ were reached at 9 a.m. and 4 p.m. (LDT), respectively. It is important to mention that Fig. (4) shows the behavior of the $G_0/Rn$ relation just until 3 p.m., as this relation becomes unstable in the following three hours due to a sign change in the $Rn$ and $G_{0R}$ fluxes, which takes place with a time lag of one hour between one and the other, a phenomenon that is called hysteresis loop, as reported by Clothier et al. (1986). It can also be observed in Fig. (4) that there is a time lag of three hours between the highest values of net radiation and the $G_{0R}/Rn$ relation. This can be due to the fact that at 3 p.m. (highest $G_{0R}/Rn$) values close to the peak of $G_{0R}$ are maintained (Fig. 3) while the net radiation has dropped considerably with respect to its peak. On the other hand, when comparing Figs. (3) and (4), a 1 hour time lag can be seen between the peak of $G_{0R}$ (13 hours) and that of $Rn$ (12 hours). According to Clothier et al. (1986), when analyzing the analytical solution of the one-dimensional heat equation by Carslaw and Jaegar (1959), $G_0$ should precede $Rn$ in 1 hour (or $\pi/12w$), which opposes what was found in this study. This could be explained by the time lags that occur when determining $G_0$ through measurements of $G_z^m$ (Eq. 31) performed at different depths. As a matter of fact, Mayocchi and Bristow (1995), report a morning time lag of 1 hour approximately, between the $G_0$ obtained through measurements of $G_z^m$ at depths of 0.02 and 0.1 m.

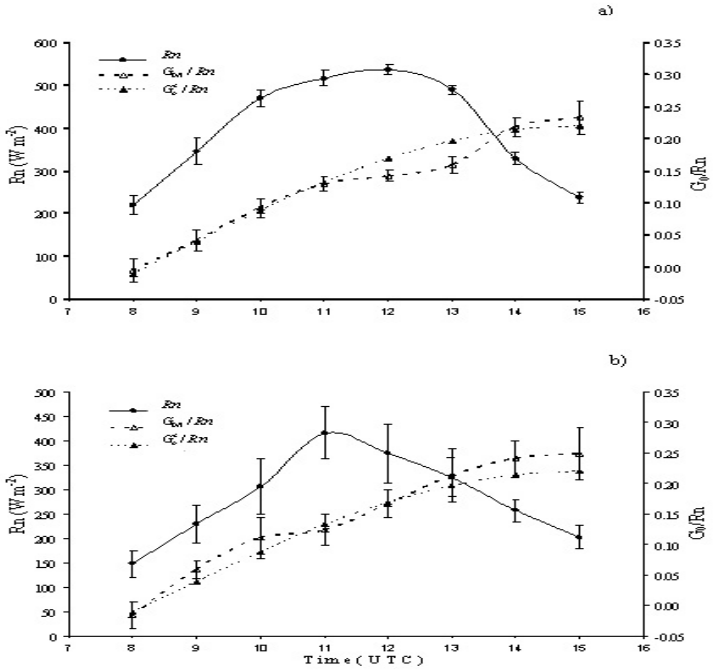


Fig. 4. Time behavior of the relation between referential heat flux density at the soil surface ($G_{0R}$) and that estimated through the model by Santanello and Friedl (2003) ($G_0^s$) with the net radiation ($Rn$) for the daylight hours, obtained from the mean of a) 8 clear days and b) 8 cloudy days. The bars show the $\pm 1$ S.D.

IV.1.4.3. Hourly estimation of $G_0$:

In general, both the two methods used and the heat flux plate calorimetry methodology show a pattern that follows the curve of $G_{0R}$ (Fig. 5).

The best approximation is achieved through the model by Santanello and Friedl ($G_0^s$) and the plate-calorimetry methodology, from 9 a.m. on. This estimation tends to improve from 2 p.m on, including the radiational model by Choudhury et al. (1987) ($G_0^{rn}$), especially on cloudy days (Fig. 5b). The Force-restore model shows results more distant from the values of $G_{0R}$, with an overestimation for every hour of daylight.

The better estimation of $G_0$ by Santanello and Friedl's model (2003) when compared with that of Choudhury et al. (1987) is due to the prediction quality of the $G_0/Rn$ ratio. In fact, the estimated relation ($G_0^s/Rn$) shows practically no difference with the observed relation ($G_{0R}/Rn$) during daylight hours (Fig. 4). In the case of the fixed $G_0^{rn}/Rn$ ratio of 0.2343, obtained with the model by Choudhury et al. (1987), (Eq. 41), there is an overestimation of $G_0$ in the early hours of the morning but it tends to converge during hours of the afternoon, when the $G_{0R}/Rn$ relation begins to increase and reaches values close to 0.23 (Fig. 4).

In the case of the plate-calorimetry methodology, the overestimation of $G_0$ can occur due to the fact that the time lag of the temperatures which determine $G_0^{pco}$ and $G_{0R}$ is bigger in the morning hours than in the afternoon hours, which is in agreement with what Mayocchi and Bristow (1995) reported: a morning time lag difference among fluxes of $G_0$, which were determined with measurements of $G_z^m$ (Eq. 31) performed at different depths.

The high values of $G_0$ estimated by the Force-restore model contradict Liebethal and Foken (2007), who determined this model was the best estimator of $G_0$. On the other hand, Gao et al. (2008) claim that this model tends to overestimate the values of $G_0$, while reports by Chandrakant and Bhumralkar (1975) showed $G_0$ values of up to 360 W m$^{-2}$ and a $G_0/Rn$ ratio close to 1 while using the Force-restore model during the summer season in the eastern area of Argentina, in bare soil.

It can also be seen in Fig. (5) that the highest values of $G_0$ for the two models and plate and gradient-calorimetry methodologies ($G_{0R}$) occur at 1 p.m., with the exception of the $G_0^{rn}$ model, which reaches its highest value at 12 hrs. This is so because $G_0^{rn}$ follows the hourly behavior of the net radiation and not that of the soil temperature.

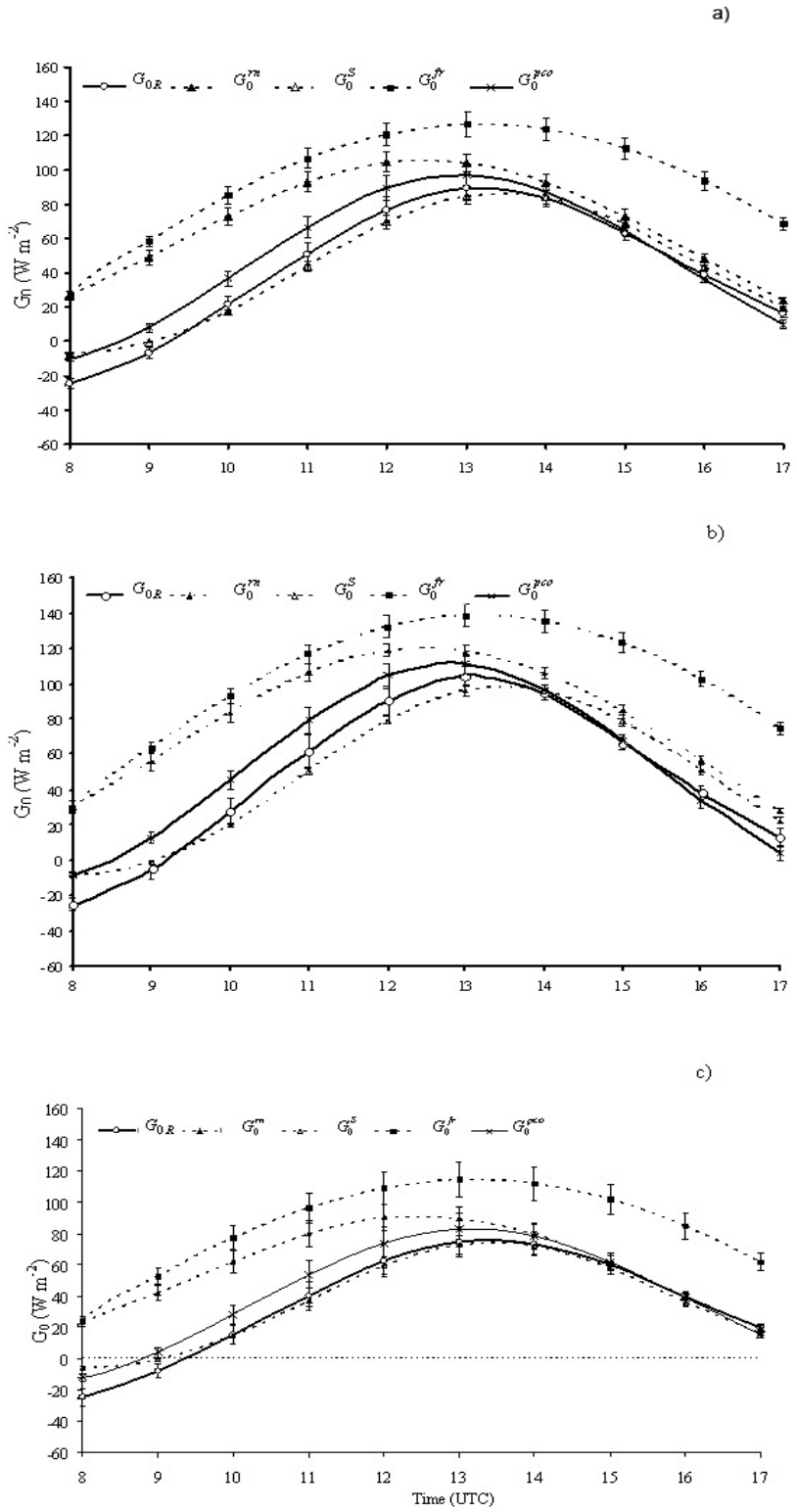


Fig. 5. Heat flux density at the soil surface ($G_0$) estimated with the radiational model by Choudhury et al. ($G_0^{rn}$), Santanello and Friedl's ($G_0^{s}$), Force-restore model ($G_0^{fr}$), plate calorimetry methodology ($G_0^{pco}$) and the referential gradient-calorimetry methodology ($G_{0R}$), during daytime hours, for a) 16 days of measurements, b) 8 cloudy days and c) 8 clear days. The bars show the $\pm 1$ S.D.

IV.1.4.4. Evaluation of $G_0$ estimation models and measurements with soil heat flux plates

The radiational model $G_0^{rn}$ overestimates the referential heat flux, $G_{0R}$, both for positive and negative values (Fig. 6a). Considering that the fraction of $Rn$ is valid for values of $Rn$ >0 (Eq. 41), the $G_0^{rn}$ estimation will always be positive, which implies that for negative values of $G_{0R}$ the error of the estimation will proportionally increase as $G_{0R}$ values decrease. In the case of Santanello and Friedl's model (2003), the $G_0^s$ estimation shows a 1:1 behavior pattern in the estimation of positive values of $G_{0R}$, which is in agreement with Liebethal and Foken's (2007) results. However, it overestimates for negative values of $G_{0R}$ (Fig. 6b). This occurs during the first hours of the morning and near twilight, due to the difference in magnitude between the model's $G_0^s/Rn$ and $G_{0R}/Rn$ ratio in the mentioned hours. The Force-restore model, $G_0^{fr}$ (Fig. 6c), is the one that shows a behavior which is more distant from the 1:1 line in the estimation of $G_{0R}$, with overestimations for both positive and negative values. This does not coincide with Liebethal and Foken's (2007) findings, which showed the best $G_{0R}$ predicting model is Force–restore. The fact this model assumes a homogeneous soil profile should be considered, because that implies that the soil physical properties do not change with depth, and that could explain the results obtained. Another reason that could explain this result is related to the magnitude of $\Delta z$ used in this study (0.1 m); a lower value might improve the results obtained, since the thermally active layer (an assumption of the model) can be found at depths less than 0.1 m. The methodology of heat flux plate measurement, $G_0^{pco}$ follows the 1:1 proportion for the positive values of $G_{0R}$; however, it overestimates for negative values of $G_{0R}$ (Fig. 6d), owing to the time lag between the temperatures determining both heat fluxes.

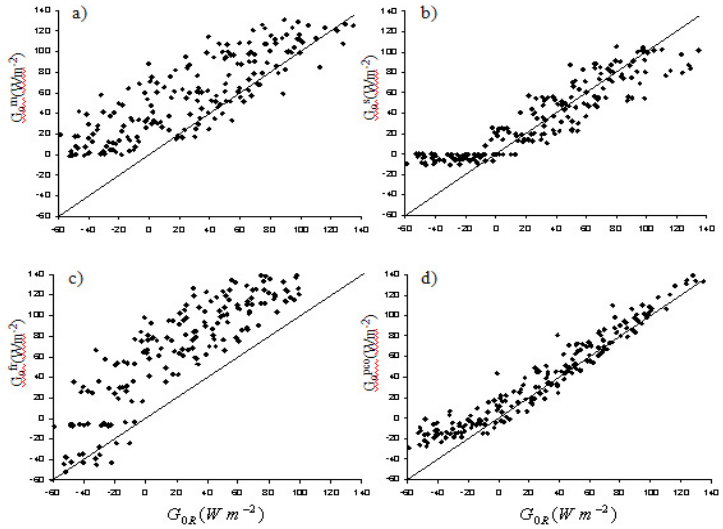


Fig. 6. 1:1 ratio of the heat flux density at the soil surface estimated a) through Eq. (41), as the fraction 0.2343 $Rn$ ($G_0^{rn}$) ; (b) Santanello and Friedl 's model (Eq. 6) ($G_0^s$) ; (c) Force- restore model (Eq. 21) ($G_0^{fr}$) ; and (d) through plate calorimetry methodology (Eq. 26) ($G_0^{pco}$), versus the referential heat flux density at the soil surface ($G_{0R}$), hourly, during daylight hours, for 16 days of study (n=192).

When evaluating the statistical efficiency indices of the three models and the heat flux plate calorimetry methodology for all days of this study (Table 1), and according to what can be observed in the 1:1 graphs, it can be observed that the $G_0^{rn}$ model performed poorly at estimating $G_{0R}$, which could be due to:

a) The fixed $G_0^{rn}/Rn$ ratio determined by Eq. (5) not being appropriate. In this respect, Fig. (7) presents a number of combinations for the fixed $G_0^{rn}/Rn$ ratio which are associated with the error caused (RMSE) in $G_0$ estimation, with respect to $G_{0R}$ for all days of the study. The relation that caused the smallest error is 0.15, associated to a RMSE of 31 W m$^{-2}$. Thus, the optimal $G_0^{rn}/Rn$ relation could have been 0.15 and not 0.2343. However, the model's behavior improved marginally since the RMSE of 39 W m$^{-2}$ ($G_0^{rn}/Rn = 0.2343$) decreases to 31 W m$^{-2}$ ($G_0^{rn}/Rn = 0.15$).

b) The $G_0^{rn}/Rn$ relation of the model by Choudhury et al. is not fixed, but variable during the day, as can be observed in Fig. (4). The impact of changing the $G_0/Rn$ relation from fixed to variable can be observed when comparing this model's RMSE and MAE, with respect to Santanello and Friedl's (2003), (Table 1), which does consider this variability.

Table 1. Efficiency evaluation indices for the hourly estimation of referential heat flux density at the soil surface ($G_{0R}$) with the model by Choudhury et al. ($G_0^{rn}$); Santanello and Friedl ($G_0^{s}$); the Force-restore model, ($G_0^{fr}$); and the heat flux plate calorimetry methodology ($G_0^{pco}$) for a) 8 clear days; b) 8 cloudy days; and c) 16 days of study.

| Model | RMSE (W m$^{-2}$) | | | MAE (W m$^{-2}$) | | | Average $G_{0R}$ (W m$^{-2}$) | | |
|---|---|---|---|---|---|---|---|---|---|
| | a | b | c | a | b | c | a | b | c |
| $G_0^{rn}$ | 42.8 | 35.4 | 39.7 | 35.9 | 28.5 | 32.7 | 33.15 | 21.2 | 28 |
| $G_0^{s}$ | 24.6 | 18.7 | 22.2 | 20.0 | 15.1 | 17.9 | | | |
| $G_0^{fr}$ | 54.4 | 46.5 | 51.1 | 49.5 | 41.0 | 45.8 | | | |
| $G_0^{pco}$ | 17.7 | 14.1 | 16.2 | 13.8 | 11.0 | 12.6 | | | |

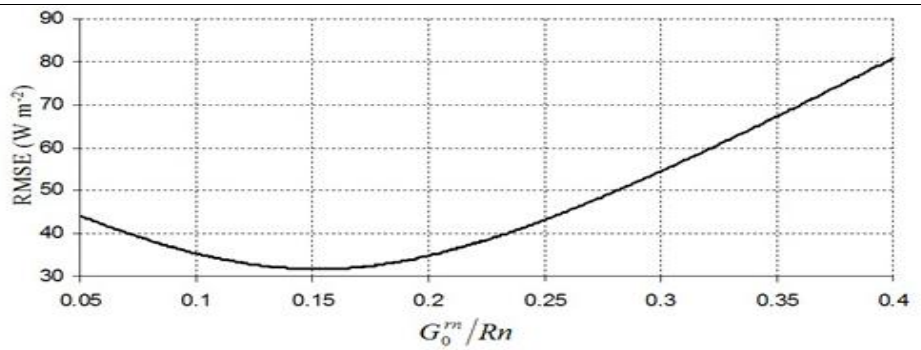


Fig. 7. Fixed relation combination of the of heat flux density at the soil surface and the net radiation ($G_0^{rn}/Rn$) of the model by Choudhury et al., and the RMSE in the estimation of the referential heat flux density at the soil surface ($G_{0R}$).

Out of the three models analyzed, Santanello and Friedl's (2003) ($G_0^s$), show the best statistical indicators for the prediction of $G_{0R}$ (Table 1), making this model a good alternative to obtain $G_0$ based on $Rn$.

On the other hand, Santanello and Friedl's model adjustment values used in this study ($A$=0.22 and $B$=97500), do not differ from the values that can be obtained using Eqs. (7) and (8), which on average, for the study period, correspond to 0.21 and 92814 for $A$ and $B$, respectively.

The least efficient model for estimating $G_{0R}$ is Force–restore ($G_0^{fr}$), according to RMSE and MAE, with an overestimation of $G_{0R}$ during daylight hours, for clear as well as cloudy days. This behavior could be explained by the assumption of homogeneity in the soil profile's physical properties, necessary for its analytical derivation, which was not observed in this study. According to estimation, soil bulk density was 1.45 Mg $m^{-3}$ for the soil surface layer (0 to 0.10 m of depth) and 1.6 Mg $m^{-3}$ for the layer between 0.1 and 0.2 m of depth. As for soil moisture, it varied in average 0.06 $m^3$ $m^{-3}$ between 5 to 10 cm of depth, and such variation increased when it was measured in the first 3 centimeters, since it is at that depth that the water phase shift from liquid to gas occurs (Mayocchi and Bristol, 1995). Therefore, the soil bulk density and moisture variation would alter the determination of the damping depth, $d$ (Eq. 17), and consequently, the determination of $G_0$. In addition, in cultivated soils, an active extraction of water is expected to occur in the soil surface layers due to root activity in that area. On the other hand, the use of a $\Delta z$ of 0.1 m. could have been inappropriate; better results might be obtained if a lower value were used since the thermally active layer (an assumption of the model) could be found at depths less than 0.1m. Even though this model has had good results in other studies (Liebethal and Foken, 2007), its implementation is not easy since it requires having the soil physical properties and soil moisture information, which is not always available.

The heat flux plate calorimetry methodology ($G_0^{pco}$) presented the highest statistical indices of efficiency, with lower RMSE and MAE values, due to the fact this is a methodology for the determination of the heat flux density at the soil surface and not an estimation. This methodology has a slight deviation with respect to $G_{0R}$, which can be due to the time lag that exists in temperature behavior at different depths. For the determination of $G_{0R}$ in this study, records of temperatures used were those read at 0.05 and 0.10 m of depth, and for the case of the plate calorimetry methodology, the records of temperature used were those at 0.025 and 0.05 m of depth. The results obtained are very close to $G_{0R}$, which implies that the use of heat flux plates is a good methodology to obtain $G_0$, despite inconveniences related to its use.

Finally, the behavior of models and plate calorimetry methods in the estimation of $G_{0R}$ is maintained for cloudy and clear days (Table 1). However, the statistical indices for cloudy days are slightly better.

### IV.1.5. Conclusions

When integrally analyzing the statistical indices, the plate-calorimetry methodology ($G_0^{pco}$) shows similar results to the gradient-calorimetry methodology ($G_{0R}$), therefore, it is a recommendable methodology to estimate the heat flux density at the soil surface, despite installation inconveniences.

The model that best estimates the hourly behavior of $G_0$ is Santanello and Friedl's model ($G_0^{s}$), what makes it highly recommendable both for its behavior and its simple implementation.

The estimation of the heat flux density at the soil surface ($G_0$) through the model by Choudhury et al. ($G_0^{rn}$), does not adequately represent its hourly behavior during daylight hours, with overestimations throughout the whole period due to the fact the $G_{0R}/Rn$ ratio is not fixed but variable during the day.

The Force-restore model ($G_0^{fr}$) proved to be the least efficient estimator of $G_0$. This condition could be attributed to the lack of homogeneity of thermal and physical soil profile properties (bulk density, moisture content and thermally active layer thickness) implied in the assumptions of the model.

### IV.1.6. References

ASCE-EWRI, 2005. The ASCE Standarized Reference Evapotranspiration Equation. Report 0-7844-0805-X, ASCE Task Committee on Standarization of Reference Evapotranspiration. Reston, VA., American Soc. Civil Engineers.

Allen, R., Pereira, L., Raes, D., Smith, M., 1998. Crop evapotranspiration: guidelines for computing crop water requirements. FAO Irrigation and drainage paper 56. FAO, Rome.

Bhumralkar, C.M., 1975. Numerical experiments on the computation of ground surface temperature in an atmospheric general circulation model. J. Appl. Meteorol. 14, 1246–1258

Blackadar, A.K., 1976. Modelling the nocturnal boundary layer. Proceedings of the 3rd International Symposium on Atmospheric Turbulence, Diffusion and Air Quality, Boston: 46–49.

Campbell GS (1985) Soil physics with basic: transport models for soil- plant systems. Elsevier, New York

Carslaw, H.S., Jaeger, J.C., 1959. Conduction of Heat in Solids, second ed. Oxford Science Publication, Oxford.

Choudhury, B.J., Idso S.B., Reginato R.J., 1987. Analysis of an empirical model for soil heat flux under a growing wheat crop for estimating evaporation by an infrared temperature based energy balance equation. Agric. For. Meteorol. 39:283-297.

Clothier, B.E., Clawson, K.L., Pinter P.J., Moran M.S., Reginato, R.J., Jackson R. D., 1986: Estimation of soil heat flux from net radiation during the growth of alfalfa. Agric. For. Meteorol. 37, 319-329.

Cobos D., Baker, J.M., 2003: In situ measurement of soil heat flux with the gradient method. Vadose Zone Journal 2, 589-594.

Deardoff, J.W., 1978. Efficient prediction of ground surface temperature and moisture with inclusion of a layer of vegetation. J. Geophys. Res 83 (4), 1889-1903

De Vries, D.A., 1963. Thermal properties of soil. In: Van Wijk, W.R. (Ed.), Physics of the Plant Environment. North-Holland. Amsterdam

Dickinson, R.E., 1988. The force-restore model for surface temperatures and its generalizations. J. Clim. 1, 1086-1097

Gao, Z., Horton, R., Wang, L., Liu, H., Wen, J., 2008. An improved force-restore method for soil temperature prediction. Euro. J. Soil Sci. doi: 10.1111/j.1365-2389.2008.01060.x

Fuchs, M., Hadas, A., 1973. Analysis of the performance of an improved soil heat flux transducer. Soil Sci. Soc. Am. J. 37, 173–175.

Fuchs, M., 1987. Heat flux. In Klute A (ed) Methods of soil analysis, part 1: Physical and mineralogical methods. Agr. Monogr. Madion:ASA and SSSA, 957-968

Howell, T.A., Tolk, J.A., 1990. Calibration of soil heat flux transducers. Theor. Appl. Climatol. 42, 263-272.

Kustas, W., Daughtry, C., 1990. Estimation of the soil heat flux/net radiation ratio from spectral data. Agric. For. Meteorol. 49, 205-223.

Kustas, W., Prueger J., Hatfield, J., Ramalingam, K., Hipps, L., 2000. Variability In Soil Heat Flux From A Mesquite Dune Site. Agric. For. Meteorol. 103, 249 – 264.

Liebethal, C., Huwe, B., Foken, T., 2005. Sensivity analysis for two ground heat flux calculation approaches. Agric. For. Meteorol. 132, 253 – 262.

Liebethal, C., Foken, T., 2007. Evaluation of six parameterization approaches for the ground heat flux. Theor. Appl. Climatol. 88, 43-56.

Lin, J.D., 1980. On the force-restore method for prediction of ground surface temperature. J. Geophys. Res. 85 (6), 3251-3254.

Mayocchi, C., Bristow, K., 1995. Soil surface heat flux: some general questions and comments on measurements. Agric. For. Meteorol. 75, 43-50.

Nuñez, C.M., Vara, E.A., Meza, J.M., 2010. Modelling soil heat flux. Theor. Appl. Climatol. 100, 251 – 260.

Philip, J.R.,1961. The theory of heat flux meters. J. Geophys. Res. 66, 571–579.

Santanello, J., Friedl, M., 2003. Diurnal covariation in soil heat flux and net radiation. J. Appl. Meteorol. 42, 851 – 862.

Sauer, D.W., Ochsner, A. R., Harris., Horton R., 2003. Errors in heat flux measurement by flux plates of contrasting design and thermal conductivity. Soil Sci. Soc. Am. J. 2, 580-588.

Sauer, T., Ochner, T., Horton, R., 2007. Soil Heat Flux Plates: Heat flow distortion and thermal contact resistance. Agron. J. 99, 304 – 310.

## IV. 2.

## Modeling hourly nocturnal temperature in frost radiative events i: development of a numerical model to estimate bare soil surface temperature

**Abstract**

During radiative frost events (hourly night time step), a numerical model was developed considering *in situ* soil temperature profile, soil water content and net outgoing long-wave radiation measurements, which are necessary to define the model's initial and boundary conditions. Thus, bare soil surface temperature prediction is based on the main variables involved in the formation of radiative frosts.The numerical model performed well in the estimation of bare soil surface temperature with RMSE and MAE of 1.6 ºC and 1.3 ºC, respectively. The numerical model performed better when the soil surface wetness content ($\theta_0$) lays between field capacity ($\theta_{fc}$) and wilting point ($\theta_{wp}$), because upper boundary conditions can be estimated with greater accuracy, and the error which can be caused in the estimation has low sensitivity in the prediction of the bare soil surface temperature at sunrise. On the other hand, to be massively applied, its initial and boundary conditions need to be parameterized since, currently, data about soil profile temperature and long wave net radiation is not available in most agricultural lands.

### IV.2.1. Introduction

Various approaches have been designed to predict the minimum air-soil temperature reached during nocturnal cooling from weather data registered the day before, generally at sunset. They can be purely empirical, obtained from statistical relationships, or mechanistic, based upon physical principles (Bagdonas *et al.* 1978). In the mechanistic models of frost radiative prediction, an accurate estimate of downward long-wave radiation is essential, due to the fact that frost occurrence is generated by a deficit in long-wave radiation (Lhome *et al*. 2007).

For a bare soil surface, the radiative frost formation process means a budget energy process whose components are the net flux density of radiation, $Rn$; sensible heat flux density, $H$; latent heat flux density, $LE$; and heat flux density in the soil, $G$. During radiative frosts, there is a loss of radiation from the ground surface to the atmosphere and a gain of radiation from the atmosphere to the ground, as well as a gain of energy by conduction of heat in the soil and by convection of heat in the air. However, more heat is lost than gained in this process (Snyder *et al.* 2010). Similarly, Figuerola and Mazzeo (1997) indicated that the evolution of night temperature on a horizontal and homogeneous surface is affected by the radiation loss from the surface, which is partially replaced by heat conduction from the ground, but also by the contribution of sensible heat from the air.

The first true physical approach was developed by Brunt (1941). It is essentially an analytical solution of a one-dimensional heat-conduction equation in bare soil considered as a semi-infinite and homogeneus medium, where the atmosphere is eliminated from de analysis (Lhomme and Guillione, 2004):

$$\frac{\partial Ts}{\partial t} = Ks \frac{\partial^2 Ts}{\partial z^2} \qquad (1)$$

where $Ts$ is the soil temperature (K or ºC), $Ks$ is the soil thermal diffusivity ($m^2\ s^{-1}$), $t$ is time (s) and $z$ is the depth into the soil (m).

The main idea behind Brunt's and associated equations is that the soil plays a major role in limiting the temperature decreasing under radiative frost conditions. Easy operation is an important advantage of these approaches; for that reason, Brunt's equations are still widely used for short time range of minimum air temperature predictions (Cellier 1993). This initial approach was extended, by several authors, to take into account the heating of the surface by the air. In this sense, Jaeger (1945) noted that the ground can be heated from the air, developing an expression similar to that of Brunt in function of net radiation, night length, thermal conductivity and thermal diffusivity of the air and soil surface (assuming all of them as constant).

As Jaeger, Reuter (1951) found an analytical solution to the one-dimensional heat equation, considering the effect of heat transfer from the atmosphere to the ground. To do this, he assumed that the air and soil thermal conductivity, net radiation, thermal gradient in depth (soil) and height (air), are constant over the course of the night; as well as assuming that during night-time at depth $z = 0$, the air temperature equals the soil surface temperature, $\left(Ta_{(0,t)} = Ts_{(0,t)}\right)$. The last condition states simply that the sum of effective net outgoing radiation ( $Rn$ ), the flow of heat from below to the surface and the flow of heat from atmosphere to the surface is equal to zero. The expression is similar to that developed by Jaeger (1945); however, Reuter`s expression considers the thermal gradient in the soil and the atmosphere media, as well as the dry adiabatic lapse rate in the air.

Anfossi *et al.* (1976) developed a one-dimensional heat equation, but instead of considering the heat diffusion from the inside of the ground to the surface as Brunt does, they looked at Brunt's problem as one of diffusion in air from the ground surface up. The conditions to find his expression are: a) initial condition, where the starting time of the process is made to coincide with the moment at which the diurnal thermal wave (near the surface) attains its maximum value before decreasing; b) lower boundary condition, where the temporal evolution of thermal gradient is constant; and c) upper boundary condition, where at a given height, the temporal evolution of thermal gradient is zero. Jaeger (1945), Reuter (1951) and Anfossi *et al*. (1976), developed models which are the result of an analytical solution of the one-dimensional heat equation, based upon Brunt's analysis plus the incorporation of energy input from the atmosphere, which should result in better estimations. However, the use of Brunt's model is still more practical since it requires the quantification of fewer variables.

The models which are the result of an analytical solution of the one-dimensional heat equation ((Brunt's, Jaeger's, Reuter's and Anfossi's) have the inconvenience of using assumptions which do not always conform to reality (thermal diffusivity, and soil physical characteristics, which are constant through the profile) and are, therefore, applicable under certain conditions. In this respect, numerical models are more flexible since assumptions which are considered constant in analytical models can be variable in numerical models, because they can be adjusted to the medium conditions that affect a given physical phenomenon. They generally simulate the evolution of air and soil temperatures near the soil surface, using more or less complex numerical solutions of the energy conservation equation. These models have two main advantages (Cellier 1993):

- They may account for most physical processes involved in nocturnal cooling.
- They may simulate very different conditions: evolution of meteorological conditions, soil type, surrounding environments and complex topography.

But, strong drawbacks must also be emphasized:

- The relative complexity of these models: even if computer programs performances are improving rapidly, most of these models are not accessible to the level at which they would be most useful (extension services or local meteorological centers).
- Some input data are not easily available for routine operation at a local scale.

The objective of this research was to develop and solve numerically a one-dimensional heat diffusion model with real initial and boundary conditions, estimating bare soil surface temperature for frost radiative events (hourly night time step).

### IV.2.2. Theory and numerical model development

The model developed in the present study numerically solves the one-dimensional heat diffusion equation (Eq. (1)), dependent on initial and boundary conditions observed in radiative frost events. In this respect, the initial and boundary conditions are according to the temporal behavior of the net radiation and the response of the temperature and wetness content at different soil depths.

Bare soil surface water content had to be indirectly determined through Richards' equation (or estimated from field observations); meanwhile soil temperature distribution is obtained solving the one-dimensional heat diffusion equation.

#### IV.2.2.1. The use of Richards' equation in the bare soil evaporation process

Because Richards' equation is nonlinear, an analytical solution is not possible except for special cases. Therefore, numerical approximations are typically used to solve the unsaturated flow equation. The standard approximations applied to the spatial domain are the finite difference method and the finite element method (Celia *et al.* 1990).

In order to estimate the temporal and spatial evolution of the soil wetness, especially that of the soil surface ($\theta_0$) at the beginning of the radiative frost event, Richards' equation is applied to the evaporation process of water in bare soil for a period of time $[0, \mathrm{T}]$, beginning six hours after the last rain or planting irrigation - previous to a frost event ($t=0$) - until the sunset that precedes this event ($t = \mathrm{T}$), and its value is variable depending on the frost event.
For the conditions of this study, Richards' equation is presented in the following manner:

$$\frac{\partial \theta}{\partial t} = \frac{\partial}{\partial z}\left( k_c \frac{\partial \psi}{\partial z} \right) + \frac{\partial k_c}{\partial z}, \quad 0 \le z \le \mathrm{Z} \quad \text{and} \quad 0 \le t \le \mathrm{T} \tag{2}$$

where $\theta$ , $k_c$, y $\psi$ are volumetric soil water content ($m^3\ m^{-3}$), soil capillary hydraulic conductivity ($m\ s^{-1}$) and matric potential of water in the soil (m). Depth *z* is considered from soil surface to the depth Z closest to the surface where soil wetness is determined either by sensors or modeling.
Because specific water retention capacity of the soil $C(\psi)$ and capillary hydraulic conductivity $(k_c)$ are nonlinear functions of soil water matric potential $(\psi)$, some linearization and/or iteration procedure must be used to solve the discrete equations. Standard iteration techniques include Picard and Newton methods. The Picard iteration method involves sequential estimation of unknown $\psi$, using the latest estimates of $C(\psi)$ and $k_c$ (Celia *et al.* 1990).

Eq. (2) was discretized as indicated by Clement *et al.* (1994), i.e., with the finite-difference method, through an implicit scheme, and through the use of Picard iteration to estimate, in every time step, the hydraulic conductivity in the non-linear part of the equation. The right side of Eq. (2) can be discretized as follows:

$$\frac{\partial}{\partial z}\left(kc\frac{\partial \psi}{\partial z}\right)+\frac{\partial kc}{\partial z}\approx\frac{1}{\Delta z}\left[\left(\frac{kc_j^{n+1,m}+kc_{j+1}^{n+1,m}}{2}\right)\left(\frac{\psi_{j+1}^{n+1,m+1}-\psi_j^{n+1,m+1}}{\Delta z}\right)-\left(\frac{kc_j^{n+1,m}+kc_{j-1}^{n+1,m}}{2}\right)\left(\frac{\psi_j^{n+1,m+1}-\psi_{j-1}^{n+1,m+1}}{\Delta z}\right)\right] \quad (3)$$
$$+\frac{1}{\Delta z}\left[\left(\frac{kc_j^{n+1,m}+kc_{j+1}^{n+1,m}}{2}\right)-\left(\frac{kc_j^{n+1,m}+kc_{j-1}^{n+1,m}}{2}\right)\right]$$

Where $\psi_{j+1}^{n+1,\,m+1}$ denotes matric potential estimated in time $t_{n+1}$(s), in node $z_{j+1}$, and at a Picard iteration level of $m+1$. Therefore, $\Delta t$ (s) corresponds to the difference between $t_{n+1}$ and $t_n$; $\Delta z$ (m) corresponds to the difference between node $z_{j+1}$ and $z_j$; then, the discretization of depth can be expressed as $z_j=(j-1)\,\Delta z$. Finally, the current and previous Picard iteration level is denoted by $m+1$ and $m$, respectively.

The soil capillary hydraulic conductivity, $k_c$, for the stratum located between the nodes $z_{j+1}$ and $z_j$, was defined as the hydraulic conductivities' mean value of nodes $z_{j+1}$ and $z_j$. The use of the arithmetic mean is justified by the finding of Kirkland *et al.* (1992), where the solution of the closely related Richards' equation is relatively insensitive to the interblock-averaging scheme used for hydraulic conductivity (Clement *et al.* 1994). Furthermore, hydraulic conductivity is a non-linear function of the volumetric soil water content, $\theta$, which is linearized by using Picard iteration scheme. On the other hand, discretization of the left side of Eq. (2) is the following:

$$\frac{\partial\theta}{\partial t}\approx\left[\frac{\theta_j^{n+1,\,m}-\theta_j^{n}}{\Delta t}\right] \quad (4)$$

Celia *et al.* (1990) expanded $\theta_j^{n+1,\,m}$ through a first-order truncated Taylor series, in terms of the potential-head perturbation arising from Picard iteration, about the expansion point, as:

$$\theta_j^{n+1,m+1}\approx\theta_j^{n+1,m}+\left.\frac{d\theta}{d\psi}\right|_j^{n+1,\,m}\left[\psi_j^{n+1,m+1}-\psi_j^{n+1,m}\right] \quad (5)$$

where $d\theta/d\psi$ represents the specific water retention capacity of the soil, $C(\psi)$. Considering that:

$$C(\psi) = \frac{d\theta}{d\psi} \tag{6}$$

by replacing Eq. (6) and Eq. (5) in Eq. (4) we have:

$$\frac{\partial\theta}{\partial t} \approx \left[\frac{\theta_j^{n+1,m} - \theta_j^n}{\Delta t}\right] + C_j^{n+1,m}\left[\frac{\psi_j^{n+1,m+1} - \psi_j^{n+1,m}}{\Delta t}\right] \tag{7}$$

The first term on the right side of Eq. (7) is an explicit estimate for the time derivative of soil water content, based on the *m*th Picard level estimates of soil water potential. In the second term on the right side Eq. (7), the numerator of the bracketed fraction is an estimate of the error in the soil water potential at node *j* between two successive Picard iterations (Clement *et al.* 1994). By rearranging the terms of equation Eq. (7) and Eq. (3) we obtain:

$$\frac{\theta_j^{n+1,m} - C_j^{n+1,m}\psi_j^{n+1,m} - \theta_j^n}{\Delta t} - \left(\frac{kc_{j+1}^{n+1,m} - kc_j^{n+1,m}}{2\Delta z}\right) = \left(\frac{kc_{j+1}^{n+1,m} + kc_j^{n+1,m}}{2\Delta z^2}\right)\psi_{j+1}^{n+1,m+1} - \left(\frac{kc_{j+1}^{n+1,m} + 2kc_j^{n+1,m} + kc_{j-1}^{n+1,m}}{2\Delta z^2} + \frac{C_j^{n+1,m}}{\Delta t}\right)\psi_j^{n+1,m+1} + \left(\frac{kc_j^{n+1,m} + kc_{j-1}^{n+1,m}}{2\Delta z^2}\right)\psi_{j-1}^{n+1,m+1} \tag{8}$$

Eq. (8) will generate the system equations of inner nodes of domain, when the subscript *j* varies from 2 to *l*-1. The cases where *j* equals 1 and *l*, the boundary conditions will be considered. For finite difference, Kirkland *et al.* (1992) found that using Crank-Nicholson scheme on the closely related mixed form of Richards' equation fails to reduce truncation error, and is, of course, subject to potential instabilities; consequently, the fully implicit formulation is used. Therefore, in this study, the one-dimensional Richards' equation is solved using finite-difference methods, employing implicit scheme and the modified Picard iteration presented by Celia *et al.* (1990).

IV.2.2.1.1. Initial condition

The use of Richards' equation implies that the soil water content on the surface at initial time ($t$ = 0 s) is associated to field capacity. Then, the initial condition of soil wetness profile was determined with the equation presented by the paper's authors:

$$\theta_{(z,0)} = \theta_{fc} + A\ \exp\left(-\frac{B}{z}\right) \tag{9}$$

where $\theta_{(z,0)}$ is the soil water content at depth $z$ in the initial time ($t$ = 0 s), that occurs six hours after the last rain or irrigation event; $\theta_{fc}$ is the field capacity soil water content at depth $z$ = 0 m; $A$ and $B$ are constants obtained by curve fitting ($\theta_{z,0} - \theta_{fc}$ v/s depth $z$), using the information recorded by the sensors of soil wetness at the initial time.

IV.2.2.1.2. Upper boundary conditions

The upper boundary condition of Richards' equation (Neumann's boundary condition) is related to the evaporative rate of bare soil. The evaporation of a bare soil can be calculated as a residual of the surface energy equation (Allen *et al.* 2007):

$$\lambda E = Rn - G_0 - H \tag{10}$$

where $\lambda E$ is the latent energy consumed by evaporation (W $m^{-2}$); $Rn$ is net radiation (W $m^{-2}$); $G_0$ is the heat flux density at the soil surface (W $m^{-2}$); and $H$ is sensible heat flux density (W $m^{-2}$).

To determine the evaporation rate (m $s^{-1}$), Eq. (10) is divided by the latent heat of vaporization of water ($\lambda$ = 2,450 J $g^{-1}$) and multiplied by a conversion factor of units:

$$E_{(0,t)} = \frac{Rn_t - G_{(0,t)} - H_{(0,t)}}{F\,\rho_w\,\lambda} \tag{11}$$

where $E_{(0,t)}$ corresponds to the evaporative rate ($m^3$ $m^{-2}$ $s^{-1}$), measured at soil surface in time *t*; $Rn_t$ is the net radiation (J $s^{-1}$ $m^{-2}$) measured directly with a net radiometer in time *t*; $G_{(0,t)}$ is the heat flow density at the soil surface in time *t*; $H_{(0,t)}$ is sensible heat flow density, measured at time *t*; $\rho_w$ is the water density (1,000 kg $m^{-3}$); and *F* corresponds to a conversion factor (1,000 g $kg^{-1}$). $H_{(0,t)}$ is determined with the following equation:

$$H_{(0,t)} = \frac{\rho_a c_a \left(\Delta T_t\right)}{rh_t} \tag{12}$$

where $\rho_a c_a$, $\Delta T_t$, and $rh_t$ are the volumetric heat capacity of air (1,200 J $m^{-3}$ $K^{-1}$), the temperature difference between the evaporative surface and the air (K), and the resistance to heat transfer (s $m^{-1}$) at time *t*, respectively. The methodology to determine the sensible heat flux density is described in Annex I.

After determining $H_{(0,t)}$, $G_{(0,t)}$, and the measured values of net radiation (*Rn*), the evaporative rate of soil may be determined according to Eq. (11).

At the upper boundary a Neumannn type condition is established for each time *t*:

$$kc\left(\frac{\partial \psi}{\partial z} + 1\right)\Bigg|_{z=0} = E_0 \tag{13}$$

Fictitious nodes to implement the boundary conditions in $z = 0$ are used. Then, the discretization of Eq. (13) and boundary considerations for capillary hydraulic conductivity, permits to define the term $\psi_{j-1}^{n+1,m+1}$ (indicated in Eq. (8)), which is expressed as:

$$\psi_{j-1}^{n+1,m+1} = \psi_{j+1}^{n+1,m+1} - \frac{4\,\Delta z\,E_0}{\left(kc_j^{n+1,m} + kc_{j+1}^{n+1,m}\right)} + 2\,\Delta z \tag{14}$$

Therefore, after introducing the Eq. (14) in Eq. (8), the first equation of the system is expressed as follows (for the first node $z_1$):

$$\frac{\theta_1^{n+1,m} - C_1^{n+1,m}\psi_1^{n+1,m} - \theta_1^n}{\Delta t} - \left(\frac{kc_2^{n+1,m} + kc_1^{n+1,m}}{\Delta z}\right) + \frac{E_0}{\Delta z} = \left(\frac{kc_2^{n+1,m} + kc_1^{n+1,m}}{\Delta z^2}\right)\psi_2^{n+1,m+1} - \left(\frac{kc_2^{n+1,m} + kc_1^{n+1,m}}{\Delta z^2} + \frac{C_1^{n+1,m}}{\Delta t}\right)\psi_1^{n+1,m+1} \tag{15}$$

IV.2.2.1.3. Lower boundary conditions (Dirichlet boundary condition)

The lower boundary condition corresponds to the soil water content ($\theta$) measured or estimated (*me*) at depth $Z = 0.025$ m, in time $t$ during the analysis period $[0, T]$, beginning six hours after the last rain or irrigation event, until the sunset previous to radiative frost event. Depth Z corresponds to the humidity sensor closest to the soil surface. Then:

$$\theta_{(0.025,\ t)} = \theta_t^{me} \tag{16}$$

It is derived from the above mentioned information, that the soil hydraulic conductivity and matric potential of the nodes, placed at 0.025 m of depth (node $z_{l+1}$), are known and, therefore, remain out of Picard iteration. Once the boundary condition is introduced, the last equation of the system is expressed in the following way:

$$\frac{\theta_l^{n+1,m} - C_l^{n+1,m}\psi_l^{n+1,m} - \theta_l^n}{\Delta t} - \left(\frac{kc_{l+1}^{n+1} - kc_l^{n+1,m}}{2\,\Delta z}\right) - \left(\frac{kc_{l+1}^{n+1} + K_l^{n+1,m}}{2\,\Delta z^2}\right)\psi_{l+1}^{n+1} = -\left(\frac{kc_{l+1}^{n+1} + 2\,kc_l^{n+1,m} + kc_{l-1}^{n+1,m}}{2\,\Delta z^2} + \frac{C_l^{n+1,m}}{\Delta t}\right)\psi_l^{n+1,m+1} + \left(\frac{kc_l^{n+1,m} + kc_{l-1}^{n+1,m}}{2\,\Delta z^2}\right)\psi_{l-1}^{n+1,m+1} \tag{17}$$

The variables which are included in the previous expressions can be determined through the following relations (Campbell, 1985):

$$b = \frac{\ln 1500 - \ln 30}{\ln \theta_{fc} - \ln \theta_{wp}} \tag{18}$$

$$a = \exp\left(\ln 30 + b \ln \theta_{fc}\right) \tag{19}$$

$$\theta_s = 1 - \frac{\rho_s}{2.65} \tag{20}$$

$$\psi = \frac{-a\,\theta^{-b}}{10} \tag{21}$$

$$kc = k_{hs}\left(\frac{\theta^n}{\theta_s}\right)^{2b+3} \tag{22}$$

$$C = -\frac{1}{10b}\psi^{\left(-1-\frac{1}{b}\right)} \tag{23}$$

Where $k_{hs}$, $\theta_s$, $\theta_{fc}$, $\theta_{wp}$, $\rho_s$, and $C$ correspond to hydraulic conductivity at saturated soil ($m^3\ m^{-2}\ s^{-1}$), volumetric soil water content at saturation ($m^3\ m^{-3}$), volumetric soil water content at field capacity ($m^3\ m^{-3}$), volumetric soil water content at permanent wilting point ($m^3\ m^{-3}$), soil bulk density ($Mg\ m^{-3}$), and specific water retention capacity of the soil $\left(m^{-1}\right)$, respectively. On the other hand, $\theta^n$ corresponds to the known soil wetness used in Eq. 4, 7, 8, 15, and 17. The system of algebraic equations is expressed as follows:

$$\begin{vmatrix} -F_1 & D_2 & 0 & 0 & 0 & 0 & 0 & 0 \\ D_1 & -FF_2 & D_3 & 0 & 0 & 0 & 0 & 0 \\ 0 & D_2 & -FF_3 & D_4 & 0 & 0 & 0 & 0 \\ 0 & 0 & \ddots & \ddots & \ddots & 0 & 0 & 0 \\ 0 & 0 & 0 & \ddots & \ddots & \ddots & 0 & 0 \\ 0 & 0 & 0 & 0 & \ddots & \ddots & \ddots & 0 \\ 0 & 0 & 0 & 0 & 0 & D_{l-2} & -FF_{l-1} & D_l \\ 0 & 0 & 0 & 0 & 0 & 0 & D_{l-1} & -FF_l \end{vmatrix} \times \begin{vmatrix} \psi_1 \\ \psi_2 \\ \psi_3 \\ \vdots \\ \vdots \\ \vdots \\ \psi_{l-1} \\ \psi_l \end{vmatrix} = \begin{vmatrix} \alpha_1 - \beta_1 + E_0/\Delta z \\ \alpha_2 - \beta_2 \\ \alpha_3 - \beta_3 \\ \vdots \\ \vdots \\ \vdots \\ \alpha_{l-1} - \beta_{l-1} \\ \alpha_l - \beta_l - G_l \end{vmatrix} \tag{24}$$

where:

$$\frac{\theta_j^{n+1,m} - C_j^{n+1,m}\psi_j^{n+1,m} - \theta_j^n}{\Delta t} = \alpha_j \tag{25}$$

$$\frac{kc_{j+1}^{n+1,m} - kc_j^{n+1,m}}{2\Delta z} = \beta_j \tag{26}$$

$$-\left(\frac{kc_j^{n+1,m} + kc_{j+1}^{n+1,m}}{2\Delta z^2}\right) = D_{j+1} \tag{27}$$

$$-\left(\frac{kc_j^{n+1,m} + kc_{j-1}^{n+1,m}}{2\Delta z^2}\right) = D_{j-1} \tag{28}$$

$$-\left(\frac{kc_2^{n+1,m} + kc_1^{n+1,m}}{\Delta z^2} + \frac{C_1^{n+1,m}}{\Delta t}\right) = F_1 \tag{29}$$

$$-\left(\frac{kc_{j+1}^{n+1,m} + 2kc_j^{n+1,m} + kc_{j-1}^{n+1,m}}{2\Delta z^2} + \frac{C_j^{n+1,m}}{\Delta t}\right) = FF_j \tag{30}$$

$$-\left(\frac{kc_{l+1}^{n+1,m} + kc_l^{n+1,m}}{2\Delta z^2}\right)\psi_{l+1}^{n+1} = G_l \tag{31}$$

and $E_0$ (Eq. (13) corresponds to the evaporative rate ($m^3\ m^{-2}\ s^{-1}$), measured at soil surface.

IV.2.2.1.4. Picard iteration:

To solve the system of algebraic equations (Eq. (24)) it is necessary to use an iterative method to linearize the equation system, since the capillary hydraulic conductivity and the specific water retention capacity are defined as non-linear functions and are dependent on the soil water content. Therefore, the iterative process begins with a known profile of soil wetness content at the $n$th time level; thus, the hydraulic

conductivity (Eq. (22)) and specific water retention capacity (Eq. (23)) profiles in the soil are known a priori, and the equation system can be solved (Eq. (24)) to determine the matric potential profile. Once these have been determined, the new wetness volumetric content profile in the soil can be obtained, clearing wetness from Eq. (21). With this profile the hydraulic conductivity and water retention capacity profiles are determined, and once again the equation system is solved and the matric potential profile in the soil is obtained. This process continues until the maximum difference in the matric potential profile, between the iterative level *m* and *m*+1, is inferior to a value given in the stopping criterion. When the iterative process is stopped, it implies the soil wetness profile at the time level $n+1$has been obtained. For the following iterative process, the wetness content profile of $n+1$ will be used as a base to attain the volumetric wetness content profile at the time level $n+2$. This process continues until the wetness content profile in soil of all time levels involved in the time period $[0, \mathrm{T}]$ are obtained.

IV.2.2.2. The use of the one-dimensional heat diffusion equation

In order to obtain a numerical solution to the one-dimensional heat diffusion equation (Eq. (1)), the finite-difference method was applied, through a Crank-Nicholson scheme:

$$\frac{Ts_k^{j+1}-Ts_k^j}{\Delta t}=\frac{1}{2}\left[\frac{Ks_{i+1}\left(Ts_{k+1}^{j+1}-Ts_k^{j+1}\right)-Ks_i\left(Ts_k^{j+1}-Ts_{k-1}^{j+1}\right)}{(\Delta z)^2}+\frac{Ks_{i+1}\left(Ts_{k+1}^{j}-Ts_k^{j}\right)-Ks_i\left(Ts_k^{j}-Ts_{k-1}^{J}\right)}{(\Delta z)^2}\right] \quad (32)$$

where $Ts_k^{j+1}$ denotes soil temperature estimated in time $t_{j+1}$(s), in node $z_k$. Therefore, $\Delta t$(s) corresponds to the difference between $t_{j+1}$ and $t_j$; $\Delta z$(m) corresponds to the difference between node $z_{k+1}$ and $z_k$. Then, the discretization of depth can be expressed as $z_k=(k-1)\,\Delta z$. On the other hand, $Ks_{i+1}$ indicates the estimated thermal diffusivity $\left(\mathrm{m}^2\,\mathrm{s}^{-1}\right)$ in the soil stratum $i+1$, which is found between the nodes $z_{k+1}$ and $z_k$. In turn, $Ks_i$ indicates the estimated thermal diffusivity in the soil stratum $i$, found between the nodes $z_k$ and $z_{k-1}$. By re-arranging and simplifying, the difference equation associated with the *kth* node is obtained, which later allows to formulate the system of linear equations associated to the inner nodes of domain, when the subscript *k* varies from *2* to *m*-1.

$$-\alpha\,Ks_{i+1}\,Ts_{k+1}^{j+1}+Ts_k^{j+1}\left[1+\alpha\left(Ks_{i+1}+Ks_i\right)\right]-\alpha\,Ks_i\,Ts_{k-1}^{j+1}=\alpha\,Ks_{i+1}\,Ts_{k+1}^{j}+Ts_k^{j}\left[1-\alpha\left(Ks_{i+1}+Ks_i\right)\right]+\alpha\,Ks_i\,Ts_{k-1}^{j} \quad (33)$$

where coefficient α corresponds to the expression:

$$\alpha=\frac{\Delta t}{2\,(\Delta z)^2} \quad (34)$$

where $Ts_{k+1}^{j+1}$ is the estimated temperature in time $t_{j+1}$(s) and node $z_{k+1}$, $\Delta t$ is the time step between $t_{j+1}$ and $t_j$. Meanwhile, $\Delta z$ is the spatial interval between the nodes $z_{k+1}$ and $z_k$. Thus, depth is expressed as: $z_k=(k-1)\,\Delta z$, for *k* = 1,...,*m*. The cases where *k* equals 1 or *m* will be discussed later considering the upper boundary conditions to obtain Eq. (37) and the lower boundary condition to obtain Eq. (39).

IV.2.2.2.1. Upper boundary conditions

At the upper boundary, a Neumann- type condition (flux condition) is implemented with fictitious nodes in z = 0:

$$\left.\frac{\partial Ts_{(z,t)}}{\partial z}\right|_{z=0} = \frac{Rn}{Cv_{i=1}\,Ks_{i=1}} \Rightarrow \frac{Ts_{k+1}^{j+1} - Ts_{k-1}^{j+1}}{2\Delta z} = \frac{Rn}{Cv_{i=1}\,Ks_{i=1}} \tag{35}$$

where $Ts_{(z,t)}$ is the soil temperature at depth $z$ in time $t$; $Rn$ is in fact the nocturnal net outgoing long-wave radiation (J $s^{-1}$ $m^{-2}$); $Cv_{i=1}$ and $Ks_{i=1}$ are the volumetric heat capacity of the soil (J $m^{-3}$ $^{o}C^{-1}$) and the soil thermal diffusivity ($m^2$ $s^{-1}$) of the first soil layer $(i=1)$, respectively. On the other hand, $Ts_{k+1}^{j+1}$ is the estimated temperature in time $t_{j+1}$(s) and node $z_{k+1}$, meanwhile $\Delta z$ is the spatial interval between the nodes $z_{k+1}$ and $z_k$. Thus, depth is expressed as: $z_k = (k-1)\,\Delta z$, for $k$=1,...,$m$. Solving for $Ts_{k-1}^{j}$ from Eq. (35):

$$Ts_{k-1}^{j} = Ts_{k+1}^{j} - \frac{2\Delta z\, Rn}{Cv_{i=1}\,Ks_{i=1}} \tag{36}$$

Therefore, after introducing the upper boundary condition (Eq. (36) in Eq. (33)), the first equation of the linear equation system (Eq. (42)) is expressed as follows:

$$-2\alpha\, Ks_1 Ts_2^{j+1} + [1+2\alpha\, Ks_1]\,Ts_1^{j+1} = 2\alpha\, Ks_1\, Ts_2^{j} + [1-2\alpha\, Ks_1]\,Ts_1^{j} - \frac{4\alpha\,\Delta z\, Rn}{Cv_{i=1}} \tag{37}$$

IV.2.2.2.2. Lower boundary conditions

At the lower boundary condition, a Dirichlet-type condition is implemented, where the soil temperature at $z = 0.20$ m is constant throughout the night, i.e.:

$$Ts_{0.2,\,t}^{j+1} = Ts_{0.2,\,t}^{j} = cte = Ts^{*} \tag{38}$$

Where $Ts^{*}$ is the soil temperature (°C) at depth $z = 0.20\,\mathrm{m}$ in time $t_j$, which it is constant during the night. Once this condition is introduced in Eq. (33), the last equation of the linear equation system (Eq. (42)) is expressed in the following manner:

$$Ts_m^{j+1}\left[1+\alpha\left(Ks_n + Ks_{n-1}\right)\right] - \alpha\, Ks_{n-1}\, Ts_{m-1}^{j+1} = Ts_m^{j}\left[1-\alpha\left(Ks_n + Ks_{n-1}\right)\right] + \alpha\, Ks_{n-1}\, Ts_{m-1}^{j} + 2\alpha\, Ks_n\, Ts^{*} \tag{39}$$

where $m$ represents the last node of the domain, and $n$ represents the deepest stratum within it.

IV.2.2.2.3. System of linear equations

After the boundary conditions are established, it is possible to formulate a system of linear equations to solve the soil temperature at each time step. Then, Eq. (37) together with the $m$-2 equations generated from Eq. (33) - making $k$ to vary from 2 to $m$-1 - and Eq. (39) conform a system of $m$ linear equations in the unknown $Ts_1, Ts_2, \cdots, Ts_m$. Considering the notations:

$$\beta = \frac{\alpha\ \Delta z\ Rn}{Cv_{i=1}} \tag{40}$$

$$\gamma_{i+1} = \left(Ks_i + Ks_{i+1}\right) \tag{41}$$

where $C_{v_{i=1}}$, $K_{s_i}$ and $K_{s_{i+1}}$ are the volumetric heat capacity of the soil (J $m^{-3}$ $K^{-1}$) and the soil thermal diffusivity ($m^2$ $s^{-1}$) of the first soil layer $(i=1)$ or the layer $i+1$, respectively. $\Delta z$ is the spatial interval between the nodes and *Rn* is, in fact, the nocturnal net outgoing long-wave radiation (J $s^{-1}$ $m^{-2}$). The system can be written in a matrix form as:

$$\begin{vmatrix} 1+2\alpha Ks_1 & -2\alpha Ks_1 & 0 & 0 & 0 & 0 & 0 & 0 \\ -\alpha Ks_1 & 1+\alpha\gamma_2 & -\alpha Ks_2 & 0 & 0 & 0 & 0 & 0 \\ 0 & -\alpha Ks_2 & 1+\alpha\gamma_3 & -\alpha Ks_3 & 0 & 0 & 0 & 0 \\ 0 & 0 & \ddots & \ddots & \ddots & 0 & 0 & 0 \\ 0 & 0 & 0 & \ddots & \ddots & \ddots & 0 & 0 \\ 0 & 0 & 0 & 0 & \ddots & \ddots & \ddots & 0 \\ 0 & 0 & 0 & 0 & 0 & -\alpha Ks_{n-2} & 1+\alpha\gamma_{n-1} & -\alpha Ks_{n-1} \\ 0 & 0 & 0 & 0 & 0 & 0 & -\alpha Ks_{n-1} & 1+\alpha\gamma_n \end{vmatrix} \begin{vmatrix} Ts_1^{j+1} \\ Ts_2^{j+1} \\ Ts_3^{j+1} \\ \vdots \\ \vdots \\ \vdots \\ Ts_{m-1}^{j+1} \\ Ts_m^{j+1} \end{vmatrix} = \begin{vmatrix} \left(1-2\alpha Ks_1\right) Ts_1^{j} + 2\,\alpha\, Ks_1\, Ts_2^{j} - 4\beta \\ \alpha\, Ks_1\, Ts_1^{j} + \left(1-\alpha\gamma_2\right) Ts_2^{j} + \alpha\, Ks_2\, Ts_3^{j} \\ \alpha\, Ks_2 Ts_2^{j} + \left(1-\alpha\gamma_3\right) Ts_3^{j} + \alpha\, Ks_3\, Ts_4^{j} \\ \vdots \\ \vdots \\ \vdots \\ \alpha\, Ks_{n-2}\, Ts_{m-2}^{j} + \left(1-\alpha\gamma_{n-1}\right) Ts_{m-1}^{j} + \alpha\, Ks_{n-1}\, Ts_m^{j} \\ \alpha\, Ks_{n-1}\, Ts_{m-1}^{j} + \left(1-\alpha\gamma_n\right) Ts_m^{j} + 2\,\alpha Ks_n\, Ts^{*} \end{vmatrix} \quad (42)$$

To clarify the calculation process, Figure 1 shows the relationship between Richards' equation and one-dimensional heat diffusion equation to obtain bare soil surface temperature.

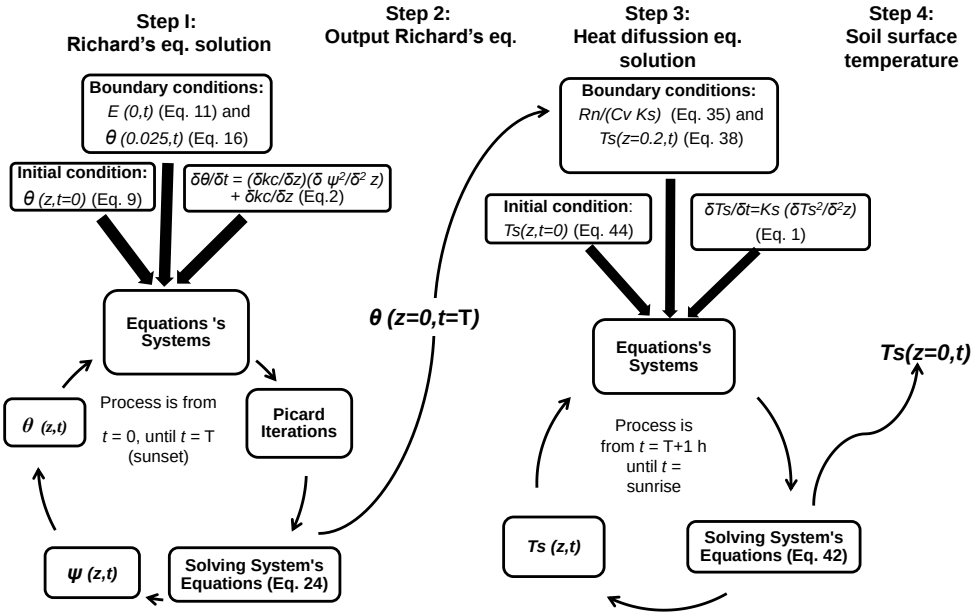


**Fig. 1** Calculation process relationship between Richards' equation - to obtain soil water content on the surface, $\theta_{(z=0,\,t=\mathrm{T})}$ - required by the one-dimensional heat diffusion equation to obtain bare soil surface temperature, $Ts_{(z=0,t)}$. $E_{(0,t)}$ is soil surface evaporation rate; $k_c$ is soil capillary hydraulic conductivity; $\psi_{(z,t)}$ is matrix potential of water in the soil; *Rn* is net outgoing long-wave radiation; *Cv* is volumetric heat capacity of the soil; and *Ks* is the soil thermal diffusivity.

## IV.2.3. Methodology

### IV.2.3.1. Experimental site

This experiment was carried out at the Agrometeorological Station of the Faculty of Agricultural Engineering, University of Concepción in Chillán-Chile (36°35′43.4″ S,

72°4′47.3″W), located at an altitude of 130 m above sea level. The soil is clay loamy, with a soil bulk density of 1.45 Mg $m^{-3}$ at a depth between 0 and 0.1 m and of 1.60 Mg $m^{-3}$ at a depth between 0.1 and 0.2 m; the soil water content at field capacity and permanent wilting point is 0.29 and 0.21 $m^3$ $m^{-3}$, respectively; the saturated hydraulic conductivity of de soil is 1.1 m $day^{-1}$; and a fraction of clay of 33 % in the first layer. It belongs to the Tres Esquinas series (member of the fine, mixed, thermic Ultic Haploxeralfs soil family), has a slightly inclined slope, and rests upon a substrate of weathering solid rock, mixed, dark brown, and reddish material with 5 YR shades under humidity. The measurement period went from September 3 of 2010 to December 31 of 2011. In this period of time only nine radiative frost events occurred at ground level. Details of these events are given in Table 1:

**Table 1** Date of radiative frost event, sunset and sunrise time, length of the night, sunset bare soil surface temperature ($Ts_{(0,\,ss)}$), and minimum bare soil surface ($Ts_{z=0}^{\min}$).

| Year | Radiative frost (DOY) | Time sunset* | Time sunrise* | Night length (hours) | $Ts_{(0,\,ss)}$ (ºC) | $Ts_{z=0}^{\min}$ (ºC) |
|---|---|---|---|---|---|---|
| 2010 | 273/274 | 20:00 | 07:15 | 11.25 | 9.5 | -2.0 |
| | 297/298 | 20:30 | 06:45 | 10.25 | 16.3 | -0.1 |
| 2011 | 105/106 | 19:30 | 08:15 | 12.75 | 13.0 | -1.1 |
| | 106/107 | 19:30 | 08:15 | 12.75 | 13.4 | -0.9 |
| | 241/242 | 19:45 | 08:00 | 12.25 | 7.4 | -1.9 |
| | 242/243 | 19:45 | 08:00 | 12.25 | 9.3 | -2.9 |
| | 243/244 | 19:45 | 08:00 | 12.25 | 9.8 | -3.0 |
| | 247/248 | 19:45 | 07:45 | 12.00 | 7.5 | -3.0 |
| | 260/261 | 20:00 | 07:30 | 11.50 | 11.9 | -1.9 |

* Local time

IV.2.3.2. Soil temperature

In order to measure the soil temperature, seven nickel/chrome nickel-type K thermocouples, of 1 mm diameter were used. These thermocouples were made at the Water Resources Department of the Faculty of Agricultural Engineering. They were buried at depths of 0.01, 0.03, 0.05, 0.09, 0.13, 0.17, and 0.22 m for the year 2010, and 0.02, 0.04, 0.07, 0.10, 0.15, and 0.25 for the year 2011. Measurements of bare soil surface temperature were made with Wahl's DHS24L heat spy infrared thermometers (Palmer Wahl Instrumentation Group, Ashville, North Caroline, USA), with an operating temperature range going from -20 ºC to 550 ºC, and a conversion factor of 1.0 ºC $mV^{-1}$, located 1.70 m above ground level. Monitoring readings were recorded every 1 second and averaged every 15 min. during the 2010-2011 period.

IV.2.3.3. Soil water content

In order to measure soil wetness, ECHO-5 capacitive sensors (Decagon Devices) were used, placed horizontally at depths of 0.05 and 0.10 m for the year 2010, and 0.025, 0.05, and 0.10 m for the year 2011. In order to estimate soil water content at 0.025 m of depth in the year 2010, the methodology used was applied as described by Venegas *et al.* (2013). The sensors were calibrated with gravimetric measurements of soil wetness *in situ*, at depths ranging from 0.0 to 0.05 m and 0.1 m. Seven repetitions at every depth were made for every measurement. Monitoring readings were recorded every 1 second and averaged every 1 hour.

IV.2.3.4. Soil heat flux density (heat flux plates)

In order to measure the soil heat flux density, two circular heat flux plates, model HFT-3 (Campbell Scientific, Inc., Logan, Utah, USA), with a diameter of 38 mm, width of 3.9 mm, and thermal conductivity of 1.22 W $m^{-1}$ $K^{-1}$ were placed at a depth of 0.05 m. The constants to transform voltage to flux density were 47.1 and 42.4 W $m^{-2}$ $mV^{-1}$, respectively. To prevent air gap formation in the soil–plate inter-phase, the soil surface under which the flux plates had been placed was moistened and compacted. Readings were recorded every 1 second and averaged every 15 min.

IV.2.3.5. Net radiation

The net radiation was measured with a net radiometer, model Q-7.1 (Campbell Scientific, Inc., Logan, Utah, USA), placed at a height of 1.55 m above bare soil. The constant to transform voltage to flux density was 9.1 W $m^{-2}$ $mV^{-1}$ for millivolts greater than zero, and 11.4 W $m^{-2}$ $mV^{-1}$ for millivolts smaller than zero. Readings were recorded every 1 second and averaged every 15 min.

IV.2.3.6. Storage of records

The net radiation and flux plate records were stored in a 21X micrologger (Campbell Scientific Inc., Logan, Utah, USA.), and thermocouple records were stored in a HL20 micrologger (Rotronic A G, Bassersdorf, Switzerland). Soil wetness records were stored in an ECHO-5 micrologger (Decagon Device, Washington, USA). Fig. 2 shows how the sensors were placed.

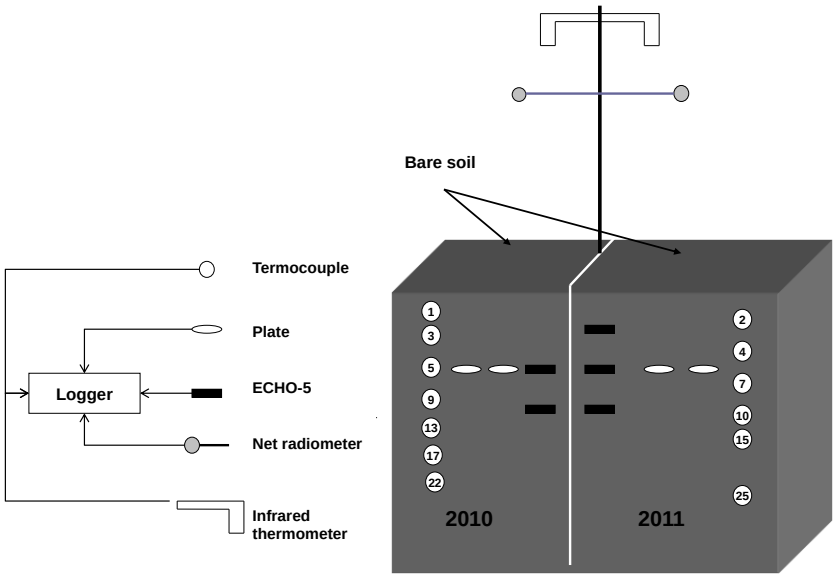


**Fig. 2** Arrangement of the sensors used in the soil profile and at the soil surface during the research period (years 2010 and 2011). The numbers inside the thermocouples show the depth (in centimeters) at which the sensors were buried.

IV.2.3.7. Richards' equation additional information

In previous behavior analysis of the proposed numerical model for prediction of frost, it was determined by the authors that the upper boundary condition of Eq. (35) is sensitive to the wetness of the soil surface (see Eq. (9)), which affects an appropriate estimation of thermal behavior on the surface and into the soil.

The soil wetness content at depth $z \approx 0$ had to be indirectly determined, through Richards' equation, because the soil wetness sensor closest to the surface remained at a depth of 0.05 m (year 2010), and at a depth of 0.025 m (year 2011).
The Eq. (9) presented by the paper's authors to determine soil moisture profile requires to obtain the constants $A$ and $B$ by curve fitting ($\theta_{z,0} - \theta_{fc}$ v/s depth z), using the information recorded by the sensors of soil wetness at depth $z$ = 0.025, 0.050, and 0.100 m, at the initial time ($t$ = 0).

In order to estimate the temporal and spatial evolution of the soil wetness, especially at the beginning of the radiative frost event, Richards' equation was applied to the evaporation process of water in bare soil for a period of time $[0, T]$, beginning six hours after the last rain ($t$ = 0) – and previous to a frost event - until the sunset that precedes this event ($t = T$).

Richards' equation was not applied to all nine frost events since in some cases, between rain and preceding sunset, there was an elapsed period of one day or less (DOY 241/242, 242/243, and 247/248). In these cases, soil surface wetness was assumed to be equivalent to field capacity. In other three cases, soil water content at 0.025 m, as measured one or more days before the sunset that precedes the radiative frost, was found to be 0.12 $m^3$ $m^{-3}$ or more below permanent wilting point (0.21 $m^3$ $m^{-3}$) (DOY 105/106, 106/107, and 297/298). Under these conditions, soil water evaporation and soil capillary hydraulic conductivity are too low for water incoming or outgoing to occur inside the soil surface stratum (0.001 m), what made the application of Richards' equation unnecessary. Then, surface wetness was assumed to be equivalent to that recorded by the ECHO-5 capacitive sensors buried at a depth of 0.025 m.

On the other hand, the time length of this period (from last rain to beginning of frost event), soil surface water content, and the days when Richards' model was applied or the surface soil water content was assumed instead, is particular to each case (Table 2).

**Table 2** Date of radiative frost occurrence (year and DOY), sunset time, date of last rain, estimated or assumed soil surface water content ($\theta_0$) at sunset that precedes the beginning of frost, and elapsed period between rain and beginning of frost event.

| Year | Radiative frost (DOY) | Time sunset* | Date last rain (DOY/time) | $\theta_0$ ($m^3$ $m^{-3}$) | Period between rain and frost (hour) |
|---|---|---|---|---|---|
| 2010 | 273/274 | 20:00 | 270/14:30 | 0.20 | $78^{R}$ |
| | 297/298 | 20:30 | 287/23:45 | 0.12 | $237^{SM}$ |
| 2011 | 105/106 | 19:30 | 103/10:45 | 0.17 | $57^{SM}$ |
| | 106/107 | 19:30 | 103/10:45 | 0.16 | $81^{SM}$ |
| | 241/242 | 19:45 | 241/14:00 | 0.29 | $6^{FC}$ |
| | 242/243 | 19:45 | 241/14:00 | 0.29 | $30^{FC}$ |
| | 243/244 | 19:45 | 241/14:00 | 0.22 | $54^{R}$ |
| | 247/248 | 19:45 | 247/17:45 | 0.29 | $2^{FC}$ |
| | 260/261 | 20:00 | 259/00:15 | 0.21 | $44^{R}$ |

* Local time. R: Richards' model was applied to obtain soil surface water content. FC: field capacity was assumed as soil surface water content. SM: soil surface water content assumed equal to ECHO-5 sensor measurement at depth z=0.025m.

After determining initial and boundary conditions, Richards' model was applied in order to estimate the evolution of soil wetness ($\theta$) during the three frost events, as

presented in Fig. 3. The final output of Richards' equation solution, obtained after 72 h (DOY 273), 48 h (DOY 243), and 38 h (DOY 260), corresponds to soil surface water content ($\theta_0$).

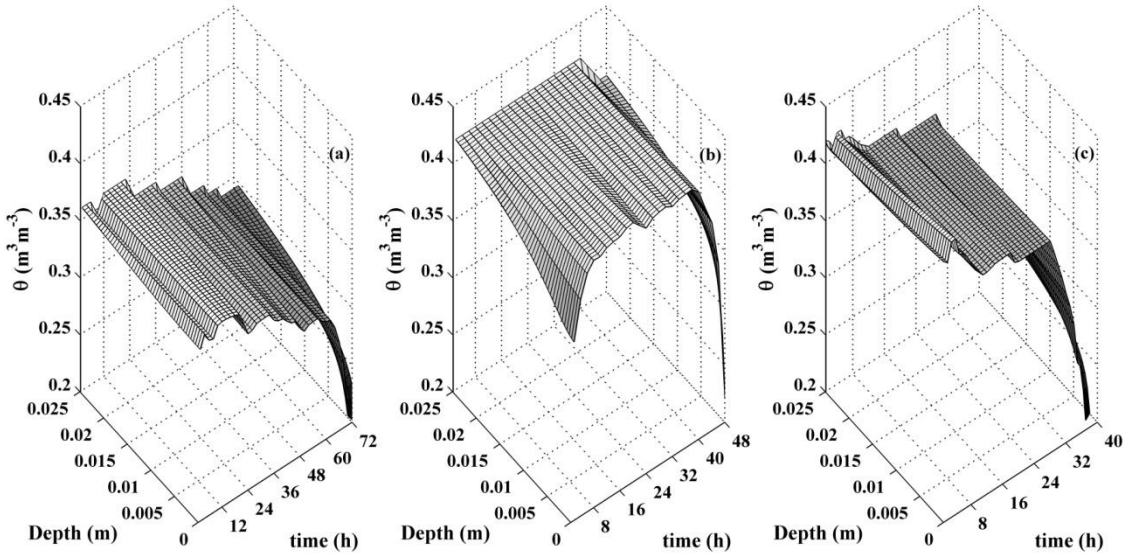


**Fig. 3** Estimation of temporal and spatial soil water content ($\theta$) behavior, after the application of Richards' model during the elapsed period of time between the rain previous to the frost and the beginning of the radiative frost event. DOY: 273/274 (a); 243/244 (b); and 260/261 (c).

IV.2.3.8. One-dimensional heat diffusion additional information

In this respect, the initial and boundary conditions are according to the temporal behavior of the net radiation and the response of the temperature and wetness content at different soil depths. During the time from one hour after sunset $(\mathrm{T}+3600\ s)$ until sunrise $(t \approx 36{,}000\ \mathrm{s})$, the temperature at depth $z = 0.2$ m is almost constant (Fig. 4), the soil thermal gradient changes (from positive to negative) at a depth of $z = 0.05$ m for $t = 0$, the net radiation remains constant, and the soil wetness profile does not change during this period. This last conclusion is necessary to determine the soil thermal conductivity profile, the volumetric heat capacity profile of the soil and, hence, the soil thermal diffusivity profile through Eq. (43):

$$Ks_z = \frac{ks_z}{Cv_z} \tag{43}$$

where $Ks_z$, $ks_z$, and $Cv_z$ are thermal diffusivity ($m^2\ s^{-1}$), thermal conductivity ($J\ m^{-1}\ s^{-1}\ K^{-1}$), and volumetric heat capacity ($J\ m^{-3}\ K^{-1}$) at depth *z*, respectively.

To illustrate these assumptions, in Fig. 4 the temporal behavior of net radiation, soil temperature, and soil moisture content is presented, for DOY 273:

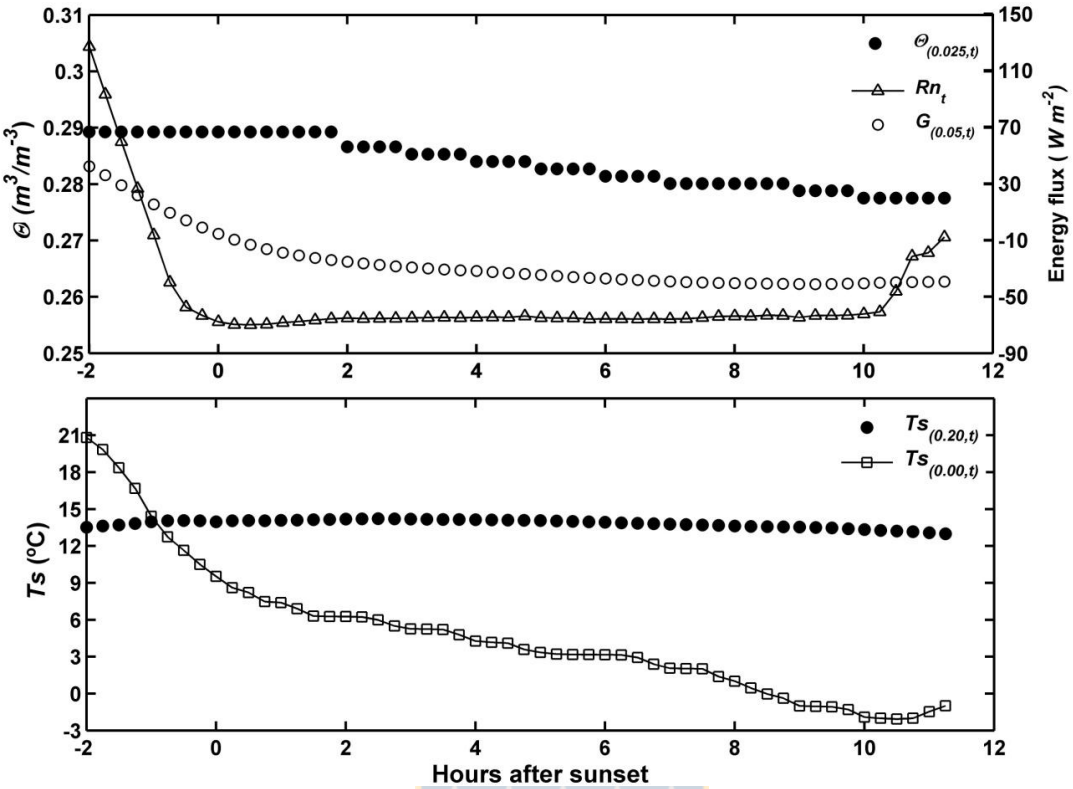


**Fig 4** Measured sunset and nocturnal hourly net radiation ($Rn_t$), soil heat flux density at depth z = 0.05 m ($G_{(0.05,\,t)}$), soil wetness content ($\theta$) at depth z = 0.025 m ($\theta_{(0.025,\,t)}$), and soil temperature ($Ts$) at depth z = 0 ($Ts_{(0,t)}$) and 0.2 m ($Ts_{(0.20,\,t)}$), for DOY 273

For the case of initial temperature distribution at one hour after sunset, soil temperature profile was determined with the records of the soil temperature measured with thermocouples (see section 3.2). The time where this condition occurs for each radiative frost event can be seen in Table 1.

The upper boundary condition was determined with the records of night time net outgoing long-wave radiation ($Rn$). The thermal diffusivity near soil surface was determined with Eq. (43). In turn, thermal conductivity was determined with the model developed by Campbell (1985), and the volumetric heat capacity of the soil was determined with De Vries (1963) model, both of them described by Venegas *et al.* (2013).

The thermal diffusivity depends on the soil water content, and the soil wetness profile was determined with Eq. (9). In this expression, the wetness of the soil surface was determined with Richards' equation in three out of nine cases; in the rest of the cases the criteria mentioned in section 3.7 was used.

The lower boundary condition was determined with the soil temperature records at depth $z = 0.20$ m, which remained almost constant during the night time (Fig. 4).
Temperature is initially assumed to present a piece-wise linear pattern, therefore, the initial condition is introduced through a piecewise linear function:

$$Ts_{(z,\,0)} \begin{cases} Ts_{(0,\,0)} + C\,z, & for \quad 0 \le z \le 0.05 \text{ m} \\ Ts_{(0.05,\,0)} - D\left(z - 0.05\right), & for \quad 0.05 < z \le 0.20 \text{ m} \end{cases} \tag{44}$$

where $Ts_{(0,\ 0)}$, $Ts_{(0.05,\ 0)}$, $Ts_{(0.20,\ 0)}$ are the soil temperature (° C) at depth $z$ equivalent to 0, 0.05 and 0.20 m, respectively, in time $t = 0$. $C$ and $D$ are the thermal gradient for the pieces presented in Eq. (44), which are determined through the following expressions:

$$C = \frac{Ts_{(0.05,\ 0)} - Ts_{(0,\ 0)}}{0.05} \tag{45}$$

$$D = \frac{Ts_{(0.05,\ 0)} - Ts_{(0.20,\ 0)}}{(0.20 - 0.05)} \tag{46}$$

In order to obtain a numerical solution for the one-dimensional heat diffusion equation (Eq. (1)) the finite-difference method was used, through a Crank-Nicholson's scheme. To achieve this, the temporal domain was discretized with time steps ($\Delta t$) of 900 seconds, while the spatial domain with intervals ($\Delta z$) of 0.001 m. Discretizaton of the problem, together with the initial and boundary conditions, make it possible to establish a system of linear equations (Eq. (42)) to be solved in every time step. The solution of this equation system allows for the determination of changes in spatial (from depth z = 0 until depth z = 0.20 m) and temporal (from 1 hour after sunset, $t$ = 0 s, until sunrise) soil temperature and, therefore, the evolution of temperature at the soil surface during the time period when the frost occurs.

IV.2.3.9. Validation of the models

The validation of the models was based on frost events selected in Table 1. Records of soil surface temperature $(Ts_{(0,t)})$ were used as reference. The validation was done through the interpretation of the following coefficients:

Graphic relation 1:1, where data of the observed bare soil surface temperatures ($Ts_{(0,t)}$) are contrasted with the temperatures estimated through the numerical model.

The mean absolute error (*MAE)* and the root mean square error (RMSE) were calculated from:

$$\mathrm{MAE} = \frac{1}{N}\sum_{i=1}^{N}|O_i - P_i| \tag{47}$$

$$\mathrm{RMSE} = \sqrt{\frac{1}{N}\sum_{i=1}^{N}(O_i - P_i)^2} \tag{48}$$

where $O_i$ is the observed temperature value and $P_i$ is the estimated temperature values, $N$ is the number of observations, and subscript $i$ denotes the ith observation.

**IV.2.4. Results and discussion**

IV.2.4.1. Hourly nocturnal estimation of soil surface temperature ($Ts_{(0,t)}$)

During all 9 radiative frost events, the numerical model developed by the authors tend to overestimate the behavior of the hourly soil surface temperature in radiative frost

events (Fig. 5), with a mean RMSE and MAE in all 9 radiative frost events of 1.6 and 1.3 ºC, respectively. What is more, the estimated bare soil surface temperature was expected to underestimate the observed temperature. As a matter of fact, the development of the numerical model implies that net radiation and soil heat flux density are the factors that explain the nocturnal temperature decrease. Then, no energy contribution coming from either convection from upper layers of the air or water vapor condensation is counted. However, in frost events where the surface moisture content in soil is significantly lower than the permanent wilting point (0.21 $m^3$ $m^{-3}$) (DOY 297, 106, and 105 – no data shown), the model's estimation errors are greater (mean RMSE and MAE of 1.9 and 1.7 ºC, respectively) than when the soil surface moisture content is between permanent wilting point and field capacity (RMSE and MAE: 1.16 and 0.98 ºC, respectively). In those events where the soil surface moisture content was estimated through Richards' equation (DOY 273, 243, 260), the error in the estimation of the surface temperature was smaller than the mean error of the 9 frost events , with a RMSE and MAE of 1.2 and 1.1 ºC, respectively.

From what was mentioned above, it can be said that the overestimation (Fig. 5 and Fig. 6) could be explained by errors in the determination of soil surface wetness (see section 5.2). As a matter of fact, during events where soil water content is equal or less to permanent wilting point (DOY 105, 106, 260, 273 and 297), variation in the estimation of soil surface temperature at sunrise is more sensitive due to possible error in the estimation of wetness content in the soil surface (variation of about 0.4 ºC per 0.01 $m^3$ $m^{-3}$ error), than when the wetness content is close to field capacity (variation of 0.2 ºC per 0.01 $m^3$ $m^{-3}$ error).

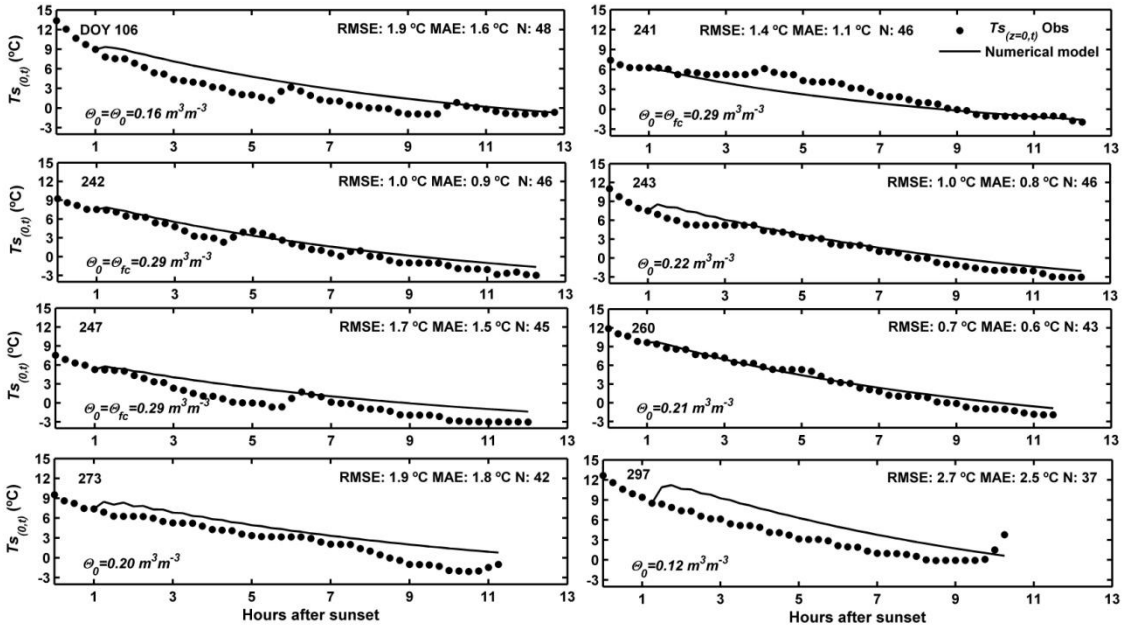


**Fig. 5** Decline of the nighttime hourly bare soil surface temperature ($Ts_{(0,\,t)}$) estimated by the numerical model, from sunset to sunrise, during 8 radiative frost events. $\theta_0$ is the estimated or assumed soil surface water content at the beginning of frost, $\theta_{fc}$ is field capacity water content, and N represents nocturnal temperature records every 15 minutes.

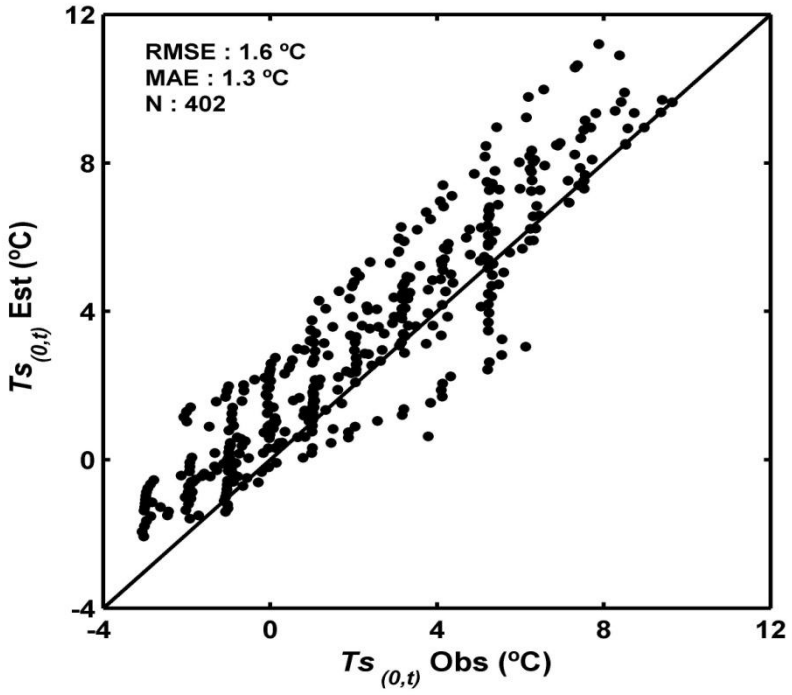


**Fig. 6** 1:1 ratio of night-time hourly bare soil surface temperature estimated ($Ts_{(0,t)}$Est) and observed ($Ts_{(0,t)}$Obs) through numerical model. N represents nocturnal temperature records every 15 minutes which were obtained during nine radiative frost events.

Although this numerical model showed a slight overestimation of bare superficial soil temperature, it is important to point out that the model does not require calibration with historical records. As a matter of fact, just a good estimation of the initial condition (soil profile temperature at sunset, from z = 0 to z = 0.20 m), upper boundary condition (net outgoing long-wave radiation one hour after sunset, and soil surface water content at the beginning of the frost event), and lower boundary condition (soil temperature at depth z=0.20 m) would be enough.

IV.2.4.2. Analysis of the numerical model's sensitivity

A sensitivity analysis was carried out for upper and lower boundary conditions and initial conditions, which have an impact on the simulation of bare soil surface temperature in a radiative frost event.

Regarding the upper boundary condition, it can be concluded that, considering the physical characteristics of the soil where this study was carried out, thermal diffusivity is sensitive to soil water content ranging from 0.10 to 0.22 $m^3$ $m^{-3}$ (Fig. 7a).Then, the upper boundary condition of this model (Eq. (35)) is more sensitive to error in the soil water estimation (Eq. (9)), within the wetness range previously mentioned. This can be observed in the variation of soil surface temperature estimation at sunrise, $Ts_{(0,sr)}$, caused by an estimation error in the soil surface wetness content at the beginning of frost event, $\theta_0$ . Fig. 7b shows the variation of bare soil surface temperature estimation at sunrise, caused by an error in the estimation of soil surface wetness, $\Delta Ts_{(0,sr)}/\Delta\theta_0$ , with respect to the wetness content in the soil surface . This variation in $Ts_{(0,sr)}$ is greater

when the error is caused within the wetness range mentioned (0.10 to 0.22 $m^3$ $m^{-3}$); that is to say, previous to the frost event an error of 0.01 $m^3$ $m^{-3}$ for an estimated surface soil water content of 0.12 $m^3$ $m^{-3}$ (corresponding to the minimum soil wetness measured at 0.025 m of depth) would produce a variation in the estimation of bare soil surface temperature at sunrise of 0.5 ºC. In the same way, an error of 0.01 $m^3$ $m^{-3}$ for estimated surface wetness of 0.19 $m^3$ $m^{-3}$ would produce a variation in the estimation of bare soil surface temperature at sunrise of 0.30 ºC (30 ºC $m^3$ $m^{-3}$ x 0.01 $m^3$ $m^{-3}$). On the contrary, an error of 0.01 $m^3$ $m^{-3}$ for an actual soil water content of 0.29 $m^3$ $m^{-3}$ (field capacity) would produce a variation in the estimation of only 0.17 ºC.

With regards to the initial condition (mainly associated to soil temperature at a depth of 0.05 m and time zero at 1 hour after sunset, $Ts_{(z=0.05,\,0)}$) and lower boundary condition (associated to soil temperature at a depth of 0.20 m and time *t* from 1 hour after sunset to sunrise, $Ts_{(z=0.20,\,0)} = Ts_{(z=0.20,\,t)}$), the variation in the estimated bare soil surface temperature at sunrise, with respect to error which can be caused in soil surface temperature at depths $z = 0.05$ and $0.20\,m$ and time zero at sunset ($\Delta Ts_{(z,\,0)}$), it was found to be 0.7 ºC per ºC error for lower boundary condition ($\Delta Ts_{(0,\,sr)} / \Delta Ts_{(0.2,\,0)}$) and 0.3 ºC per ºC error for initial condition ($\Delta Ts_{(0,\,sr)} / \Delta Ts_{(0.05,\,0)}$). This means that an error of 1 ºC in the estimation of soil temperature at a depth of 0.20 m, would imply an error of 0.7 ºC in the estimation of bare soil surface temperature at sunrise. On the contrary, the same error of 1 ºC in the estimation of soil temperature at a depth of 0.05 m, would imply an error of 0.3 ºC in the estimation of bare soil surface temperature at sunrise. Therefore, the numerical model is more sensitive to the soil temperature's lower boundary condition (depth of 0.20 m and time from one hour after sunset to sunrise) than to the initial condition (depth of 0.05 m and time zero at one hour after sunset).

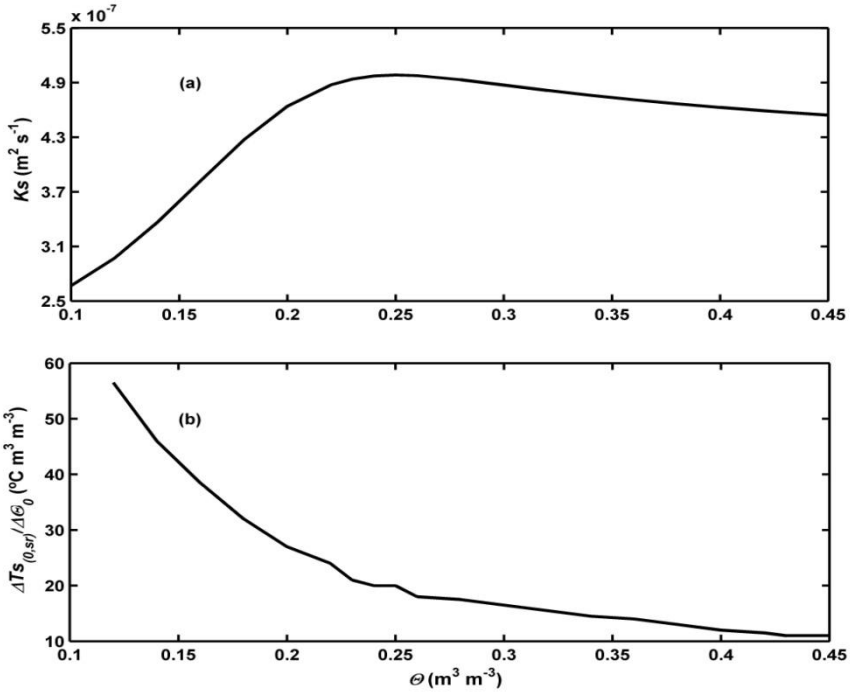


**Fig. 7:** Effect of soil water content ($\theta$) on thermal diffusivity (*Ks*) (a), and relationship between variation of estimated bare soil surface temperature at sunrise ($\Delta Ts_{(0,\,sr)}$), as a result of an error in the estimation of soil surface wetness content ($\Delta\theta_0$), depending on soil water content ($\theta$) (b).

### IV.2.5. Conclusions

The numerical model performed better when the soil surface wetness content ($\theta_0$) lays between field capacity ($\theta_{fc}$) and wilting point ($\theta_{wp}$), because upper boundary conditions can be estimated with greater accuracy, and the error which can be caused in the estimation has low sensitivity in the prediction of the bare soil surface temperature at sunrise. In order to implement this model in a practical manner, the initial boundary conditions need to be parameterized: profile of soil temperature from z = 0 to z = 0.20 m at one hour after sunset, soil temperature at a depth of 0.20 m at one hour after sunset, nocturnal net outgoing long-wave radiation, and soil surface wetness content at sunset previous to radiative frost event.

In the frost events where Richards' equation was applied, , the resultant error of soil surface temperature was below the mean error value of the 9 frost events Then, it is possible to infer that applying Richards' equation would produce a good estimation of bare soil surface wetness.

The implementation of the numerical model, through the development of the heat diffusion equation, only considered the intervention of net outgoing long-wave radiation (*Rn*) and soil heat flux density (*G*); sensible and latent heat flux density were not considered. Given the numerical model's performance on bare soil surface temperature estimation, it is possible to establish, for the condition of this research, that the most important variables taking part in the formation of nocturnal radiative frosts would be *Rn* and *G*.

### IV.2.6. References

Allen RG, Tasumi M, Trezza R (2007) Satellite-baased energy balance for mapping evapotranspiration with internalized calibration (metric)-model. J. Irrig. Drain. E-ASCE doi: 10.1061/(ASCE)0733-9437(2007)133:4(380)

Anfossi D, Bacci P, Longhetto A (1976) Forecasting of vertical temperature profiles in the atmosphere during nocturnal radiation inversions from air temperature trend at screen height. Quart J. Roy. Meteorol. Soc. 102:173-180

Bagdonas A, Georg JC, Gerber JF (1978) Techniques of frost prediction and methods of frost and cold protection. W.M.O. Technical Note, No. 157. Geneva, Switzerland. 160 p

Brunt D (1941) Physical and dynamical meteorology 2nd edn Cambridge University Press, New York

Campbell GS (1985) Soil physics with basic: transport models for soil- plant systems. Elsevier, New York

Campbell GS, Norman JH (1998) An introduction to environmental biophysics. Springer-Verlag, New York

Celia MA, Bouloutas ET, Zarba RL (1990) A general mass-conservative numerical solution for the unsaturated flow equation. Water Resour. Res. 26:1483-1496

Cellier P (1993) An operational model for predicting minimum temperatures near the soil surface under clear sky conditions. J. Appl. Meteorol. 32: 871-883

Clement TP, William RW, Molz FJ (1994) A physically based, two-dimensional, finite-difference algorithm for modeling variably satured flow. J. Hydrol. 161:71-90

De Vries DA (1963) Thermal of soil. In:Van Wijk WR (ed) Physics of the plant environment. North-Holland, Amsterdam

Figuerola PI, Mazzeo NA (1997) An analytical model for the prediction of nocturnal and dawn surface temperatures under calm, clear sky conditions. Agric For. Meteorol. 85:229-237

Jaeger JC (1945) Note on the effect of wind on nocturnal cooling. Quart J. Roy. Meteorol. Soc. 71:388-390

Kirkland MR, Hills RG, Wierenga PJ (1992) Algorithms for solving Richards' equation for variably saturated soils. Water Resour. Res. 28:2049-2058

Lhomme JP, Guilioni L (2004) A simple model for minimum crop temperature forecasting during nocturnal cooling. Agric For Meteorol 123:55-68

Lhomme JP, Vacher JJ, Rocheteau A (2007) Estimating downward long-wave radiation on the Andean Altiplano. Agric. For. Meteorol. 145:139-148

Reuter H (1951) Forecasting minimum temperatures. Tellus 3:141-147

Snyder RL, Melo-Abreu JP, Villar-Mir JM (2010) Protección contra las heladas: fundamentos, práctica y economía. FAO serie sobre medio ambiente y la gestión de recursos naturales. FAO, Roma

Venegas P, Grandon A, Jara J, Paredes J (2013) Hourly estimation of soil heat flux density at the soil surface with three models and two field methods. Theor Appl Climatol 112:45-59

# ANNEX 2.I

In order to determine the temperature difference between evaporative surface and air, $\Delta T_t$ (Eq. (12)) was obtained through the following equation:

$$\Delta T_t = -\left( \frac{H_{(0,t)}}{(\rho_a \; c_a) \; k_v \; u^*} \right) \ln\left( \frac{z-d}{z_H} \right) \tag{I.1}$$

where $k_v$, $d$, $u^*$, and $z_H$ are Von Karman's constant (0.41), the aerodynamic surface of energy exchange (m), friction speed of wind (m $s^{-1}$), and the roughness length for heat (m), respectively. The remaining variables have already been defined, and $z$ corresponds to the height in the atmosphere where wind speed and air temperature are measured.

The factor that multiplies the logarithmic function in the right term of Eq. (I.1), corresponds to the inverse of the slope between $\ln((z-d)/z_H)$ (dependent variable) and the measured air temperature at different heights (independent variable), which is obtained through curve fitting.

The heat transfer resistance $rh_t$ is determined based on the measured wind speed at two meters above the ground, $u_{(2)}$, occupying the following criterion:

If $u_{(2)} < 0.1$ m $s^{-1}$ it is determined by the air's thermal diffusivity (Campbell and Norman, 1998):

$$rh_t = \frac{l}{D_{a(t)}} \tag{I.2}$$

where $l$ and $D_{a(t)}$ correspond to the distance between the evaporating surface and the reference height (2 m), and the air thermal diffusivity ($m^2$ $s^{-1}$) at time $t$, respectively.

If $u_{(2)} \geq 0.1$ m $s^{-1}$, the expression which determines heat transfer resistance is the following:

$$rh_t = \frac{\left[ \ln\left( \frac{z-d}{z_M} \right) + \Psi_M \right] \left[ \ln\left( \frac{z-d}{z_M} \right) + \Psi_H \right]}{k_v^2 \; u_{(z,t)}} \tag{I.3}$$

where $z_M$, $\Psi_M$, $\Psi_H$, and $u_{(z,\,t)}$ correspond to the roughness length for momentum (m), profile diabatic correction factor for momentum (dimensionless), profile diabatic correction factor for heat (dimensionless), and wind speed at height $z$ (m $s^{-1}$) at time $t$, respectively. The remaining variables have been defined.

The aerodynamic surface energy exchange ($d$) is related to the height of the crop (0.65 times the height of the crop). The roughness length for momentum and heat are a

proportion of *d*. For bare soil, the roughness length for momentum currently has a value of 0.002 m (Campbell and Norman, 1998).

To compute $\Psi_M$ and $\Psi_H$, it is necessary to determine the Monin-Obukhov atmospheric stability parameter, $\xi$, according to the following expression (Campbell and Norman, 1998):

$$\xi = -\frac{k_v\, g\, z\, H}{\rho_a\, c_a\, Ta\, \mu^{*3}} \tag{I.4}$$

where $g$ is gravitational constant ($9.8\ \mathrm{m\ s^{-2}}$); $z$ is the height measurement (m); $H$ is the sensible heat flux density ($\mathrm{W\,m^{-2}}$); $\rho c_a$ is the air volumetric heat capacity ($\mathrm{J\,m^{-3}\,K^{-1}}$); $Ta$ is the air temperature ($\mathrm{K}$); and $\mu^*$ is the friction speed of wind ($\mathrm{m\,s^{-1}}$). By replacing Eq. (12) in Eq. (I.4):

$$\xi = -\frac{k_v\, z\, g\,(T_s - T_a)}{T_a\, u^{*3}\, r_h} \tag{I.5}$$

where $T_a$ and $T_s$ correspond to air and surface temperature (*K*), respectively. The other variables have been defined.

If $\xi \geq 0$ it implies stable atmospheric conditions, then the expression that determines the diabatic correction factors for momentum and heat is (Campbell and Norman, 1998):

$$\Psi_m = \Psi_H = 6\ln(1+\xi) \tag{I.6}$$

If $\xi < 0$ it implies unstable atmospheric conditions, then the expressions that determine the diabatic correction factors for momentum and heat are:

$$\Psi_H = -2\ln\left[\frac{1+(1-16\xi)^{0.5}}{2}\right] \tag{I.7}$$

$$\Psi_m = 0{,}6\ \Psi_H \tag{I.8}$$

# IV.3.
## Modeling hourly nocturnal in frost radiative events ii: empirical, regression, physical and numerical models to estimate air and bare soil surface temperature


### Abstract

During radiative frost events (hourly night time step), two estimation models of air temperature were evaluated: Allen's empirical model and the regression model by Gandia *et al.* Also, for the same conditions, four other estimation models were tested to estimate bare soil surface temperature: Brunt's physical model; a Numerical model with real initial and boundary conditions; Allen's empirical model and the regression model by Gandia *et al.* applied to bare soil surface condition. The Numerical model developed considered *in situ* temperature profile, wetness content and net radiation measurements, which are necessary to define the initial and boundary conditions for the model. Air temperature (2 m above soil) and bare soil surface temperature records served as reference. The best performance for air temperature estimations was the regression model by Gandia *et al.* (RMSE: 1.6 ºC). For soil surface temperature on bare soil, the best performance was by Allen's empirical model (RMSE: 1.3 ºC), followed by the Numerical model (RMSE: 1.6 ºC), the regression model by Gandia *et al.* (RMSE: 2.0 ºC) and, lastly, by Brunt's physical model (RMSE: 2.9 ºC). The calibration of Allen's model can be used to estimate air and bare soil surface temperature. Brunt's model underestimated soil surface temperature and can be used as the lower boundary in the estimation of minimum soil surface temperature.


### IV.3.1. Introduction

Technically, the word "frost" refers to the formation of ice crystals on surfaces, either by freezing of dew or a phase change from vapour to ice (Blanc *et al*. 1963, Bettencourt 1980; Mota 1981, Cunha 1982); however, the word is widely used by the public to describe a meteorological event when crops and other plants experience freezing injury (Snyder *et al.* 2010). Nevertheless, it also can be defined as the occurrence of temperatures lower than or equal to 0 °C measured in a "Stevenson-screen" shelter at a height between 1.25 and 2.0 m (Hogg 1971, Lawrence 1952).

Snyder *et al.* (1987) and Kalma *et al.* (1992) have defined frost as falling into two categories: "advective" and "radiative". Advective frosts are associated with large-scale incursions of cold air with a well-mixed, windy atmosphere and a temperature that is often sub-zero, even during daytime. And radiative frosts are associated with cooling due to energy loss through radiant exchange during clear, calm nights, and with air temperature inversions. In some cases, a combination of both advective and radiative conditions occurs (Snyder *et al.* 2010).

Usually, under ideal conditions of radiative frost, that is clear nights with no wind, the air temperature decreases due to the release of radiation from the ground and may reach the point of freezing at dawn (Ellison 1928). However, under conditions of cloudiness or haze, the radiation from the atmosphere to the ground increases, depending on the temperature of clouds or haze; therefore, the net energy loss is small (Snyder *et al.* 2010).

The frost formation process causes various agricultural crop damages, especially in frost-sensitive plants, including herbaceous annuals, flowers of deciduous fruit trees, and the fruit of many plant species which cannot tolerate ice formation within their tissues. Ice forming in or on frost sensitive plants spreads rapidly, both intercellular and intracellularly, and mechanical disrupting is usually manifested in flaccidity and or discoloration when the plant is warm again (Lindow 1983).

In many areas prone to low temperature occurrence, significant losses in agricultural production may result from frost damage (Lhomme and Guilioni 2004). In the U.S.A, economic losses are greater by frosts than any other agro-climatic phenomenon (Snyder *et al.* 2010).

In order to provide reliable forecast of night-time temperatures to allow the use of active or passive frost protection methods, thus avoiding damage in agriculture, many studies have developed a wide range of models. Some of these methods are: (1) empirical methods of frost prediction, (2) regression models, (3) physical models, and (4) numerical models.

### IV.3.2. Background

As noted, various approaches have been designed to predict the minimum air temperature reached during nocturnal cooling from weather data registered the day before, generally at sunset. They can be purely empirical, obtained from statistical relationships, or mechanistic, based upon physical principles (Bagdonas *et al.* 1978). In the mechanistic models of frost prediction, an accurate estimate of downward long-wave radiation is essential, due to the fact that frost occurrence is generated by a deficit in long-wave radiation (Lhomme *et al*. 2007**).**

IV.3.2.1. Empirical methods of frost prediction

Initially, predicting minimum night temperatures implied occupying empirical expressions involving biophysical factors, such as dew point temperature ($Tdw$), wet bulb temperature ($Tbw$), vapor pressure ($e_w$), wind speed ($v$) and relative humidity ($hr$). Such expressions were developed using historical records, obtained from weather stations for specific areas and under certain environmental conditions (Bagdonas *et al.* 1978).

Some of the earliest empirical equations simply related the minimum air temperature with the air temperature, measured at a reference height and time. Nichols (1920) proposed a "maximum-minimum" relationship which gave as a direct function of the maximum air temperature, from which the minimum air temperature may be determined (Bagdonas *et al.* 1978).

Smith (1920) correlated the difference between evening values of air temperature and evening dew point temperatures, with the difference between evening dew point temperatures and the ensuing minimum air temperatures (Bagdonas *et al.* 1978).

Inasmuch as radiation from the ground is a function of the soil temperature and the absolute air humidity, a simple mathematical formula was developed by Young (1920)

which expresses these factors quantitatively and shows the probable minimum air temperature (Allen 1939).

Angström (1920) (cited by Allen 1957) expressed the minimum air temperature in terms of the dry-bulb temperature and the wet bulb temperature, both measured at a reference height, at 16:45 p.m. (local time).

Another way of confronting the problem of frost is through regression equations that predict the behavior of the air temperature overnight. In this regard, Allen (1957) developed a model for predicting frost simple trend, using historical records of air temperature and dew point, as well the minimum air temperatures observed during clear calm and frosty nights. The criterion is to begin modeling air temperature two hours past sunset ( $ss$ ) until sunrise, since the author of this model has concluded that this time period corresponds to the time when the net radiation has reached its most negative value. The expression that describes it is:

$$Ta_{(z\,ref\,,\,t)} = Ta_{(z\,ref\,,\,ss+2)} + b\sqrt{t} \qquad (1)$$

and $b$ (ºC hour$^{-0.5}$) is obtained with the following expression:

$$b = \frac{Ta_{z\,ref}^{\min} - Ta_{(z\,ref\,,\,ss+2)}}{\sqrt{h}} \qquad (2)$$

where $Ta_{(z\,ref\,,\,t)}$ is the air temperature (K or ºC) measured at a reference height $z\,ref$ (m) in time $t$ (hours); $Ta_{(z\,ref\,,\,ss+2)}$ is the air temperature (K or ºC) measured at a reference height $z\,ref$, two hours after sunset $(ss+2)$; $t$ is the time (hours) counted from two hours after sunset ( $ss+2$ ) until sunrise; $Ta_{z\,ref}^{\min}$ is the minimum air temperature (K or ºC) measured at a reference height $z\,ref$ ; and $h$ is the time period (hours) elapsed between two hours after sunset and sunrise.

IV.3.2.2. Regression models

Later, Gandia *et al.* (1985) used an exponential technique in order to predict the minimum air temperature, during a clear-sky night with low wind speeds over the area being investigated. More precisely, minimum air temperature was estimated based on data providing sunset air temperature and the air temperature at time $t$, both temperatures measured at a reference height starting from sunset to sunrise, by the following equation:

$$\ln\left(\frac{Ta_{(z\,ref\,,\,t)} - Ta_{z\,ref}^{\min}}{Ta_{(z\,ref\,,\,ss)} - Ta_{z\,ref}^{\min}}\right) = A_G\,t + B_G \qquad (3)$$

where $Ta_{(z\,ref\,,\,ss)}$, $Ta_{z\,ref}^{\min}$ and $Ta_{(z\,ref\,,\,t)}$ are sunset air temperature, minimum air temperature, and air temperature in time $t$, measured at a reference height $z\,ref$ . The coefficients $A_G$ (hour$^{-1}$) and $B_G$ (dimensionless) were obtained by means of a least squares adjustment using a large database of past observations; $t$ is the time recorded

from sunset until sunrise (hours).Once the constants $A_G$ and $B_G$ are known, $Ta_{(z\,ref,\,t)}$ is cleared from Eq. (3):

$$Ta_{(zref,t)} = Ta_{zref}^{\min} + \left(Ta_{(zref,ss)} - Ta_{zref}^{\min}\right)\exp\left(A_G\, t + B_G\right) \tag{4}$$

In order to determine the minimum air temperature, Gandia *et al.* (1985) proposed the following expression:

$$Ta_{zref}^{\min} = \frac{Ta_{(zref,t)} - Ta_{(zref,ss)}\exp\left(A_G\, t + B_G\right)}{1 - Ta_{(zref,ss)}\exp\left(A_G\, t + B_G\right)} \tag{5}$$

In accordance with Gandia *et al.* (1985), $Ta_{(z\,ref,\,t)}$ was measured four hours after sunset $Ta_{(z\,ref,4)}$. Similarly, Emmanouil *et al.* (2006) proposed a third degree polynomial model, where its coefficients were obtained through curve fitting.

IV.3.2.3. Physical models

The temperature of the earth's surface at night should be highly correlated with that of the air in the surface layer. Therefore, a good forecast of the minimum soil temperature should provide a good forecast of the minimum air temperature. This logic resulted in the development of several semi-empirical and theoretical techniques early in the past century (Bagdonas *et al.* 1978).

An analytical solution of a one-dimensional heat-conduction equation in bare soil considered as a semi-infinite medium was developed by Brunt (1941):

$$\frac{\partial Ts}{\partial t} = Ks\frac{\partial^2 Ts}{\partial z^2}, \quad z \geq 0 \quad \text{and} \quad t > 0 \tag{6}$$

where $Ts$ is the soil temperature (K or ºC), $Ks$ is the soil thermal diffusivity ($m^2\ s^{-1}$), $t$ is time (s) and $z$ is the depth into the soil (m). In this case, the atmosphere is eliminated from the analysis (Lhomme and Guilione 2004). In order to develop the equation, Brunt assumed as an upper boundary condition that the temperature gradient at depth $z = 0$, $\left(\partial Ts/\partial z\right)_{z=0}$, is equivalent to the constant ratio between net radiation and soil thermal conductivity. Besides, Brunt considered the ground to be a semi-infinite and homogeneous medium, with uniform physical properties, and that the soil temperature is initially constant throughout depth (Brunt 1941). Details of Brunt's expression derivation are presented in Annex I. The final expression developed is:

$$Ts_{(0,\,t)} = Ts_{(0,\,ss)} - \frac{2}{\sqrt{\pi}}\frac{Rn}{\rho s_0\, Cs_0\sqrt{Ks_0}}\sqrt{t} \tag{7}$$

where $Ts_{(0,\,t)}$ is the temperature of the soil surface (K or ºC) estimated at time $t$, $Ts_{(0,\,ss)}$ is the temperature of the soil surface (K or ºC) at the time of sunset, $Rn$ is the net outgoing long-wave radiation ($J\ s^{-1}\ m^{-2}$), $\rho s_0$ is the bulk density of the soil surface ($kg\ m^{-3}$), $Cs_0$ is the specific heat of the soil surface ($J\ K^{-1}\ kg^{-1}$), $Ks_0$ is the thermal diffusivity of the soil surface ($m^2\ s^{-1}$), and $t$ is the time (s) counted from the sunset to sunrise. Brunt assumed $Rn$ as constant throughout the night.

When considering the conditions during night thermal inversion, there is heat transfer from air to ground, tending to prevent the decrease of the ground's temperature. Therefore, this model gives a limit to the maximum temperature dropping at the surface, where the main factor that determines the temperature decreasing is the net radiation (Brunt 1941). In this sense, the earth's surface radiates effectively as a black body, and the amount of heat which it sends into the atmosphere is independent on the nature of the ground. The amount of energy which the earth's surface gains from the atmosphere depends upon the distribution of temperature and humidity in the lower layers on the atmosphere. Thus, the net outward radiation at night from the earth's surface depends only on atmospheric conditions and on the temperature of the earth's surface (Brunt 1941).

However, to avoid the problem of determining the soil parameters, mean values of the term $\rho_{s_0} c_{s_0} \sqrt{Ks_0}$ were found from solutions of the heat equation, after good estimation of nocturnal net outgoing long-wave radiation. In some cases, the mean values of this term were unrealistic, while in others they were quite acceptable. Although there is no problem in finding suitable soil bulk density and specific heat values, the soil surface thermal diffusivity limits the equation's usefulness (Bagdonas *et al.* 1978).

IV.3.2.4. Numerical model

Since analytical solutions of the one-dimensional heat equation have the inconvenience of using assumptions which do not always conform to reality, numerical models are more flexible since assumptions which are considered constant in analytical models can be variable in numerical models, because they can be adjusted to the medium conditions that affect a given physical phenomenon.

In order to obtain the bare soil surface temperature in radiative frost condition, Venegas *et al*. (submitted) developed a model, which solves the one-dimensional heat equation (Eq. (6)), dependent on initial and boundary conditions observed in radiative frost events. These conditions only consider soil temperature profile, soil water content, outgoing long-wave radiation (*Rn*) and soil heat flux density (*G*). Therefore, a Neumann-type condition (flux condition) was implemented at the upper boundary condition, a Dirichlet-type condition was implemented at the lower boundary condition, and thermal profile in the soil as initial condition. In order to obtain a numerical solution for the one-dimensional heat diffusion equation the finite-difference method was used, through a Crank-Nicholson scheme.

### IV.3.3. Objective

The objective of this research was to evaluate, during a frost event (hourly night time step), two estimation models of air temperature: Allen's empirical model (Eq. (1)) and the regression model by Gandia *et al.* (Eq. (4)); and four estimation models of bare soil surface temperature: Brunt's physical model (Eq. (7)); Numerical model, which solves the one-dimensional heat diffusion equation, with real initial and boundary conditions, proposed previously by the authors; Allen's empirical model and the regression model by Gandia *et al.* applied to bare soil surface condition. The records of the soil surface temperature and the air temperature (2 m above soil) will be used as a comparison or reference.

## IV.3.4. Methodology

### IV.3.4.1. Experimental site

This experiment was carried out at the Agrometeorological Station of the Faculty of Agricultural Engineering, University of Concepción in Chillán-Chile (36°35′43.4″ S, 72°4′47.3″W), located at an altitude of 130 m above sea level. The soil is clay loamy, with a soil bulk density of 1.45 Mg $m^{-3}$ at a depth between 0 and 0.1 m and of 1.60 Mg $m^{-3}$ at a depth between 0.1 and 0.2 m; the soil water content at field capacity and permanent wilting point is 0.29 and 0.21 $m^3$ $m^{-3}$, respectively; the saturated hydraulic conductivity of de soil is 1.1 m $day^{-1}$; and a fraction of clay of 33 % in the first layer. It belongs to the Tres Esquinas series (member of the fine, mixed, thermic Ultic Haploxeralfs soil family), has a slightly inclined slope, and rests upon a substrate of weathering solid rock, mixed, dark brown, and reddish material with 5 YR shades under humidity. The measurement period went from September 03 of 2010, day of the year (DOY) 246, to December 31 of 2011 (DOY 365). In this period of time only nine radiative frost events occurred. Details of these events are given in Table 1:

**Table 1** Date of radiative frost event, sunset and sunrise time, length of the night, sunset soil surface temperature ($Ts_{(0,\,ss)}$), minimum soil surface ($Ts_{z=0}^{\min}$), minimum air temperature measured at 2 m height ( $Ta_{z=2}^{\min}$), and estimated or assumed soil surface water content ( $\theta_0$ ) reached during each event.

| Year | Radiative frost (DOY) | Time sunset* | Time sunrise* | Night length (hours) | $Ts_{(0,\,ss)}$ (º C) | $Ts_{z=0}^{\min}$ (º C) | $Ta_{z=2}^{\min}$ (º C) | $\theta_0$ ($m^3$ $m^{-3}$) |
|---|---|---|---|---|---|---|---|---|
| 2010 | 273/274 | 20:00 | 07:15 | 11.25 | 9.5 | -2.0 | 1.5 | 0.20 |
| | 297/298 | 20:30 | 06:45 | 10.25 | 16.3 | -0.1 | 2.5 | 0.12 |
| 2011 | 105/106 | 19:30 | 08:15 | 12.75 | 13.0 | -1.1 | 3.0 | 0.17 |
| | 106/107 | 19:30 | 08:15 | 12.75 | 13.4 | -0.9 | 2.6 | 0.16 |
| | 241/242 | 19:45 | 08:00 | 12.25 | 7.4 | -1.9 | 0.1 | 0.29 |
| | 242/243 | 19:45 | 08:00 | 12.25 | 9.3 | -2.9 | -0.1 | 0.29 |
| | 243/244 | 19:45 | 08:00 | 12.25 | 9.8 | -3.0 | -0.4 | 0.22 |
| | 247/248 | 19:45 | 07:45 | 12.00 | 7.5 | -3.0 | -1.0 | 0.29 |
| | 260/261 | 20:00 | 07:30 | 11.50 | 11.9 | -1.9 | -0.3 | 0.21 |

* Local time

### IV.3.4.2. Soil surface temperature and soil water content

The measurements of soil surface temperature were made with Wahl's DHS24L heat spy infrared thermometers (Palmer Wahl Instrumentation Group, Ashville, North Caroline, USA), with an operating temperature range going from -20 ºC to 550 ºC, and a conversion factor of 1.0 ºC $mV^{-1}$, located 1.70 m above ground level. Monitoring readings were recorded every 1 second and averaged every 15 min during the 2010-2011 period.

In orden to measure soil wetness, ECHO-5 capacitive sensors (Decagon Devices, Washington, USA) were used, placed horizontally at depths of 0.05 m and 0.10 m for the year 2010, and 0.025, 0.05, and 0.10 m for the year 2011. Details of methodology applied to obtain soil surface water content are given by Venegas *et al* (submitted)

IV.3.4.3. Net radiation

The net radiation was measured with a net radiometer, model Q-7.1 (Campbell Scientific, Inc., Logan, Utah, USA), placed at a height of 1.55 m above bare soil. The constant to transform voltage to flux density was 9.1 W $m^{-2}$ $mV^{-1}$, for millivolts greater than zero, and 11.4 W $m^{-2}$ $mV^{-1}$, for millivolts smaller than zero. Readings were recorded every 1 second and averaged every 15 min.

IV.3.4.4. Air temperature, wind speed and solar radiation

Air temperature was measured using a Vaisala probe (HMP35C, Campbell Scientific Inc., Logan, Utah, USA) located 2.0 m above ground level. Additionally, air temperature was measured with copper constant thermocouples, located at 0.5 and 1.0 m above the ground. Wind speed was measured using a cup anemometer and wind vane (Young Co, 03001, Michigan, USA) located 2.0 m above ground level. Solar radiation was measured with a silicon piranometer (LI-200X, Campbell Scientific Inc., Logan, Utah, USA) located 2.0 m above ground level, which are part of the sensors belonging to the Agrometeorological Station of the Faculty of Agricultural Engineering. Readings were recorded every 1 second and averaged every 15 min.

IV.3.4.5. Storage of records

The net radiation and flux plate records were stored in a 21X micrologger (Campbell Scientific Inc., Logan, Utah, USA.), and thermocouple records were stored in a HL20 micrologger (Rotronic A G, Bassersdorf, Switzerland). Soil wetness records were stored in an ECHO-5 micrologger (Decagon Devices, Washington, USA).

IV.3.4.6. Calibration of Allen's empirical model

From the year 2000 to 2009 and for 55 nights with radiative frost conditions, wind speed and solar radiation records were selected at the Agrometeorological Station of the Faculty of Agricultural Engineering. Subsequently, the calibration was done with the records of air temperature at 2 m height.

The criteria employed to determine radiative frost nights were air temperature below or equal to 0 ° C, wind speed of less than 2 m $s^{-1}$, and the absence of clouds. In the latter case, the criterion used by Lhomme and Guilioni (2004) was adopted, who show that cloudy conditions do not change dramatically between the day prior to frost and the night when this event occurs, and that one way to determine the percentage of clear sky ($n/N$) is through the expression proposed by Prescott (1940):

$$\frac{Rs}{Rs_0} = 0.18 + 0.55\left(\frac{n}{N}\right) \tag{8}$$

where $Rs_0$ is the extraterrestrial solar radiation (MJ $m^{-2}$ $day^{-1}$), $Rs$ is the measured incoming solar radiation at the soil level (MJ $m^{-2}$ $day^{-1}$), $n$ is actual duration of sunshine (hours), $N$ is the duration of daylight (hours), and $n/N$ is the fraction of clear day.

The fraction of cloud cover ($Fcc$) was estimated by the following expression:

$$Fcc = 1 - \frac{n}{N} \tag{9}$$

In the case of this study, we considered a clear night (nonexistence of cloudiness) when $Fcc \leq 0.25$.

The criterion to determine sunset time was the last diurnal record of instant solar radiation that had a non-zero positive value. For the case of sunrise time, the last night record of zero solar radiation (before the start of positive values) was considered. This information was used to obtain the times *t*, *h* (Eq. (1 and 2) of Allen's empirical model) and *t* (Eq. (3, 4 and 5) of Gandia *et al.* regression model.

To calibrate Allen's empirical model, Eq. (2), *b* values were determined for 55 radiative frost events selected from the years 2000 to 2009. Once *b*' range of variation was determined, it was found that the lowest RMSE is obtained with a *b* value of -2.4 $^{o}$C hour$^{-0.5}$ (Fig. 1):

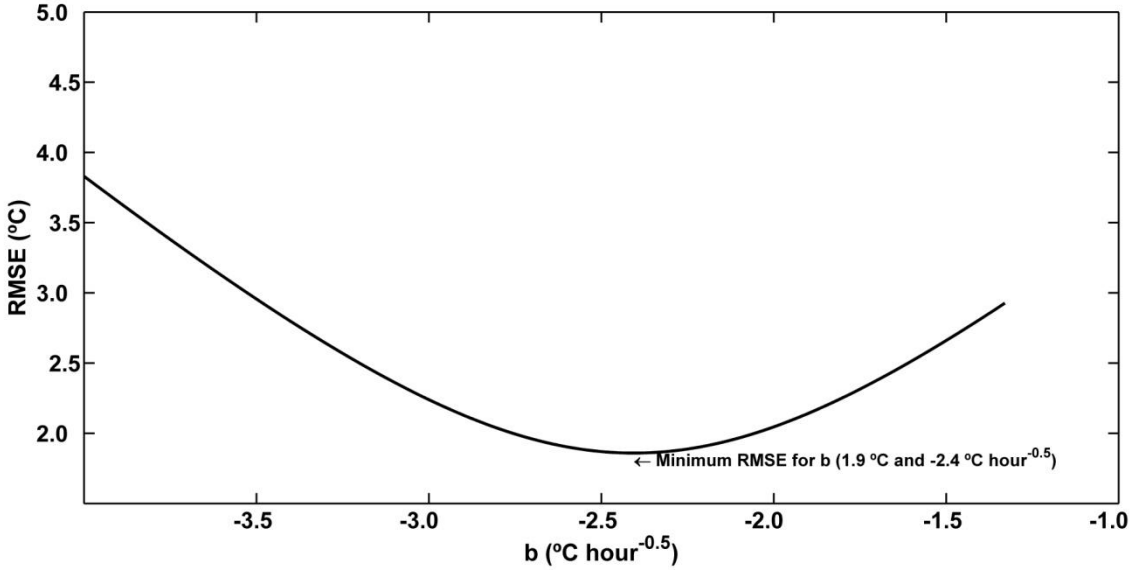


**Fig. 1** Relation between b`s range of variation (Allen's empirical model, Eq. (2)), and the RMSE response, with respect to the estimation of air temperature and observed air temperature, during night time in radiative frost events.

The calibrated value of *b* was used to estimate the air (2 m) and soil surface temperature. For this reason, the equations applied to estimate air temperature at a height of 2 m and the temperature of the soil surface, in the 9 radiative frost events presented in Table 1 are the following:

$$Ta_{(z\,ref,\,t)} = Ta_{(z\,ref,\,ss+2)} - 2.40\sqrt{t} \tag{10}$$

$$Ts_{(z=0,\,t)} = Ts_{(z=0,\,ss+2)} - 2.40\sqrt{t} \tag{11}$$

IV.3.4.7. Calibration of the regression model by Gandia *et al.*

To determine the coefficients $A_G$ and $B_G$ of the regression model by Gandia *et al.* (Eq. (4)), curve fitting by least squares was used for 55 radiative frost events selected from the years 2000 to 2009. Therefore, the range of variation of each constant was obtained.

Based on this range of variation, the combination of constants with the lowest RMSE value over all analyzed frost events was selected. The calibrated values of $A_G$ and $B_G$ (Eq. (3)) with the lowest RMSE were -0.19 $h^{-1}$ and 0.025, respectively (Fig. 2):

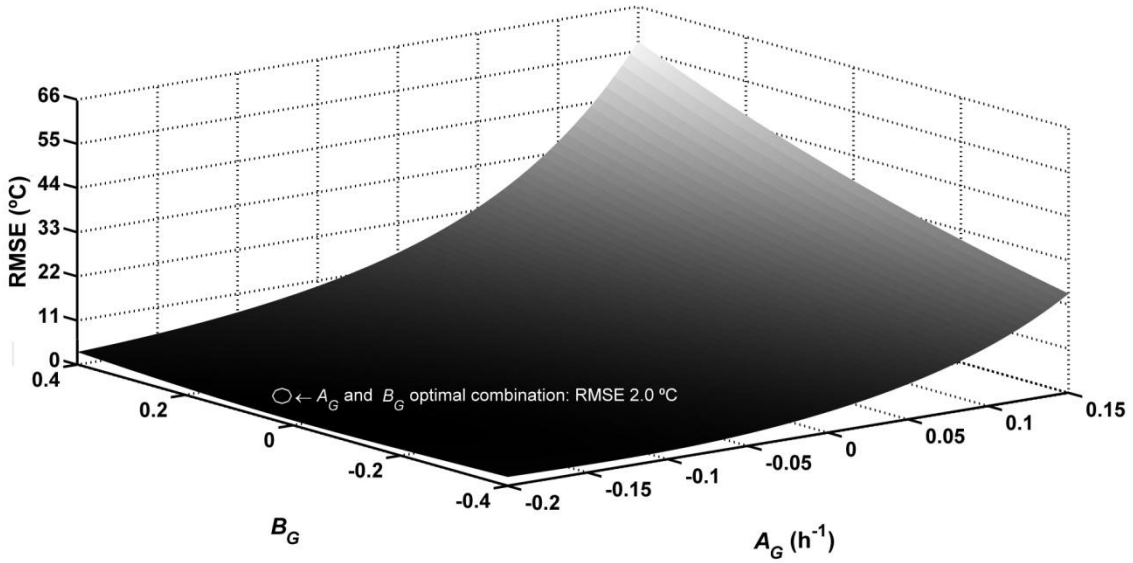


**Fig. 2** RMSE response surface, in relation to the combination of coefficients $A_G$ and $B_G$ values (Eq. (4)) by Gandia *et al.* (1985) regression model, for air temperature estimation in comparison to observed air temperature.

Based on the before-mentioned observations, the expressions which were used to estimate air temperature at a height of 2 m ( $z\,ref$ ) and that of the soil surface( $z = 0\,\mathrm{m}$ ), in all nine radiative frost events included in Table 1, correspond to Eq. (4) with the values of coefficients $A_G$ and $B_G$ previously indicated :

$$Ta_{(zref,t)} = Ta_{zref}^{\min} + \left(Ta_{(zref,ss)} - Ta_{zref}^{\min}\right)\exp\left(-0.19t + 0.025\right) \tag{12}$$

$$Ts_{(0,t)} = Ts_{z=0}^{\min} + \left(Ts_{(0,ss)} - Ts_{z=0}^{\min}\right)\exp\left(-0.19t + 0.025\right) \tag{13}$$

So as to determine the minimum air temperature, $Ta_{zref}^{\min}$, from Eq. (5) the following equation is obtained:

$$Ta_{zref}^{\min} = \frac{Ta_{(zref,t)} - Ta_{(zref,ss)}\ \exp\left(-0.19\ t + 0.025\right)}{1 - Ta_{(zref,ss)}\ \exp\left(-0.19\ t + 0.025\right)} \tag{14}$$

First of all, in agreement with Gandia *et al.* (1985), $Ta_{(zref,t)}$ was measured four hours after the sunset $\left(Ta_{(zref,4)}\right)$. However, our observations determined that $Ta_{(zref,t)}$ best estimates $Ta_{zref}^{\min}$ were obtained using air temperature recorded 0.25 hours after sunset ($Ta_{(zref,0.25)}$). Therefore, $Ta_{(zref,0.25)}$ was used as criterion in this research.

By replacing $Ta_{z\,ref}^{\min}$ from Eq. (14) in Eq. (12) and Eq. (13), it is possible to estimate, in radiative frost events, air and soil surface temperature behavior, respectively.

Eq. (14) was also used to determine the minimum soil surface temperature by using the soil surface temperature parameters and the criterion just described ($Ts_{(z=0,\ t)} = Ts_{(z=0,\ 0.25)}$).

IV.3.4.8. Brunt's physical model (Eq. (7))

To implement this model, it was necessary to quantify the thermal diffusivity of the soil surface $(Ks_0)$, and the volumetric heat capacity of the soil $(Cv_0 = \rho s_0\, Cs_0)$, both in $z = 0$, as well as the net radiation $(Rn)$, the soil surface temperature at sunset time $Ts_{(0,\ ss)}$ and the time period in which the model was applied (length of night).

The variables $Cv_0$ and $Ks_0$ are dependent on soil water content, so it became necessary to determine the wetness in the soil surface, $\theta_0$ (first millimeter deep). Richards' equation was applied to the soil evaporation process in the period [0,T], beginning six hours after the last rain or planting irrigation - previous to a frost event (*t=0*) - until the sunset that precedes this event ($t = \mathrm{T}$), and its value is variable depending on the frost event. (Venegas *et al*. submitted).

Soil surface water content, $\theta_0$ (Table 1), was obtained either by applying Richards' equation (in three out of nine frost event cases) or using the criteria mentioned in 3.7 section of Venegas *et al.* (submitted): soil water content was assumed to be equivalent to field capacity because rain fall one day or less before the sunset that preceded radiative frost; or soil water content was assumed to be equivalent to that recorded by the ECHO-5 capacitive sensor buried at a depth of 0.025 m, because soil wetness was much lower than permanent wilting point.

The soil thermal conductivity was determined with Campbell's model (1985), the volumetric heat capacity of the soil was determined with De Vries (1963) model, and, lastly the thermal diffusivity with Eq. (8). These procedures have been described in detail by Venegas *et al*. (2013).

To determine the sunset time, the same methodology outlined in section 5.6 was considered. The period in which the model was applied corresponds to the time between sunset and sunrise. Finally, the net radiation used in the model corresponds to the net radiation observed overnight at each frost event. Table 1 indicates the measured soil surface temperature at the time of sunset, $Ts_{(0,\ ss)}$, for each frost event.

The time step of *t* indicated in Eq. (7) was 900 seconds (15 min), in order to match the temperature value time steps estimated by the model and those observed in this study.

.

IV.3.4.9. Heat diffusion equation through the Numerical model

In order to apply the Numerical model it was necessary to determine the initial and boundary conditions for each radiative frost event, according to the temporal behavior

of the net radiation and the response of the temperature and wetness content at different soil depths (for more details see 2.2 section of Venegas *et al.* (submitted)). Defined these, it is possible to discretize the one-dimensional heat equation (Eq. (6)) through finite-difference method and the Crank-Nicholson scheme. The last approach permits to establish a system of linear equations to be solved in every time step. The solution of this equation system allows for the determination of changes in spatial (from depth z = 0 until depth z = 0.20 m) and temporal (from 1 hour after sunset, $t$ = 0 s, until sunrise) temperature and, therefore, the evolution of temperature at the soil surface during the time period the frost occurs.

IV.3.4.10. Validation of the models

The validation of the models was based on frost events selected in Table 1. For the case of calibrated models (Gandia *et al.* (1985) and Allen (1957)) records of air temperature at 2 m above soil, ($Ta_{(z=2,t)}$), and soil surface temperature, ($Ts_{(z=0,t)}$), were used as reference, and for the remaining models (Numerical model and Brunt's model) only records of soil surface temperature ($Ts_{(z=0,t)}$) were used as reference. The validation was done through the interpretation of the following coefficients:

Graphic relation 1:1, where data of the observed temperatures ($Ta_{(2,t)}$ and $Ts_{(0,t)}$) are contrasted with the temperatures estimated through the four models.

The mean absolute error (MAE) and the root mean square error (RMSE) were calculated from:

$$MAE = \frac{1}{N}\sum_{i=1}^{N}|O_i - P_i| \quad (26)$$

$$RMSE = \sqrt{\frac{1}{N}\sum_{i=1}^{N}(O_i - P_i)^2} \quad (27)$$

where $O_i$ is the observed temperature value and $P_i$ is the estimated temperature values, N is the number of observations, and subscript $i$ denotes the ith observation.

**IV.3.5. Results and discussion**

IV.3.5.1. Hourly estimation of air temperature (*Ta*)

Regarding the estimation of hourly air temperature at a height of 2 m during radiative frost events, the regression model by Gandia *et al.* performed better than Allen's model (Fig. 3). This prediction capacity agrees with results reported by Gandia *et al.* (1985), who found that modeling night air temperature at 1.5 m above ground surface had an average error of 1.1 ºC and a correlation coefficient of 0.96. However, Anfossi (1989) reported that the nocturnal observations of air temperature measured at Philippsburg, Germany, were overestimated by this model. On the other hand, Allen's model showed a tendency towards greater dispersion in the hourly estimation of air temperature by overestimating some cases and underestimating others. As an example of these two models' behavior, eight nocturnal air temperature estimation events are shown in Fig. 4:

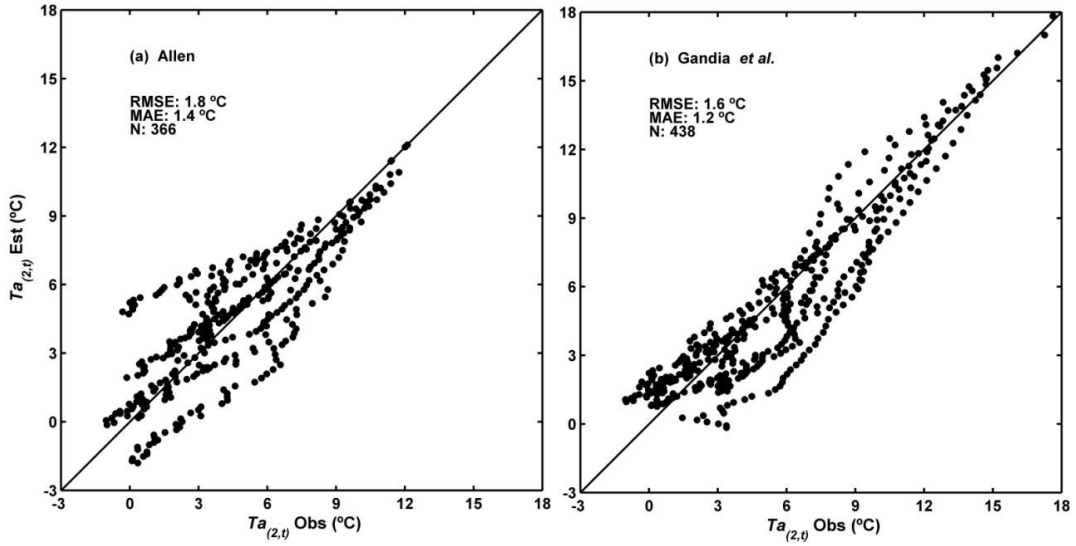


**Fig. 3** 1:1 ratio of night-time hourly air temperature estimated ($Ta_{(2,t)}$ Est) and observed ($Ta_{(2,t)}$ Obs) through Allen's empirical model (a), and the regression model by Gandia *et al.* (b). N represents nocturnal temperature records every 15 minutes which were obtained during nine radiative frost events.

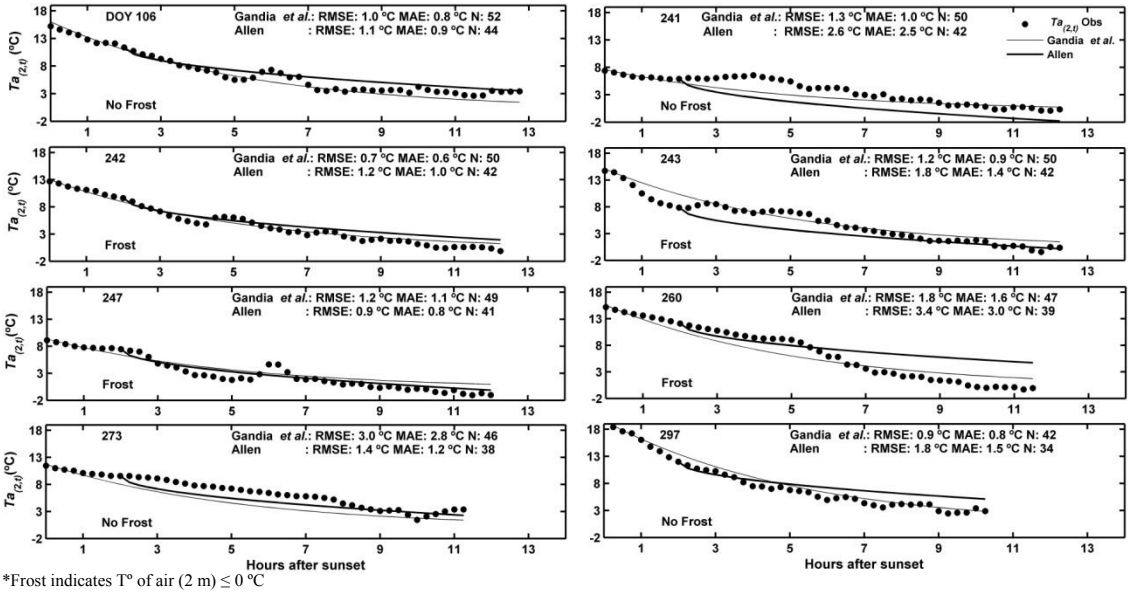


*Frost indicates Tº of air (2 m) ≤ 0 ºC

**Fig. 4** Decline of the nighttime hourly air temperature, $Ta_{(2,t)}$, estimated by Gandia *et al.* and Allen's models, from sunset to sunrise, during 8 radiative frost events. N represents nocturnal temperature records every 15 minutes.

It should be mentioned that in 4 out of the 9 radiative frost events recorded, the minimum air temperature observed at a height of 2 m was below to 0 ºC (see Table 1). The RMSE for these four radiative frost event in the estimation of minimum air temperatures was of 2.8 and 1.9 ºC for the models by Allen and Gandia *et al.*, respectively**.** On the other hand, for the other five days, where the minimum air temperature was above or close to 0 ºC, the RMSE in the estimation was of 1.8 and 1.1 ºC for the models by Allen and Gandia *et al.*, respectively.

IV.3.5.2. Hourly estimation of bare soil surface temperature ($Ts_{(0,t)}$)

With regards to the hourly estimation of bare soil surface temperature, $Ts_{(0,t)}$, during all 9 radiative frost events, Brunt's model underestimated $Ts_{(0,t)}$ in all cases (Fig. 5a), with differences of up to 5 ºC by the end of the night period. This is in agreement with what Brunt (1941) indicated referring to the use of this model as a lower boundary in the estimation of the minimum soil surface temperature. Moreover, Bagdonas *et al.* (1978) reported that in a study carried out between the years 1966 and 1967 in Florida, USA, Brunt's model underestimated the minimum soil surface temperature in 21 out of 30 frost events, where the mean error was 2.1 ºC.

On the other hand, the Numerical model developed by the authors overestimates the behavior of the hourly soil surface temperature in radiative frost events (Fig. 5b). However, differences with observed values did not surpass 2 ºC. Despite this, the Numerical model displayed the second best behavior out of the four models evaluated for their estimation of bare soil surface temperature during radiative frost events (Table 2), and overestimation (Fig. 6) could be explained by errors in the determination of soil surface wetness (Venegas *et al.* submitted). Also, it should be mentioned that when soil surface volumetric water content ($\theta_0$) is between field capacity and permanent wilting point, the average RMSE value corresponds to 1.2 ºC, and when $\theta_0$ is lower than permanent wilting point the average RMSE value corresponds to 2.2 ºC. Therefore, the numerical model presents a better behavior when the soil surface water content is over permanent wilting point that when it is under. On the other hand, in order to implement this model in a practical manner, the initial boundary conditions need to be parameterized: initial temperature distribution at sunset, soil temperature at a depth of 0.2 m at sunset, nocturnal net radiation, and soil surface wetness content at sunset.

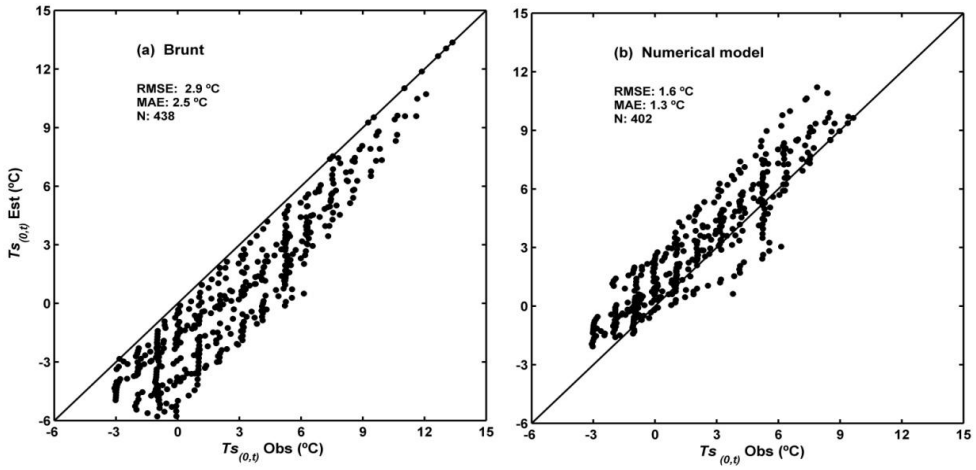


**Fig. 5** 1:1 ratio of night-time hourly bare soil surface temperature estimated ($Ts_{(0,t)}$Est) and observed ($Ts_{(0,t)}$Obs) through Brunt`s model (a) and Numerical model (b). N represents nocturnal temperature records every 15 minutes which were obtained during nine radiative frost events.

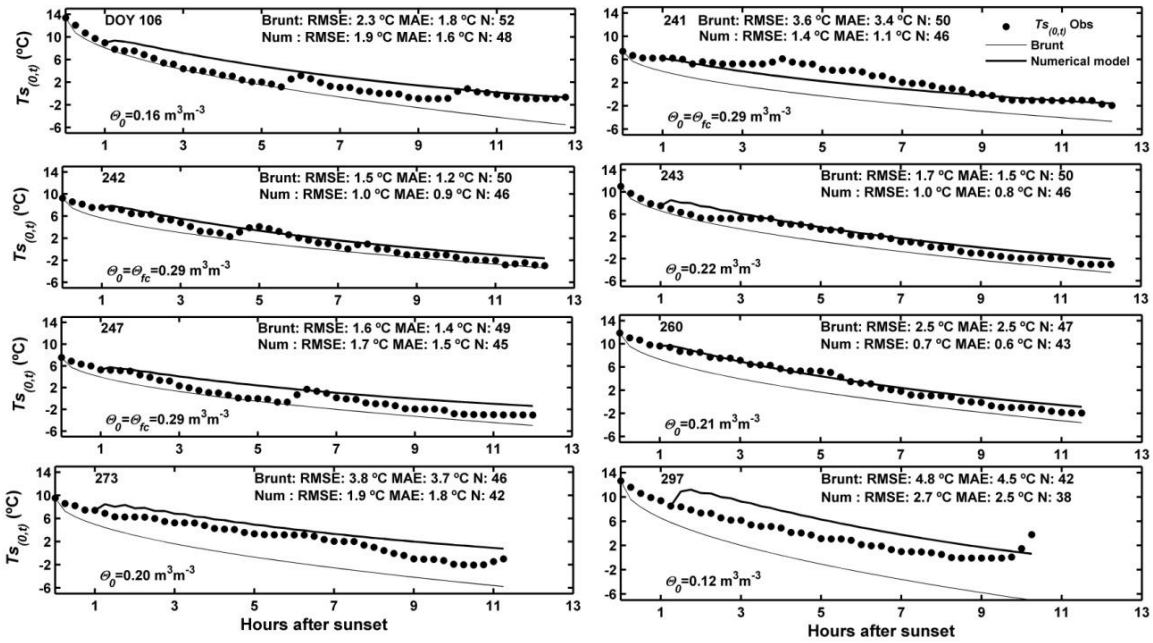


**Fig. 6** Decline of the nighttime hourly bare soil surface temperature ($Ts_{(0,t)}$) estimated by the Numerical (Num) and Brunt's models, from sunset to sunrise, during 8 radiative frost events. $\theta_0$ is the estimated or assumed soil surface water content at the beginning of each frost event, $\theta_{fc}$ is field capacity water content, and N represents nocturnal temperature records every 15 minutes.

Brunt's model's behavior was expected since its derivation implies the cooling of the soil surface is caused only by effects of net radiation, with no energy contributions by convection from the air, conduction from the soil (initial and boundary conditions: $\partial T/\partial z = 0$, see Annex I) or condensation.

When rain occurs close to the frost event (Fig. 6 DOY: 241, 242 and 247) the hourly estimation of bare soil surface temperature gives a MAE of 2.0 ºC, while those cases where the frost events are more separated in time from the last rain (DOY 106, 273 and 297), the MAE is 3.3 ºC. This is so because the contribution coming from soil heat flux density is smaller when the rain occurs very close to the frost event (DOY 241, 242 and 247) than when it occurs a longer period before the radiative frost (DOY 106, 273 and 297).

The thermal gradient is smaller in the first case than in the second (Fig. 7). Therefore, when the rain is very close to the frost event, the energy exchange conditions are more similar to those considered in Brunt's model than when the last rain occurs a longer time prior to the frost event.

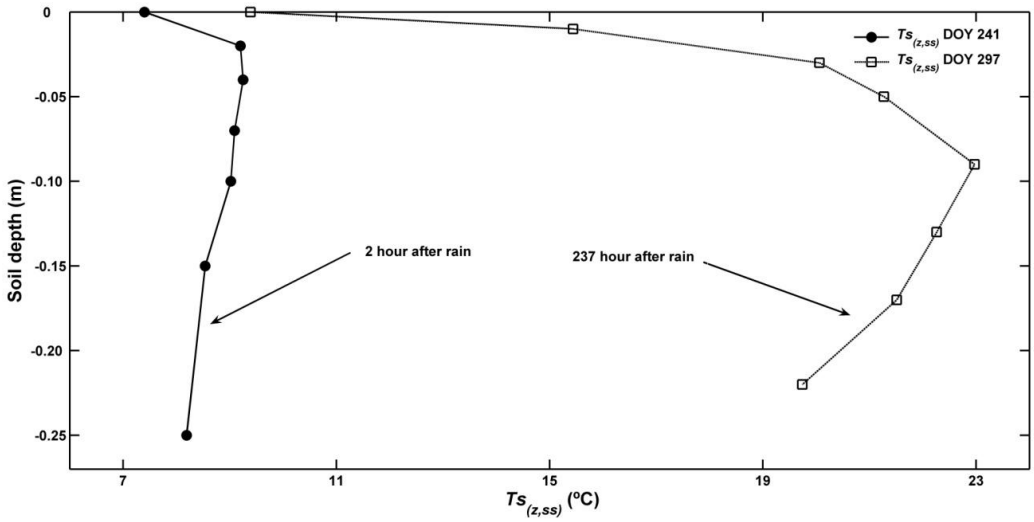


**Fig. 7** Soil temperature profile previous to radiative frost event at sunset ($Ts_{(z,\,ss)}$), 2 hours after the last rain (DOY 241/2011) and 237 hours after the last rain (DOY 297/2010)

The calibrations of coefficients in Gandia *et al.* ($A_G$ and $B_G$) and Allen's ($b$) models, based on the 55 radiative frost events selected from the air temperature records of years 2000 to 2009, were used to model the soil surface temperature (Fig. 8). As can be seen in Fig. 9 Allen's model underestimates, in most cases, hourly surface temperatures when they are above 0 ºC. However, it performs better when estimating temperatures below 0 ºC, and that is the reason why the calibration of this model with air temperatures could be applied to the behavior of minimum bare soil surface temperatures. The model by Gandia *et al.* overestimates bare soil surface temperatures in most cases, especially with temperatures observed below 0 ºC, which is similar to a situation reported by Emmanouil *et al.*, (2006).

One possible explanation for this could be the fact that the methodology proposed by Gandia *et al.* (1985) to obtain the coefficients $A_G$ and $B_G$, considers all nocturnal air temperatures of the frost events (Eq. (3)), which is the procedure used in this study. Probably, if only the minimum air temperatures of each event were used to obtain the coefficients $A_G$ and $B_G$ (Eq. ( 13)), the estimation of the bare soil surface temperatures could improve. However, in this study the value of coefficient $A_G$ (-0.19 $h^{-1}$) - which is associated to Eq. (3)'s gradient - is similar to that reported by Gandia *et al.* (1985), with values ranging from -0.176 to -0.227 $h^{-1}$. On the contrary, differences can be seen in the value of coefficient $B_G$, for which Gandia *et al.* (1985) reported values ranging between 0.138 and 0.254, as opposed to the value of 0.025 obtained in this study. Nonetheless, Anfossi (1989) indicates that the value of constant $B_G$ should be equal to zero, so that it fulfills Eq. (4)'s requirement in time $t$ = 0 s: the estimated temperature ($Ta_{(z\,ref,\,t)}$) should equal the observed temperature ($Ta_{(z\,ref,\,ss)}$) at the beginning of the modeling (sunset).

Considering the above-mentioned elements, the alternative of obtaining the coefficients $A_G$ and $B_G$ from minimum air temperatures should be explored, so that the model by Gandia *et al*. also can be used for the estimation of bare soil surface temperatures in radiative frost events.

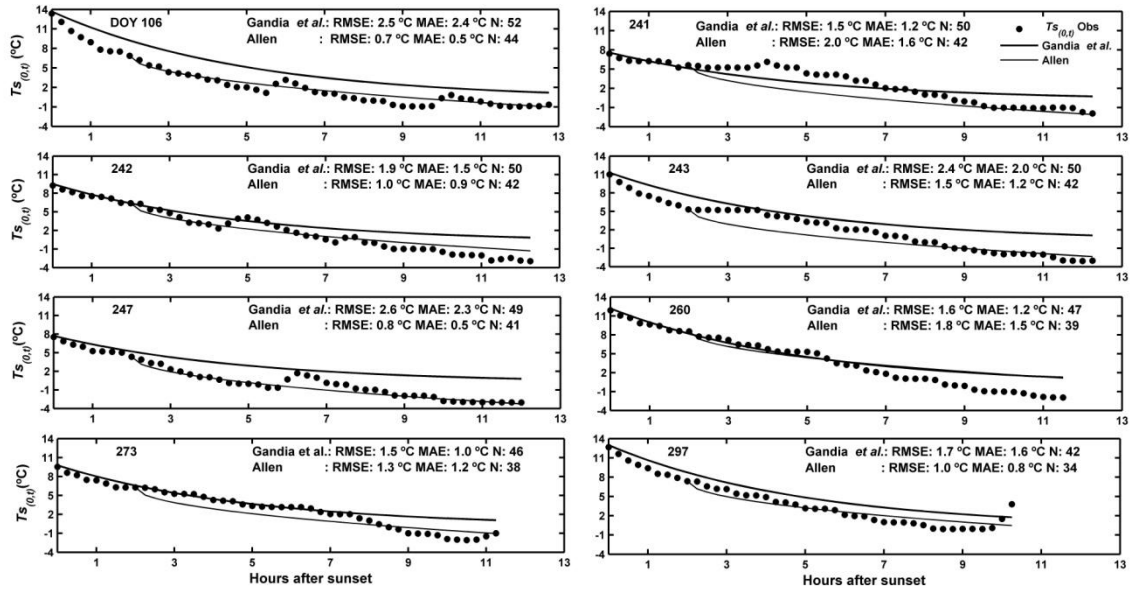


**Fig. 8** Decline of the nighttime hourly air temperature, $Ts_{(0,t)}$, estimated by Gandia *et al.* and Allen's models, from sunset to sunrise, during 8 radiative frost events. N represents nocturnal temperature records every 15 minutes.

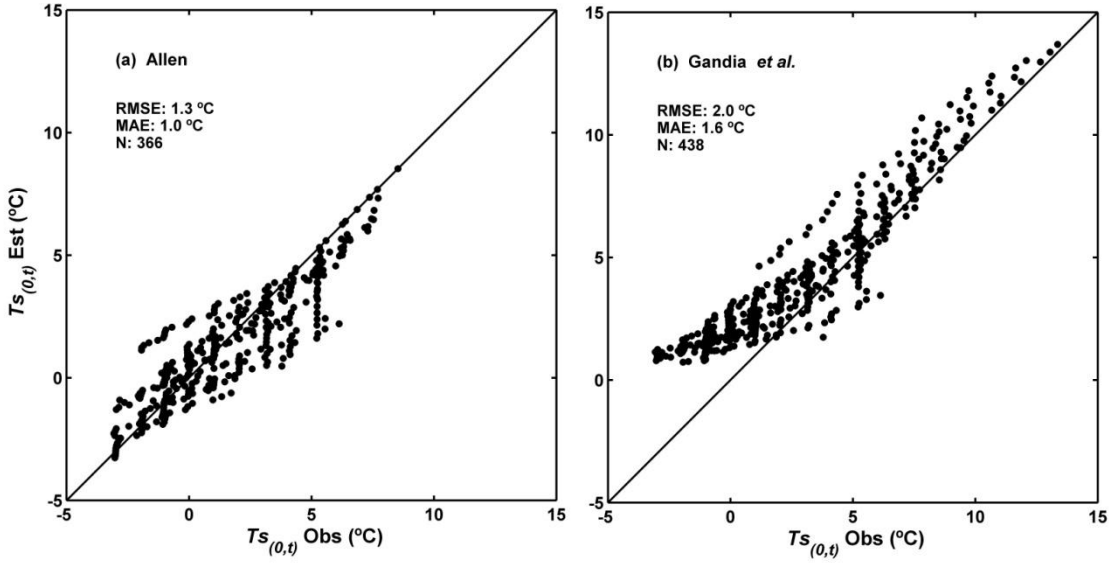


**Fig. 9** 1:1 ratio of bare soil surface temperature estimated ($Ts_{(0,t)}$Est) and observed ($Ts_{(0,t)}$Obs) through Allen's empirical model (a**)** and the regression model by Gandia *et al.* (b). N represents nocturnal temperature records every 15 minutes which were obtained during nine radiative frost events.

IV.3.5.3. Evaluation of $T_s$ and $T_a$ estimation models

After revising the models' performance in the estimation of air and bare soil surface temperatures, a summarized evaluation of each of them is presented in Table 2. It is shown that the best efficiency indices in the estimation of air temperatures in radiative frost events are those obtained by Gandia's model. For bare soil surface temperature estimation, out of the four models evaluated, the best performance was obtained by Allen's model, followed by the Numerical model, and Brunt's model in the last place.

Tabla 2: Efficiency evaluation indices for the hourly estimation of air ($Ta_{(2,t)}$) and bare soil surface temperature ($Ts_{(0,t)}$) by Allen's (Eq. (1)); Gandia's (Eq. (3)); Brunt's (Eq. (5)); and Numerical models for nine frost events.

| Model | Estimation | RMSE (º C) | MAE (º C) | N* |
|---|---|---|---|---|
| Allen | $Ta_{(2,t)}$ | 1.8 | 1.4 | 366 |
| Gandia | $Ta_{(2,t)}$ | 1.6 | 1.2 | 438 |
| Brunt | $Ts_{(0,t)}$ | 2.9 | 2.5 | 438 |
| Numerical | $Ts_{(0,t)}$ | 1.6 | 1.3 | 402 |
| Allen | $Ts_{(0,t)}$ | 1.3 | 1.0 | 366 |
| Gandia | $Ts_{(0,t)}$ | 2.0 | 1.6 | 438 |

*shows nocturnal temperature records every 15 minutes which were obtained during nine radiative frost events.

Despite the estimation of *Ta* by Gandia *et al.* and estimation of *Ts* by Allen's model had the best values in the efficiency indices, it is possible to observe the Numerical model had the second best performance to estimate bare soil surface temperature. On the other hand, it should be taken into account that Gandia *et al.* and Allen's model are specific for certain places and need to be calibrated, which implies having historical records of air temperature that might not always be available. This last reason is where the importance of the Numerical model lies since it does not require calibration, or historical records, just a good estimation of initial and boundary conditions.

Also, it should be mentioned that for the 9 radiative frost events recorded, the RMSE obtained on the estimation of minimum bare soil surface temperatures was of 1.3, 1.3, 3.1, and 3.6 ºC for the models by Allen, Numerical, Gandia *et al.*, and Brunt, respectively**.**

### IV.3.6. Conclusions

When historical air temperature records are available, Gandia *et al.* (1985) proved to be the best model at estimating air temperature in radiative frost events, out of the two models analyzed.

The calibration of Allen's model with air temperature records can be extrapolated to the estimation of nocturnal soil surface temperature behavior. Thus, out of the four models evaluated on the estimation of bare soil surface temperature, the model that best performed was Allen's (1957).

The Numerical model performed better when the rain is close to frost events. This is so because upper boundary conditions can be estimated with greater accuracy, especially by associating the initial soil surface wetness content in bare soil to that of field capacity ($\theta_0 \approx \theta_{fc}$) or when $\theta_0$ is above volumetric soil water content at permanent wilting point, where the error which can be caused in the estimation has low sensitivity in the prediction of the bare soil surface temperature at sunrise.

Brunt's model underestimates the minimum soil surface temperatures in radiative frost events, and can be used as a lower boundary in the estimation of the minimum surface temperature in bare soils.

**IV.3.7. References**

Allen CC (1939) Minimum temperature forecasting in the central California Citrus district. Mon. Weather Rev. 67:286-293

Allen CC (1957) A simplified equation for minimum temperature prediction. Mon. Weather Rev. 85:119-120

Angström A (1920) Studies of the frost problem. Geogr Ann. A. 2:20-32

Anfossi D (1989) A discussion on nocturnal temperature profiles. Atmos. Environ. 23:1177-1186

Bagdonas A, Georg JC, Gerber JF (1978) Techniques of frost prediction and methods of frost and cold protection. W.M.O. Technical Note, No. 157. Geneva, Switzerland. 160 p

Bettencourt ML (1980) Contribuição para o estudo das geadas em Portugal Continental. In: O Clima de Portugal, Fasc. XX Lisboa: INMG

Blanc ML, Gelin H, Holzberg IA, Mason B (1963) Protection against frost damage. W.M.O. Technical Note, No. 51. Geneva, Switzerland. 62 p

Brunt D (1941) Physical and dynamical meteorology 2nd edn Cambridge University Press, New York

Campbell GS (1985) Soil physics with basic: transport models for soil- plant systems. Elsevier, New York

Cunha FR (1982) O problema da geada negra no Algarve. INIA Divulgação No. 12 125p

De Vries DA (1963) Thermal of soil. In:Van Wijk WR (ed) Physics of the plant environment. North-Holland, Amsterdam

Ellison ES (1928) A critique on the construction and use of minimum temperature formulas. Mon. Weather Rev. 55:485-495

Emmanouil G, Galanis G, Kallos G (2006) Statistical methods for the prediction of night-time cooling and minimum temperature. Meteorol. Appl. 13:169-178

Gandia S, Melia J, Segarra D (1985) Application of radiative cooling model to daily minimum temperature prediction. J. Clim. 5:681-686

Hogg WH (1971) Spring frosts. Agriculture 1:28-31

Jaeger JC (1945) Note on the effect of wind on nocturnal cooling. Quart J. Roy. Meteorol. Soc. 71:388-390

Kalma JD, Laughlin GP, Caprio JM, Hamer JC (1992) Advances in Bioclimatology, 2. The Bioclimatology of Frost. Berlin: Springer-Verlag. 144p

Lawrence EN (1952) Frost investigation. Meteorol. Mag. 81:65-74

Lhomme JP, Guilioni L (2004) A simple model for minimum crop temperature forecasting during nocturnal cooling. Agric For Meteorol 123:55-68

Lhomme JP, Vacher JJ, Rocheteau A (2007) Estimating downward long-wave radiation on the Andean Altiplano. Agric. For. Meteorol. 145:139-148

Lindow SE (1983) Methods of preventing frost injury caused by epiphytic ice nucleation-active bacteria. Plant. Dis. 67:327-333

Mota FS (1981) Meteorologia Agrícola 5th ed São Paulo, Brazil: Liv. Nobel

Nichols ES (1920) Notes on damage to fruit by low temperatures; prediction of minimum temperatures. Mon. Weather Rev. 16:37-45

Prescott JA (1940) Evaporation from a water surface in relation to solar radiation. T. Roy. Soc. South Aust 64:114-125

Reuter H (1951) Forecasting minimum temperatures. Tellus 3:141-147

Smith JW (1920) Predicting minimum temperatures from hygrometric data. Mon. Weather Rev. 16:6-19

Snyder RL, Paw KT, Thompson JF (1987) Passive frost protection of trees and vines. University of California DANR Leaflet No 21429

Snyder RL, Melo-Abreu JP, Villar-Mir JM (2010) Frost protection: fundamentals, practice, and economics.Environment and natural resources series 10, FAO Rome

Venegas P, Grandon A, Jara J, Paredes J (2013) Hourly estimation of soil heat flux density at the soil surface with three models and two field methods. Theor Appl Climatol 112:45-59

Venegas et al. Submitted. Modeling hourly nocturnal temperature in frost radiative events I: development of a numerical model to estímate bare soil surface temperature. Theor Appl Climatol

Young FD (1920) Forecasting minimum temperatures in Oregon and California. Mon. Weather Rev. 16:53-60

ANNEX 3.I

**Method of heat equation characteristics: David Brunt**

Consider the P.D.E :

$$\frac{\partial S}{\partial t} = Ks\frac{\partial^2 T}{\partial z^2} \tag{I.1}$$

where $S = \frac{\partial T}{\partial z}$

The conditions for $S$ are at the boundary of the interval $[0, +\infty[$. The physical interpretation of this interval's right side (depth) is that it is far enough not to affect the phenomenon:

$$S(0,t) = \frac{Rn}{\rho s_0\, cs_0\, Ks_0} \tag{I.2}$$

$$S(+\infty, t) = 0,\ \forall t > 0 \tag{I.3}$$

The initial condition is:

$$S(z,o) = \begin{cases} \dfrac{Rn}{\rho s_0\, cs_0\, Ks_0}; & z = 0 \\ 0 \qquad\qquad\quad ; & z > 0 \end{cases} \tag{I.4}$$

By applying the method of characteristics, it is possible to obtain the solution to the problem (Eq. (I.1)) to Eq. ((I.4)):

$$S(z,t) = \frac{Rn}{\rho s_o\, cs_0\, Ks_0}\left[1 - \frac{2}{\sqrt{\pi}}\int_0^{\frac{z}{2\sqrt{t\,Ks_0}}} e^{-\theta^2} d\theta\right] \equiv \frac{2\,Rn}{\rho s_0\, cs_0\, Ks_0\,\sqrt{\pi}}\int_{\frac{z}{2\sqrt{t\,Ks_0}}}^{+\infty} e^{-\theta^2} d\theta \tag{I.5}$$

To recover $T(z,t)$, we must integrate the expression found previously, i.e.:

$$T(z,t) = \frac{2\,Rn}{\rho s_0\, cs_0\, Ks_0\,\sqrt{\pi}}\int\left[\int_{\frac{z}{2\sqrt{Ks_0\,t}}}^{\infty} e^{-\theta^2} d\theta\right] dz + C \tag{I.6}$$

To solve this expression, it must be integrated by parts and we obtain:

$$T(z,t) = C - \frac{2}{\sqrt{\pi}}\frac{Rn}{\rho s_0\, cs_0\, Ks_0}\left[\sqrt{Ks_0\,t}\; e^{\frac{-z^2}{4\,Ks_0 t}} - z\int_{\frac{z}{2\sqrt{Ks_0\,t}}}^{\infty} e^{-\theta^2} d\theta\right] \tag{I.7}$$

From Eq. (I.7), if $z = 0$ we obtain:

$$T(0,t) = C - \frac{2}{\sqrt{\pi}}\frac{Rn}{\rho s_0\, cs_0\,\sqrt{Ks_0}}\sqrt{t} \tag{I.8}$$

where $C = T(0,t)$ when $t \to 0^+$, and it corresponds to the soil surface initial temperature $T(0,0)$, that it is the temperature of the soil surface at the time of sunset $Ts_{(0,\,ss)}$ (Eq. (7)

## IV.4

## Desarrollo de un modelo simple de predicción de la temeperatura superficial del suelo en eventos de heladas radiativas, en condición de suelo sin cubierta vegetal


### Resumen

Se desarrolló un modelo mecanístico simple de predicción de la temperatura superficial del suelo, en condición de suelo desnudo, considerando para su funcionamiento información de radiación solar, contenido de humedad en la estrata superior del suelo y la temperatura superficial del suelo al crepúsculo. El modelo se comportó bien en la estimación de la temperatura superficial del suelo en estas dos condiciones, con idénticos indicadores de bondad de ajuste de 1.3 y 1.0 ºC para RMSE y MAE, respectivamente. Debido a que la estimación del contenido de humedad en la estrata superior del suelo es fácil de obtener a inicios de primavera, el modelo es de mayor utilidad en este periodo, el cual coincide con la época de mayor riesgo de heladas radiativas


### IV.4.1. Introducción

La importancia de las heladas como factor medioambiental que afecta al desarrollo de los cultivos es bien conocido. Esto puede causar una parcial o total destrucción de los cultivos, como también un retardo en su desarrollo (Bagdonas *et al.* 1978).

Algunas plantas tropicales y subtropicales padecen daños por efecto de las bajas temperaturas aún por encima de 0ºC. En cambio, las de regiones templadas sufren daños severos y hasta la muerte cuando la temperatura desciende por debajo de 0ºC. Los efectos varían marcadamente durante la vida de las plantas y es diferente según el estado de su crecimiento y desarrollo (Snyder *et al.*, 2010).

En Estados Unidos de América, las pérdidas económicas son mayores por heladas que por cualquier otro fenómeno agroclimático. Por lo tanto, el impacto de este fenómeno puede afectar sustancialmente la economía de los agricultores (Snyder *et al.*, 2010).

Las etapas de mayor riesgo, en muchos cultivos, es/son el estado de floración y formación del fruto. Por lo tanto, los agricultores requieren la predicción de la temperatura mínima con el fin de decidir la implementación de alguna técnica de protección de los cultivos (Figerola y Mazzeo, 1997). En este mismo sentido, Bagdonas *et al.*, (1978) y Cellier (1992) mencionan que muchos de los daños causados por las heladas pueden ser evitados usando métodos pasivos o activos de protección, en donde el uso de técnicas de predicción de heladas es de gran utilidad.

Coincidentemente, Figuerola y Mazzeo (1997) señalan que una correcta predicción permite tomar medidas para reducir el daño de cultivos, producto de la helada o de temperaturas críticas. Por lo tanto, una predicción confiable de heladas radiativas es una problemática importante en muchas áreas de la agricultura.

### IV.4.2. Revisión bibliográfica

Existe una diversidad de modelos predictivos de temperaturas nocturnas. Los primeros modelos desarrollados (Smith, 1917; Nichols, 1920; Angstrom, 1920) predicen las temperaturas mínimas en base a información medioambiental previa a la helada. Tales expresiones fueron desarrolladas ocupando registros históricos, obtenidos de estaciones agroclimáticas, para zonas específicas y bajo determinadas condiciones ambientales.

Otra forma de confrontar la predicción de las heladas es a través de modelos de regresión (Allen, 1957; Gandia, 1985; Emmanouil *et al.*, 2006), los cuales predicen el comportamiento nocturno de la temperatura del aire. Al igual que en el caso anterior, para determinar las tasas de disminución de la temperatura nocturna éstas se basan en registros históricos de temperatura del aire observadas durante noches claras, calmas donde se produjeron heladas.

Dentro de las críticas a la implementación de estas expresiones es que no son extrapolables, y además requieren para su aplicación grandes registros de datos meteorológicos (Cellier, 1992).

Otra crítica es que, debido a que la pérdida neta de calor desde el suelo depende de complejos procesos radiativos y de transferencia de calor, la debilidad de cualquier ecuación empírica es la validación de los supuestos establecidos para asignar valores promedios a varios parámetros físicos que, en conjunto, dan origen a varios coeficientes que se ocupan en dichas ecuaciones (Allen, 1957).

Por otra parte, se han desarrollado modelos semi empíricos con base teórica, los cuales predicen el comportamiento nocturno de la temperatura superficial del suelo. Ellos se basan en la solución analítica de la ecuación unidimensional de conducción de calor, donde los supuestos que se asumen para su desarrollo son condiciones de homogeneidad del suelo y de la estrata atmosférica cercana a éste, específicamente el perfil de temperaturas, la difusividad y conductividad termal (Brunt, 1941; Jaeger, 1945; Groen, 1947). Su desventaja es que bajo los supuestos en que fueron formulados, no se ajusta a todas las condiciones medioambientales en que se desarrollan las heladas.

Posteriormente se desarrollaron modelos numéricos, los que para su formulación asumen supuestos que se ajustan a las condiciones de borde e inicial, ya sea del suelo como del aire (baja atmósfera), lo cual permite simular de mejor forma un determinado fenómeno físico. Las principales ventajas de los modelos numéricos son que consideran los procesos físicos que involucran los eventos de heladas, como también simulan diversas condiciones meteorológicas, tipo de suelo y topografía. Sin embargo, sus principales desventajas son su alta complejidad para su desarrollo, como también que requieren para su funcionamiento información que no siempre está disponible, lo cual provoca que no sean de uso masivo (Cellier, 1993).

En este sentido, el objetivo de esta investigación fue desarrollar un modelo mecanístico simple para predecir la temperatura superficial del suelo en eventos de heladas radiativas en condición de suelo desnudo. Se considera sólo la radiación neta de onda larga y la densidad de flujo de calor en la superficie del suelo como principales variables que influyen en el balance de energía durante el proceso de formación de heladas radiativas.

### IV.4.3. Teoria y desarrollo del modelo mecanístico

Para una superficie de suelo desnudo, el proceso de formación de heladas, implica un proceso de balance de energía cuyos componentes son: la radiación neta nocturna (*Rn*); la densidad de flujo de calor sensible (*H*); la densidad de flujo de calor latente (*LE*) y la densidad de flujo de calor en la superficie del suelo ($G_0$):

$$Rn - G_0 - H - \lambda E = 0 \quad (1)$$

Durante las heladas radiativas, hay una pérdida de la radiación de la superficie del suelo a la atmósfera y una ganancia de radiación de la atmósfera al suelo, así como una ganancia de energía por convección de calor en el aire y por conducción de calor al suelo, donde el último componente es el más importante en el suministro de energía al sistema; sin embargo, en este proceso más calor se pierde que el que se gana (Snyder *et al.*, 2010). De manera similar, Figuerola y Mazzeo (1997) indicaron que la evolución de la temperatura nocturna sobre una superficie de suelo horizontal y homogéneo se ve afectada por la pérdida de radiación de la superficie, que está parcialmente sustituida por conducción de calor desde el suelo, como también por el aporte de calor sensible desde el aire debido a la inversión térmica.

Sin embargo, para el desarrollo del modelo mecanístico, que permite predecir el comportamiento de la temperatura de la superficie del suelo en eventos de heladas radiativas, se consideró que las variables más importantes que participan en la formación de heladas son la radiación neta de onda larga ($Rn^j$) y la densidad de flujo de calor en la superficie del suelo $G_0^{m,j}$ medido o estimado en el tiempo $t_j$, ambos expresados en W m$^{-2}$. La expresión utilizada es:

$$Rn^j - G_0^{m,j} = 0 \quad (2)$$

Es importante destacar que $Rn^j$ tiene signo negativo debido a la pérdida de energía en la superficie del suelo durante el período nocturno. Por otra parte, se puede obtener $G_0^{m,j}$ mediante la expresión de Mayocchi y Bristow (1995):

$$G_o^{m,j} = G_z^{m,j} + \Delta S_z^{m,j} \quad (3)$$

donde $G_z^{m,j}$ es la densidad de flujo de calor en el suelo a la profundidad z, en el tiempo $t_j$ (s); $\Delta S_z^{m,j}$ es el cambio del almacenamiento de calor en el suelo, medida en el tiempo $t_j$ entre la profundidad z y la superficie del suelo. Las variables son expresadas en W m$^{-2}$.

Remplazando la Eq.(3) en la Eq.(2) se obtiene:

$$Rn^j - \left(G_z^{m,j} + \Delta S_z^{m,j}\right) = 0 \quad (4)$$

Con el objeto de estimar o medir $G_z^{m,j}$, la siguiente expression es usada, de acuerdo a Fuchs (1987):

$$G_z^{m,j} = -k_s \frac{\partial Ts^j}{\partial z} \quad (5)$$

donde $k_s$ es la conductividad termal del suelo $\left(\mathrm{J\,m^{-1}\,s^{-1}\,{}^{o}C^{-1}}\right)$ y $Ts^j$ es la temperatura del suelo (ºC) en el tiempo $t_j$ (s). Sin embargo, para mediciones discretas de temperatura en el tiempo y en el perfil de suelo, la Eq.(5) puede ser expresada como:

$$G_z^{m,j} = -k_s \left( \frac{Ts^j_{z+\Delta z} - Ts^j_{z-\Delta z}}{(z+\Delta z)-(z-\Delta z)} \right) \quad (6)$$

donde $k_s$ es la conductividad termal del suelo (J $s^{-1}$ $m^{-1}$ $ºC^{-1}$) para la estrata localizada entre $z+\Delta z$ y $z-\Delta z$; $Ts^j_{z+\Delta z}$ es la temperatura del suelo (ºC) medida en el tiempo $t_j$ (s) a la profundidad $z+\Delta z$ (m); $Ts^j_{z-\Delta z}$ es la temperatura del suelo (ºC) medida en el tiempo $t_j$ (s) a la profundidad $z-\Delta z$ (m); y $\Delta z$ es un arbitrario grosor de la estrata de suelo (m). El signo negativo del lado derecho de la Eq.(6) indica que $G_z^{m,j}$ es positivo cuando la temperatura declina al incrementar la profundidad (densidad de flujo de calor del suelo hacia el interior de éste).

Para obtener $G_z^{m,j}$ implica determinar *ks*, que es obtenida a partir de la expresión desarrollada por Campbell (1985):

$$k_s = A + B\,X_w - (A-D)\exp\left[-(C\,X_w)^E\right] \quad (7)$$

$$A = 0.65 - 0.78\rho + 0.6\rho^2 \quad (8)$$

$$B = 1.06\,\rho^{X_w} \quad (9)$$

$$C = 1 + 2.6\,m_c^{-0.5} \quad (10)$$

$$D = 0.03 + 0.1\rho^2 \quad (11)$$

$$E = 4 \quad (12)$$

donde $\rho$ es la densidad aparente del suelo (Mg $m^{-3}$), $X_w$ es la humedad volumétrica del suelo ($m^3$ $m^{-3}$), y $m_c$ la fracción de arcilla del suelo.

También, de acuerdo a Fuchs (1987), $\Delta S_z^{m,j}$ (Ec.(4)) puede ser expresado como sigue, dependiendo de la capacidad de calor volumétrica del suelo ($Cv$) y la relación de cambio de temperatura del suelo con respecto al tiempo $(\partial Ts/\partial t)$:

$$\Delta S_z^{m,j} = \int_z^0 Cv \frac{\partial Ts^j}{\partial t} dz = Cv \frac{\partial Ts^j}{\partial t}\, z \quad (13)$$

Sin embargo, para las mediciones discretas de tiempo y de la temperatura del perfil del suelo, la Eq.(13) se puede expresar numéricamente como sigue:

$$\Delta S_z^{m,j} = \frac{\left[\left(Ts^j_{z/2} - Ts^{j-1}_{z/2}\right) z\; Cv_{z/2}\right]}{\Delta t} \quad (14)$$

Donde $\Delta S_z^{m,j}$ corresponde al cambio en el almacenamiento de calor del suelo (W $m^{-2}$) medido en el tiempo $t_j$ (s) entre la profundidad z (m) y la superficie del suelo; $Ts_{z/2}^j$ es la temperatura del suelo (º C) medida en el tiempo $t_j$ (s) en la profundidad $z/2$ (m); $z$ (m) es la profundidad de medición de la densidad de flujo de calor, $G_z^{m,j}$; $\Delta t$ es el intervalo de tiempo entre $t_j$ y $t_{j-1}$ (s), y $Cv_{z/2}$ es la capacidad de calor volumétrica del suelo (J $m^{-3}$ º $C^{-1}$) medido en profundidad $z/2$ (m). $Cv$ se determina por la adición del calor específico de los componentes del suelo, que incluye minerales, materia orgánica, agua y aire (De Vries, 1963):

$$Cv = \left[4.19\, X_w + 2.51\, X_0 + 1.93(1-\varepsilon - X_0)\right]10^6 \tag{15}$$

donde $X_w$, $X_0$ y $\varepsilon$ corresponden a la fracción volumétrica de agua, materia organica y porosidad del suelo, respectivamente.

Para los fines de esta investigación, se consideró que se puede definir $Ts_{z/2}^j$ como la temperatura media del suelo entre la superficie del suelo (z = 0) y la profundidad z:

$$Ts_{z/2}^j = \frac{Ts_0^j + Ts_z^j}{2} \tag{16}$$

Reemplazando la Eq.(16) en Eq.(14) se obtiene:

$$\Delta S_z^{m,j} = \left(Ts_0^j + Ts_z^j - Ts_0^{j-1} - Ts_z^{j-1}\right)\frac{z\,Cv_{z/2}}{2\Delta t} \tag{17}$$

Entonces, sustituyendo $\Delta S_z^{m,j}$, expresado a través de Eq.(17), en la Eq.(4), se obtiene la siguiente expresión:

$$\left(Rn^j - G_z^{m,j}\right) - \left(Ts_0^j + Ts_z^j - Ts_0^{j-1} - Ts_z^{j-1}\right)\frac{z\,Cv_{z/2}}{2\Delta t} = 0 \tag{18}$$

despejando $Ts_0^j$ desde Eq.(18), y considerando que la radiación neta de onda larga ($Rn^j$) permanece prácticamente constante durante la noche ( $Rn^j = Rn$):

$$Ts_0^j = Ts_0^{j-1} + \frac{2\Delta t\left(Rn - G_z^{m,j}\right)}{z\,Cv_{z/2}} + Ts_z^{j-1} - Ts_z^j \tag{19}$$

### IV.4.4. Metodología

IV.4.4.1 Sitio experimental

Este experimento se llevó a cabo en la estación agrometeorológica de la Facultad de Ingeniería Agrícola de la Universidad de Concepción sede Chillán, Chile (36 ° 35' 43 .4 " S, 72 ° 4' 47.3" W), situado a una altitud de 130 metros sobre el nivel del mar. El suelo es franco arcilloso, con una densidad aparente de 1.45 Mg $m^{-3}$ a una profundidad entre 0 y 0.1 m y de 1.60 Mg $m^{-3}$ a una profundidad entre 0.1 y 0.2 m, y el contenido de humedad volumétrico del suelo a capacidad de campo y punto de marchitez permanente es 0.29 y 0.21 $m^3$ $m^{-3}$, respectivamente, y una fracción de arcilla de 33% en la primera estrata. Este suelo pertenece a la serie Tres Esquinas (familia de suelo thermic Ultic

Haploxeralfs), tiene una pendiente ligeramente inclinada, y descansa sobre un sustrato de roca sólida, de un color marrón oscuro, y material rojizo con tonos 5 YR en condiciones de humedad. El período de medición fue del 3 de septiembre de 2010, día del año (DOY) 246, al 31 de diciembre de 2011 (DOY 365). En este periodo de tiempo sólo nueve días con heladas radiativas se produjeron a nivel del suelo, en condiciones de suelo desnudo. Los detalles de estos eventos se detallan en la Tabla 1:

**Tabla 1:** Fecha de eventos de heladas radiativas, hora al anochecer y al amanecer, duración de la noche, temperatura superficial del suelo al atardecer ($Ts_{(0,ss)}$) y la temperatura mínima de la superficie del suelo ($Ts_{z=0}$ min) en condiciones de suelo desnudo.

| Año | Helada radiativa (DOY) | Hora al atardecer* | Hora al amanecer* | Longitud noche (horas) | $Ts_{(0,\,ss)}$ (ºC) | $Ts_{z=0}$ min (º C) |
|---|---|---|---|---|---|---|
| 2010 | 273/274 | 20:00 | 7:15 | 11.25 | 9.5 | -1.5 |
| | 297/298 | 20:30 | 6:45 | 10.25 | 16.3 | -0.1 |
| 2011 | 105/106 | 19:30 | 8:15 | 12.75 | 13.0 | -1.1 |
| | 106/107 | 19:30 | 8:15 | 12.75 | 13.4 | -0.9 |
| | 241/242 | 19:45 | 8:00 | 12.25 | 7.4 | -1.9 |
| | 242/243 | 19:45 | 8:00 | 12.25 | 9.3 | -2.9 |
| | 243/244 | 19:45 | 8:00 | 12.25 | 9.8 | -3.0 |
| | 247/248 | 19:45 | 7:45 | 12.00 | 7.5 | -3.0 |
| | 260/261 | 20:00 | 7:30 | 11.50 | 11.9 | -1.9 |

*hora local

IV.4.4.2. Temperatura del suelo

Con el fin de medir las temperaturas del suelo se usaron termocuplas de níquel / cromo níquel tipo K, de 1 mm de diámetro. Estas termocuplas se elaboraron en el Departamento de Recursos Hídricos de la Facultad de Ingeniería Agrícola. Fueron enterradas en siete diferentes profundidades. Lecturas de monitoreo se registraron cada segundo y se promediaron cada 15 minutos. La disposición de las termocuplas se presenta en la Tabla 2.

**Tabla 2:** Profundidades de entierro de termocuplas para diferentes años y condición de suelo

| Año | Condición de suelo | Profundidad de entierro de termocuplas (m) |
|---|---|---|
| 2010 | Suelo desnudo | 0.01 0.03 0.05 0.09 0.13 0.17 0.22 |
| 2011 | Suelo desnudo | 0.02 0.04 0.07 0.10 0.15 0.25 0.30 |

Las mediciones de temperatura en la superficie de suelo desnudo se hicieron con un termómetro infrarojo marca Wahl, modelo DHS24L (Palmer Wahl Instrumentación Group, Ashville, North Carolina, EE.UU.), con un rango de temperatura de funcionamiento que va de -20 º C a 550 º C, y un factor de conversión de 1.0 º C $mV^{-1}$, localizado a 1.70 m sobre el nivel del suelo. Las lecturas de monitoreo se registraron cada segundo y promediadas cada 15 minutos durante el período septiembre 2010 – diciembre 2011.

IV.4.4.3. Contenido de humedad del suelo

Con el fin de medir el contenido de humedad del suelo, se utilizaron sensores de capacitancia ECHO-5 (Decagon Devices), tanto en el suelo desnudo como en suelo con cubierta vegetal, colocados horizontalmente a una profundidad de 0.05 y 0.10 m para el año 2010, y 0.025, 0.05, y 0.10 m para el año 2011. Con el fin de estimar el contenido de humedad del suelo a 0.025 m de profundidad en el año 2010, se aplicó la metodología utilizada según lo descrito por Venegas *et al.,* (2013). Los sensores fueron calibrados *in situ* con mediciones gravimétricas de humedad del suelo, a profundidades que van desde 0.0 hasta 0.05 m y 0.1 m. Siete repeticiones a cada profundidad se hicieron para cada medición. Las lecturas de monitoreo se registraron cada 1 segundo, y promediadas cada hora 1.

IV.4.4.4 Densidad de flujo de calor en el suelo

El cambio de la temperatura del suelo respecto a la profundidad de éste fue determinado por las lecturas de las termocuplas enterradas a diferentes profundidades, aplicando metodología de interpolación lineal para las temperaturas del suelo que se encuentran a profundidades distintas que el de las termocuplas. Luego se determinó $\Delta Ts/\Delta z$ a las profundidades de 0.025, 0.05, 0.10, 0.15 y 0.20 m. Estos valores se utilizaron para determinar la densidad de flujo de calor del suelo multiplicando por la conductividad termal del suelo (Eq.(6)). Sin embargo, para la medición de la densidad de flujo de calor del suelo a 0.05 m de profundidad se usaron platos de flujo de calor modelo HFT-3 (Campbell Scientific, Inc.), de 38 mm de diámetro, 3.9 mm de grosor y 1.22 W $m^{-1}$ $K^{-1}$ de conductividad termal.

IV.4.4.5 Radiación neta, radiación solar y velocidad de viento

La radiación neta se midió con dos radiómetros netos, modelo Q-7.1 (Campbell Scientific, Inc.), localizados a una altura de 1.55 m sobre el suelo, tanto en suelo desnudo como con cubierta vegetal. Las constantes para transformar el voltaje a densidad de flujo fue de 9.1 W $m^{-2}$ $mV^{-1}$, para milivoltios mayores que cero, y 11.4 W $m^{-2}$ $mV^{-1}$, para milivoltios menores que cero. Las lecturas se realizaron cada 1 segundo y se promediaron cada 15 minutos. La radiación solar se midió con un piranómetro de silicio (LI-200X, Campbell Scientific Inc., Logan, Utah, EE.UU.) localizado a 2.0 m sobre el nivel del suelo, el cual forma parte de los sensores pertenecientes a la Estación Agrometeorológica de la Facultad de Ingeniería Agrícola. La velocidad del viento se midió usando un anemómetro de cazoleta y veleta (Co Young, 03001, Michigan, EE.UU.), localizado a 2.0 m sobre del nivel del suelo. Las lecturas se registraron cada segundo y se promediaron cada 15 min.

IV.4.4.6. Almacenamiento de registros

Los registros de radiación neta y de platos de flujo de calor se almacenaron en un Micrologger 21 X (Campbell Scientific Inc., Logan, Utah, EE.UU.), los registros de termocuplas se almacenaron en un Micrologger HL20 (Rotronic AG, Bassersdorf, Suiza), y los registros de humedad del suelo fueron almacenadas en un ECHO 5 Micrologger (Decagon Device, Washington, EE.UU.).

IV.4.4.7. Información adicional

La conductividad térmica del suelo se estimó a profundidades de 0.025, 0.05 y 0.10 m, lo que implicaba la determinación de la densidad aparente y la humedad del suelo a estas profundidades. La fracción de arcilla fue constante, con un valor de 0.33 (33%). Para profundidades mayores de 0.1 m, se asumió un contenido de humedad volumétrico de suelo igual al contenido volumétrico del suelo a 0.1 m de profundidad.

IV.4.4.8. Condición de suelo desnudo

Teniendo en cuenta que es relevante aplicar $Cv$ a una profundidad lo más cerca posible a la superficie del suelo (Ec. (19)), porque es allí donde los cambios de temperatura del suelo ocurren en los eventos de heladas, es deseable asignar un pequeño valor a z / 2 , independiente de la profundidad z en el que se miden la temperatura del suelo ($Ts_z^j$) y $G_z^{m,j}$. Si $Cv$ se asocia a los datos medidos a la profundidad z = 0.025 m, entonces la Eq. (19). podría expresarse de la siguiente manera:

$$Ts_0^j = Ts_0^{j-1} + \frac{2\,\Delta t\left(Rn - G_z^{m,j}\right)}{z\ Cv_{0.025}} + Ts_z^{j-1} - Ts_z^j \qquad (20)$$

En la Eq.(20) está implícito que las mediciones de temperatura ($Ts_z^{j-1}$ y $Ts_z^j$) y $G_z^{m,j}$ deberían hacerse a una profundidad z. Por lo tanto, para cinco eventos donde no ocurrió una helada radiativa en suelo desnudo, pero donde la temperatura superficial del suelo estuvo cercana a 0 ºC a la hora del amanecer (DOY 113/114; 279/280; 283/284; 284/285; y 286/287 del año 2011), la Eq.(20) fue aplicada desde el atardecer hasta el amanecer, con cuatro profundidades z (0.05, 0.10, 0.15 y 0.20 m). La mejor predicción de la temperatura superficial del suelo se obtuvo usando la densidad de flujo de calor del suelo ($G_z^{m,j}$) y la temperatura del suelo a una profundidad z = 0.15 m (Tabla 3)

Tabla 3: Error cuadrático medio (RMSE) en la estimación de la temperatura superficial del suelo (Eq.(20)), desde el atardecer al amanecer, usando cuatro profundidades de referencia (*z*) para cinco eventos donde no hubo helada radiativa sobre suelo desnudo, año 2011

| DOY | RMSE (ºC) | | | |
|---|---|---|---|---|
| | z = 0.05 m | z = 0.10 m | z = 0.15 m | z = 0.20 m |
| 113/114 | 7.1 | 4.1 | 2.3 | 2.2 |
| 279/280 | 2.3 | 2.1 | 1.7 | 1.7 |
| 283/284 | 4.4 | 2.5 | 2.4 | 2.6 |
| 284/285 | 2.1 | 1.2 | 1.6 | 2.0 |
| 286/287 | 2.0 | 1.8 | 1.1 | 2.1 |

Por lo tanto, la Eq.(20) puede ser expresada como sigue:

$$Ts_0^j = Ts_0^{j-1} + \frac{2\,\Delta t\left(Rn - G_{0.15}^{m,j}\right)}{0.15\ Cv_{0.025}} + Ts_{0.15}^{j-1} - Ts_{0.15}^j \qquad (21)$$

Con el objeto de disminuir el número de variables de la Eq.(21), se procedió a expresar la temperatura de suelo, $Ts_{0.15}^{j-1}$ y $Ts_{0.15}^j$, en función de $G_{0.15}^{m,j}$ (ver Eq. (I.6)), obteniendo la siguiente expresión:

$$Ts_0^j = Ts_0^{j-1} + \frac{2\,\Delta t\,\left(Rn - G_{0.15}^{m,j-1}\right)}{0.15\;Cv_{0.025}} + \frac{\Delta z}{k_s}\left(G_{0.15}^{m,j-1} - G_{0.15}^{m,j}\right) \quad (22)$$

Detalles en la obtención de Eq.(22) se presentan en Anexo I.

Para utilizar la Eq.(22) sin la necesidad de disponer de registros directos de flujo de calor en el suelo a 0.15 m de profundidad, se estimó el comportamiento temporal de $G_{0.15}^{m,j}$ a través de la Eq.(6), la Eq.(7), y usando un $\Delta z = 0.05$ m (Eq.(6)). Se utilizaron los registros de temperatura de suelo desnudo a 0.10 y 0.20 m de profundidad, como también los registros de contenido volumétrico de humedad en suelo desnudo a 0.10 m de profundidad, comprendidos en 71 días: DOY 247 al 260 para el año 2010; 210 al 230 y 270 al 305 para el año 2011. Sin embargo, algunos días comprendidos dentro de los rangos señalados no se consideraron por presentar registros de temperatura incompletos. En la figura 1 se presenta el comportamiento temporal de $G_{0.15}^{m,j}$ entre los días (DOY) 285 y 289 del año 2011.

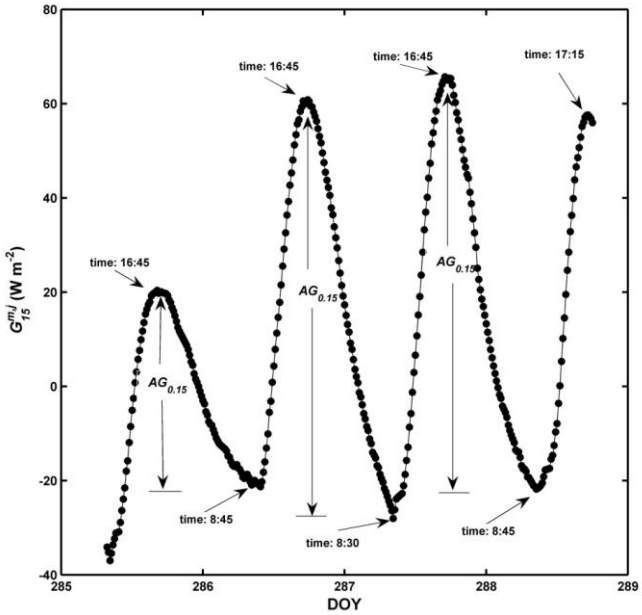


**Fig 1:** Comportamiento temporal de la densidad de flujo de calor en el suelo a la profundidad z = 0.15 m( $G_{0.15}^{m,j}$ ) en condición de suelo desnudo, estimada entre los DOY 285 y 289 del año 2011. A $G_{0.15}$ representa la diferencia entre $G_{0.15}^{m,j}$ máximo del día actual y el $G_{0.15}^{m,j}$ mínimo del día siguiente. La hora está expresada como hora local

En la Fig. 1 se observa que el máximo valor de $G_{0.15}^{m,j}$ ocurre entre las 16:45 y 17:15 horas y el mínimo ocurre entre las 8:30 y 8:45 (hora local). Sin embargo, en los 71 días analizados, la hora promedio en que ocurre el valor máximo y mínimo de $G_{0.15}^{m,j}$ fue a las 17:00 y 09:00 horas, respectivamente. Se encontró que la variable que mejor explica el comportamiento de $G_{0.15}^{m,j}$ es la sumatoria de la radiación solar (*Rs*) recibida en la superficie del suelo entre las 10:00 y las 17:00 horas (hora local), expresada en MJ $m^{-2}$. Es decir, la densidad de flujo radiante recibida durante este lapso de tiempo en un día determinado, permite predecir el valor máximo de $G_{0.15}^{m,j}$ ( $G_{0.15}^{peak}$ ) para ese día, como también permite obtener la amplitud de $G_{0.15}^{m,j}$ ( $AG_{0.15}$ ), que corresponde a la diferencia

entre $G_{0.15}^{peak}$ de ese día y el valor mínimo de $G_{0.15}^{m,j}$ del día siguiente (variación peak-to-peak). En la figura 2 y 3 se presenta la relación entre $G_{0.15}^{peak}$ vs. *Rs* and $AG_{0.15}$ vs. *Rs* , respectivamente.

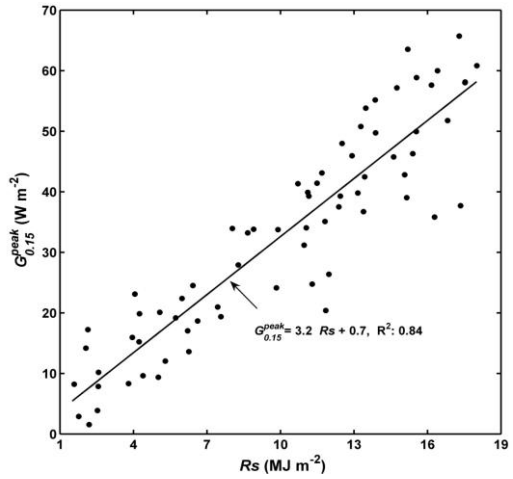


**Fig 2:** Relación entre la sumatoria de la radiación solar recibida en la superficie del suelo desnudo ($\sum Rs_{10-17}$) entre las 10:00 y 17:00 (hora local) y el valor máximo de la densidad de flujo de calor en el suelo a una profundidad de 0.15 m ($G_{0.15}^{peak}$).

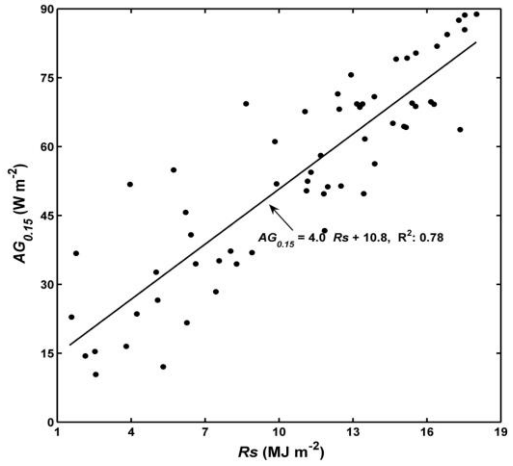


**Fig 3:** Relación entre la sumatoria de la radiación solar recibida en la superficie del suelo ($\sum Rs_{10-17}$) entre las 10:00 y 17:00 (hora local) y la amplitud de la densidad de flujo de calor en el suelo a una profundidad de 0.15 m ($AG_{0.15}$).

En las figuras 2 y 3 se ajustan las expresiones para determinar $G_{0.15}^{peak}$ y $AG_{0.15}$ :

$$G_{0.15}^{peak} = 3.2\sum Rs_{10-17} + 0.7 \quad (23)$$

$$AG_{0.15} = 4.0\sum Rs_{10-17} + 10.8 \quad (24)$$

Luego de obtener las relaciones entre $G_{0.15}^{peak}$ and $AG_{0.15}$ vs. *Rs*, se realizó la parametrización de la Eq.(22), obteniendo la siguiente expresión:

$$Ts_0^j = Ts_0^{j-1} + \frac{2\Delta t\left(Rn - G_{0.15}^{peak} - AG_{0.15}\sin\left(\frac{\pi\left(3600(15+ss)+t_{j-1}\right)}{115200}\right)\right)}{0.15Cv_{0.025}} - \frac{0.05}{k_s}\frac{\Delta t\, AG_{0.15}\pi}{115200}\cos\left(\frac{\pi\left(3600(15+ss)+t_j\right)}{115200}\right) \quad (25)$$

Detalles de la derivación de Eq.(25) se presentan en el Anexo II.

La operatoria de la Eq.(25) comienza una vez que se disponga de la sumatoria de la radiación solar entre las 10:00 y 17:00 horas, del contenido de humedad del suelo y de la radiación neta de onda larga al momento del crepúsculo. Con esta información es posible determinar *Rn*, $Cv_{0.025}$ (Eq.(15)), $k_s$ (Eq.(7)), $G_{0.15}^{peak}$ (Eq.(23)) y $AG_{0.15}$ (Eq.(24)). Dado que la Eq.(25) se aplica a partir del atardecer ($t_j$ = *0*), en este instante la temperatura superficial del suelo en el tiempo $t_{j-1}$ ($Ts_0^{j-1}$) es igual a la temperatura superficial del suelo al atardecer, es decir: $Ts_0^{ss} = Ts_0^{j-1}$. Con los valores definidos de *Rn*, $Cv_{0.025}$, $k_s$, $G_{0.15}^{peak}$, $AG_{0.15}$, $Ts_0^{j-1}$ y $t_j$, es posible determinar $Ts_0^j$. Para el siguiente paso de tiempo $\Delta t$ (definido arbitrariamente), el valor de $Ts_0^j$ calculado en el paso de tiempo anterior pasa a ser $Ts_0^{j-1}$ en el paso de tiempo actual, y dado que el único factor que cambiaría en el transcurso del evento de helada es $t_j$, es posible determinar el nuevo valor de $Ts_0^j$. Esta operatoria continúa hasta llegar al momento en que se produce el amanecer.

Para aplicar la Eq.(25) en los eventos de heladas señalados en la Tabla 1, se utilizó la información presentada en la Tabla 4.

Tabla 4: Fecha de inicio de evento de helada radiativa (DOY), energía acumulada de radiación solar incidente en la superficie del suelo entre las 10:00 y 17:00 ($\sum Rs_{10-17}$), valor máximo de la densidad de flujo de calor en el suelo a una profundidad de 0.15 m $\left(G_{0.15}^{peak}\right)$, amplitud de la densidad de flujo de calor en el suelo a *z* = 0.15 m ($AG_{0.15}$), radiación neta de onda larga para condición de suelo desnudo (*Rn*), y contenido volumétrico de humedad del suelo a una profundidad de *z* = 0.025 m $\left(\theta_{0.025}\right)$

| DOY | $\sum_{Rs_{10-17}}$ (MJ m$^{-2}$) | $G_{0.15}^{peak}$ (W m$^{-2}$) | $AG_{0.15}$ (W m$^{-2}$) | *Rn* (W m$^{-2}$) | $\theta_{0.025}$ (m$^3$ m$^{-3}$) |
|---|---|---|---|---|---|
| 105 | 14.6 | 47.4 | 69.1 | -68 | 0.22 |
| 106 | 15.0 | 48.8 | 70.9 | -68 | 0.22 |
| 241 | 4.9 | 16.2 | 30.2 | -65 | 0.45 |
| 242 | 13.2 | 42.9 | 63.5 | -68 | 0.36 |
| 243 | 12.7 | 41.3 | 61.6 | -68 | 0.33 |
| 247 | 6.1 | 20.4 | 35.4 | -68 | 0.42 |
| 260 | 16.0 | 51.8 | 74.7 | -68 | 0.28 |
| 273 | 16.8 | 54.6 | 78.1 | -65 | 0.27 |
| 297 | 20.5 | 66.4 | 92.9 | -70 | 0.15 |

IV.4.4.9. Validación del modelo

La validación de los modelos se basó en los eventos de heladas señalados en la Tabla 1. Los registros de temperatura de la superficie del suelo en suelo desnudo se utilizaron como referencia. La validación se realiza a través de la interpretación de los siguientes coeficientes: Relación gráfica 1:1, donde los datos de las temperaturas observadas en suelo desnudo ($Ts_{(0,t)}$) se contrastan con las temperaturas estimadas por el modelo. El error absoluto medio (MAE), la raíz del error cuadrático medio (RMSE), y el sesgo se calcularon a partir de:

$$\mathrm{MAE} = \frac{1}{N}\sum_{i=1}^{N}\left|O_i - P_i\right| \quad (26)$$

$$\mathrm{RMSE} = \sqrt{\frac{1}{N}\sum_{i=1}^{N}\left(O_i - P_i\right)^2} \quad (27)$$

$$sesgo = \left(\overline{O_i} - \overline{P_i}\right) \quad (28)$$

donde $O_i$ es el valor de temperatura observada, $P_i$ es el valor de la temperatura estimada, $\overline{O_i}$ es el valor medio de la temperatura observada $\overline{P_i}$ es el valor medio de la temperatura estimada, N es el número de observaciones y el subíndice denota la observación i-ésima.

### IV.4.5. Resultados y discusión

IV.4.5.1. Caracterización de los eventos de heladas radiativas:

De la Tabla 5 se observa que para condición de suelo desnudo la tasa promedio de disminución de la temperatura del suelo varía entre 0.8 y 1.6 (ºC $h^{-1}$). Cabe destacar que las menores tasas se producen en los DOY 241 y 247 (0.8 y 0.9 ºC $h^{-1}$) y corresponden a eventos en que la lluvia finalizó horas antes de la ocurrencia de la helada. En estos casos, la amplitud termal entre el atardecer y el amanecer es baja (6.5 y 6.6 ºC para DOY 241 y 247, respectivamente), como también lo es la densidad de flujo de calor en el suelo. Esto último implica que el aporte de energía desde el interior del suelo hacia la superficie de éste es bajo y, por tanto, la energía neta que sale del suelo se explica por la radiación neta de onda larga (*Rn*). Por otra parte, estos eventos presentaron un alto contenido de humedad volumétrico del suelo a z = 0.025 m, el cual estuvo sobre 0.40 $m^3$ $m^{-3}$ (ver Tabla 4). Este alto contenido de humedad del suelo aumenta la capacidad volumétrica de calor del suelo, lo que se traduce en que se requiere una mayor extracción de energía para que la temperatura del suelo disminuya en una determinada magnitud y, por tanto, la tasa promedio de disminución termal es menor.

Tabla 5. Caracterización de los eventos de heladas radiativas, a través de velocidad del viento promedio durante la noche ($\overline{V}$), amplitud termal entre el atardecer y el amanecer para condición de suelo desnudo ($\Delta Ts$), tasa de disminución promedio de temperatura para condición de suelo desnudo ($\Delta Ts/\Delta t$)

| DOY | $\overline{V}$ (m $s^{-1}$) | $\Delta Ts$ (ºC) | $\Delta Ts/\Delta t$ (ºC $h^{-1}$) |
|---|---|---|---|
| 105 | 0.30 | 14.2 | 1.1 |
| 106 | 0.05 | 14.3 | 1.1 |
| 241 | 0.40 | 9.3 | 0.8 |
| 242 | 0.10 | 12.2 | 1.0 |
| 243 | 0.00 | 12.8 | 1.0 |
| 247 | 0.01 | 10.5 | 0.9 |
| 260 | 0.30 | 13.8 | 1.2 |
| 273 | 1.60 | 11.0 | 1.0 |
| 297 | 0.01 | 16.4 | 1.6 |

Por otra parte, se observa que para eventos de heladas en que ha transcurrido más de 1 día entre la lluvia y ésta, la tasa promedio de disminución termal varía entre 1.0 y 1.6 ºC

$h^{-1}$. Estas tasas de disminución termal están asociadas principalmente al contenido de humedad en la estrata superior del suelo, la densidad de flujo de calor en el suelo y radiación neta de onda larga (aunque esta última fue similar en todos los eventos de heladas). En el caso del DOY 105, 106, 242 y 243, la densidad de flujo de calor en el suelo fue similar (ver Tabla 4). Sin embargo, el contenido de humedad del suelo fue menor para los DOY 105 y 106, lo que se tradujo en que la capacidad volumétrica de calor en el suelo fuera menor y, por tanto, la extracción de energía para que la temperatura del suelo disminuyera en una determinada magnitud también fue menor. Por ende, la tasa promedio de disminución termal fue mayor para los DOY 105 y 106 (1.1 ºC $h^{-1}$) que para los DOY 242 y 243 (1.0 ºC $h^{-1}$).

En el caso del DOY 273, el contenido de humedad fue baja (0.27 $m^3$ $m^{-3}$), similar al contenido de humedad del DOY 260 (ver Tabla 4); sin embargo, su tasa de disminución termal fue comparativamente baja respecto al DOY 260 (1.0 v/s 1.2 ºC $h^{-1}$). Esto se podría explicar porque la velocidad de viento promedio durante este evento de helada fue alto (1.6 m $s^{-1}$), incluso en algunos momentos de la noche superó los 3 m $s^{-1}$ y, por tanto, el aporte de la densidad de flujo de calor sensible hacia la superficie del suelo podría haber sido comparativamente mayor para este evento que para el resto de los eventos de heladas analizados. Este aporte de energía de calor sensible se traduce en un incremento de la temperatura del suelo en los instantes en que la velocidad del viento fue alta.

En el caso del DOY 297, la velocidad promedio del viento fue prácticamente cero, la radiación neta similar al resto de los eventos de heladas, y su contenido de humedad volumétrico fue comparativamente el más bajo entre los eventos de heladas analizados. Por otra parte, el aporte de energía desde el interior del suelo hacia la superficie de éste fue comparativamente mayor que el resto de los eventos de heladas. A pesar de esto último, la tasa de disminución termal fue la más alta (1.6 ºC $h^{-1}$), lo que implica que la disminución de la capacidad tampón del suelo (expresada a través de la capacidad volumétrica de calor del suelo) es de mayor importancia relativa que el aporte de energía desde el interior del suelo, respecto a la influencia en la tasa promedio de disminución termal.

IV.4.5.2. Estimación horaria de la temperatura superficial del suelo en el transcurso de la noche y en condición de suelo desnudo $\left(Ts_{(0,\,t)}\right)$

Durante los nueve eventos de heladas radiativas, el modelo mecanístico desarrollado por la Eq.(25) tendió a sobrestimar en 0.4 ºC las temperaturas observadas (Sesgo: -0.4 ºC), sin embargo, tendió a sobreestimar las temperaturas cuando éstas eran igual o mayores a 5 ºC y tendió a estimar de mejor manera la temperatura superficial del suelo cuando las temperaturas eran menores a 5 ºC (Fig. 4), con un promedio de RMSE y MAE en los nueve eventos de heladas radiativas de 1.3 y 1.0 ºC, respectivamente. Esto implica que este modelo no simula adecuadamente el comportamiento de la temperatura superficial del suelo en las primeras horas del evento de heladas radiativas. Sin embargo, mejora su predicción de la temperatura en las horas finales del evento de helada, periodo en el que se alcanzan las temperaturas mínimas.

En la Fig. 5 se presenta el comportamiento del modelo para 8 de los 9 eventos de heladas radiativas. En ella se observa para los días 106 (Sesgo: -0.9 ºC y RMSE: 2.1 ºC) y 297 (Sesgo: -1.1 ºC y RMSE: 1.4 ºC), una sobreestimación de la temperatura

superficial del suelo en la primera fase del evento de helada. Esto se produce porque este modelo simula el comportamiento de $G_{0.15}^{m,j}$ a través de una función seno, la que es prácticamente una recta en casi todo el periodo de duración del evento de helada, y se hace cóncava al final de este periodo. Por lo tanto, una forma de mejorar la simulación es usando una función que presente una leve concavidad desde inicios del evento de helada. Otra forma de mejorar la estimación sería probando con otra profundidad de suelo para efectuar la medición del contenido de humedad, el cual incide sobre la magnitud de la capacidad volumétrica de calor del suelo, y que en este estudio se consideró a 0.025 m. A pesar de lo anterior, hay que destacar que el modelo presenta un buen comportamiento en la simulación de la temperatura superficial del suelo.

Por otra parte, se realizó un análisis de sensibilidad respecto del comportamiento del modelo y del contenido de humedad del suelo en condición de suelo desnudo. En la figura 6 se presenta el comportamiento de la tasa promedio de disminución estimada de la temperatura ($\Delta Ts / \Delta t$), expresada en ºC $h^{-1}$, durante eventos de heladas, respecto a diferentes contenidos de humedad a una profundidad $z = 0.025$ m. En esta figura se observa que $\Delta Ts / \Delta t$ disminuye linealmente a medida que el contenido de humedad del suelo aumenta, lo cual se puede explicar porque a medida que el contenido de humedad del suelo disminuye, $Cv$ también disminuye y, por lo tanto, la cantidad de energía a extraer para disminuir la temperatura de la superficie del suelo en una magnitud determinada también es menor. Hay que hacer notar que se puede atribuir al contenido de humedad del suelo el efecto en la tasa de disminución de la temperatura, debido a que la radiación neta de onda larga, durante los eventos de heladas radiativas, fue prácticamente constante.

Al comparar estas tasas con las observadas en la Tabla 5 se aprecia que son muy similares y sólo existen diferencias con la tasas de los DOY 105 y 106, donde la tasa observada es de 1.1 y la estimada corresponde a 1.35 ºC $h^{-1}$. Sin embargo, hay que destacar que las heladas radiativas tienen relevancia en la agricultura a inicios de primavera y, en esas condiciones, las tasas observadas y estimadas son similares y varían entre 0.84 y 1.03 ºC $h^{-1}$.

Para complementar el análisis anterior, se realizó un análisis de sensibilidad respecto a la variación del paso de tiempo $\Delta t$ ocupado en la simulación de la condición de suelo desnudo. Se encontró que al incrementar el $\Delta t$ de 900 s a 3600 s, disminuyó la estimación de la temperatura mínima en -0.4 ºC en promedio, y en el caso de disminuir el $\Delta t$ de 900 s a 450 s, ésta se incrementó en 0.06 ºC .Por lo anterior, se considera que el paso de tiempo usado en este estudio es adecuado.

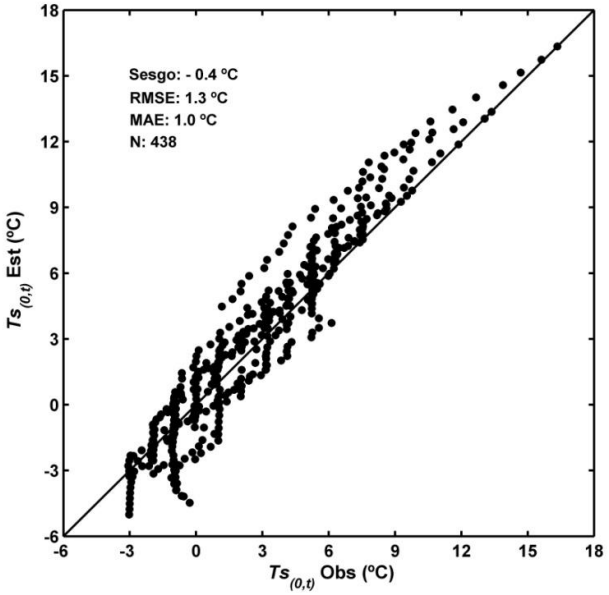


**Fig. 4** Relación 1:1 entre la temperatura estimada de la superficie del suelo ($Ts_{(0,t)}$ Est) y la observada ($Ts_{(0,t)}$ Obs). N representa los registros nocturnos, entre el crepúsculo y el amanecer, de temperatura cada 15 minutos que se obtuvieron durante nueve eventos de heladas radiativas.

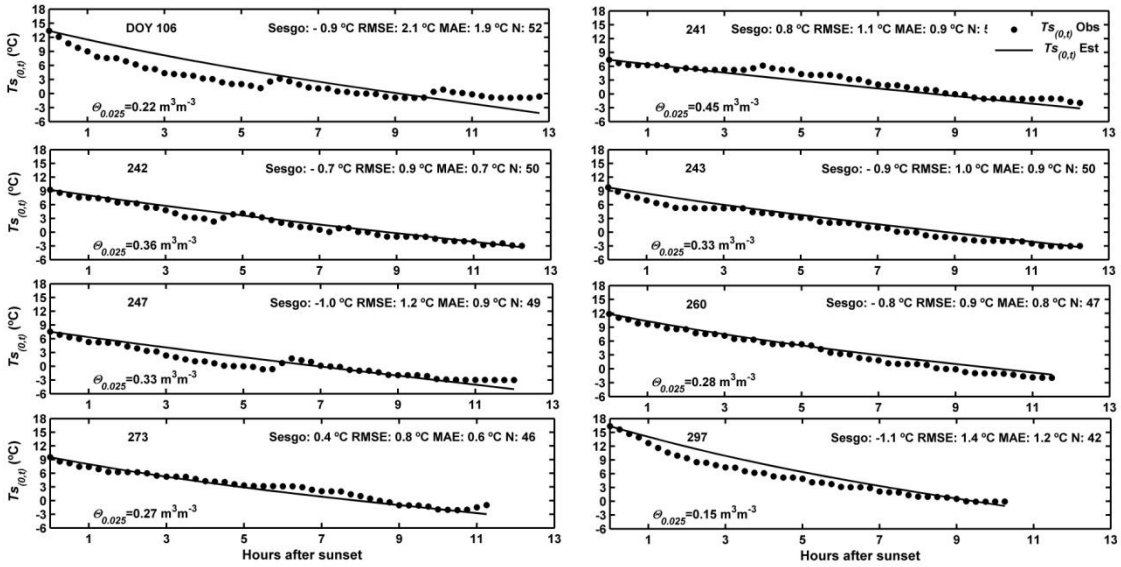


**Fig. 5** Disminución horaria de la temperatura superficial del suelo estimada ($Ts_{(0,t)}$ Est) y observada ($Ts_{(0,t)}$ Obs), desde el atardecer hasta el amanecer, durante 8 eventos de heladas radiativas. N representa los registros de temperatura cada 15 minutos

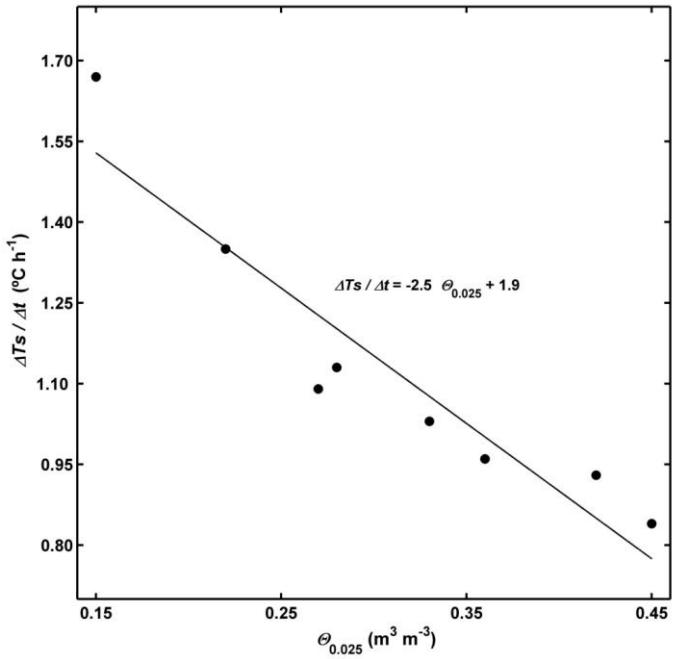


**Fig. 6** Relación entre la tasa promedio estimada de disminución de la temperatura en la superficie del suelo (ΔTs / Δt) y el contenido de humedad volumétrico a una profundidad z = 0.025 m ($\theta_{0.025}$), en condición de suelo desnudo

### IV.4.6. Conclusiones

Dado que el modelo presenta un buen comportamiento podría afirmarse que los supuestos considerados para su desarrollo son los adecuados; es decir, que los eventos de heladas radiativas son afectadas principalmente por las condiciones del suelo y de radiación neta nocturna de onda larga.

El modelo desarrollado para ambas condiciones de suelo presenta un mejor comportamiento con contenidos de humedades iguales o superiores a capacidad de campo, condición que se presenta a inicios de primavera, cuando las bajas temperaturas afectan fuertemente el desarrollo de diversos cultivos.

### IV.4.7. Referencias

Allen CC (1957) A simplified equation for minimum temperature prediction. Mon. Weather Rev. 85:119-120

Angström A (1920) Studies of the frost problem. Geogr Ann. A. 2:20-32

Bagdonas A, Georg JC, Gerber JF (1978) Techniques of frost prediction and methods of frost and cold protection. W.M.O. Technical Note, No. 157. Geneva, Switzerland. 160 p

Brunt D (1941) Physical and dynamical meteorology 2nd edn Cambridge University Press, New York

Campbell GS (1985) Soil physics with basic: transport models for soil- plant systems. Elsevier, New York

Campbell GS, Norman JH (1998) An introduction to environmental biophysics. Springer-Verlag, New York

Cellier P (1993) An operational model for predicting minimum temperatures near the soil surface under clear sky conditions. J. Appl. Meteorol. 32: 871-883

De Vries DA (1963) Thermal of soil. In:Van Wijk WR (ed) Physics of the plant environment. North-Holland, Amsterdam

Emmanouil G, Galanis G, Kallos G (2006) Statistical methods for the prediction of night-time cooling and minimum temperature. Meteorol. Appl. 13:169-178

Figuerola PI, Mazzeo NA (1997) An analytical model for the prediction of nocturnal and dawn surface temperatures under calm, clear sky conditions. Agric For. Meteorol. 85:229-237

Fuch, M., 1987. Heat flux. In Klute A (ed) Methods of soil analysis, part 1: Physical and mineralogical methods. Agr. Monogr. Madion: ASA and SSSA, 957-968

Gandia S, Melia J, Segarra D (1985) Application of radiative cooling model to daily minimum temperature prediction. J. Clim. 5:681-686

Jaeger JC (1945) Note on the effect of wind on nocturnal cooling. Quart J. Roy. Meteorol. Soc. 71:388-390

Mayocchi, C., Bristow, K., 1995. Soil surface heat flux: some general questions and comments on measurements. Agric. For. Meteorol. 75, 43-50.

Nichols ES (1920) Notes on damage to fruit by low temperatures; prediction of minimum temperatures. Mon. Weather Rev. 16:37-45

Reuter H (1951) Forecasting minimum temperatures. Tellus 3:141-147

Smith JW (1920) Predicting minimum temperatures from hygrometric data. Mon. Weather Rev. 16:6-19

Snyder RL, Melo-Abreu JP, Villar-Mir JM (2010) Frost protection: fundamentals, practice, and economics.Environment and natural resources series 10, FAO Rome

Venegas P, Grandon A, Jara J, Paredes J (2013) Hourly estimation of soil heat flux density at the soil surface with three models and two field methods. Theor Appl Climatol 112:45-59

Venegas P, Jara J, Paredes J (Submitted) Modeling hourly nocturnal temperature in frost radiative events I: development of a numerical model to estimate bare soil surface temperature. Theor Appl Climatol

ANEXO 4.I

Según Eq. (6), la densidad de flujo de calor del suelo a la profundidad z se puede expresar como:

$$G_z^{m,j} = -k_s\left(\frac{Ts_{z+\Delta z}^{j} - Ts_{z-\Delta z}^{j}}{2\,\Delta z}\right) \tag{I.1}$$

Despejando $Ts_{z-\Delta z}^{j}$ de Eq.(I.1), se obtiene:

$$Ts_{z-\Delta z}^{j} = \frac{2\,\Delta z\, G_z^{m,j}}{k_s} + Ts_{z+\Delta z}^{j} \tag{I.2}$$

Por otra parte, la temperatura del suelo a la profundidad z y tiempo $t_j$, $Ts_z^j$, puede ser expresada como:

$$Ts_z^j = \frac{Ts_{z-\Delta z}^{j} + Ts_{z+\Delta z}^{j}}{2} \tag{I.3}$$

Sustituyendo Eq. (I.2) en Eq.(I.3) se obtiene:

$$Ts_z^j = \frac{\Delta z\, G_z^{m,j}}{k_s} + Ts_{z+\Delta z}^{j} \tag{I.4}$$

Desde la Eq.(I.4), $Ts_z^{j-1} - Ts_z^j$ puede ser expresado como:

$$Ts_z^{j-1} - Ts_z^j = \frac{\Delta z\, G_z^{m,j-1}}{k_s} + Ts_{z+\Delta z}^{j-1} - \frac{\Delta z\, G_z^{m,j}}{k_s} - Ts_{z+\Delta z}^{j} \tag{I.5}$$

Tal como se señala en la Eq.(20) y la Eq.(21), la temperatura del suelo a la profundidad z medida en el tiempo $t_j$ equivale a la temperatura del suelo a la profundidad de 0.15 m medida en el tiempo $t_j$ $\left(Ts_z^j = Ts_{0.15}^j\right)$ y considerando que $\Delta z = 0.05\,\text{m}$, entonces $Ts_{z-\Delta z}^{j}$ y $Ts_{z+\Delta z}^{j}$ equivalen a $Ts_{0.10}^{j}$ y $Ts_{0.20}^{j}$, respectivamente. Según Venegas *et al* (enviado), la temperatura del suelo a 0.20 m de profundidad permanece prácticamente constante durante la noche, por lo anterior se puede asumir que $Ts_{z+\Delta z}^{j-1} - Ts_{z+\Delta z}^{j} \approx 0$, por ende la Eq.(I.5) puede expresarse como:

$$Ts_z^{j-1} - Ts_z^j = \frac{\Delta z}{k_s}\left(G_z^{m,j-1} - G_z^{m,j}\right) \tag{I.6}$$

Al reemplazar $Ts_z^{j-1} - Ts_z^j$ de la Eq.(I.6) en la Eq.(21), para z = 0.15 m y $\Delta z = 0.05\,\text{m}$ se obtiene:

$$Ts_0^j = Ts_0^{j-1} + \frac{2\,\Delta t\left(Rn - G_{0.15}^{m,j-1}\right)}{0.15\,Cv_{0.025}} + \frac{0.05}{k_s}\left(G_{0.15}^{m,j-1} - G_{0.15}^{m,j}\right) \tag{I.7}$$

ANEXO 4.II.

A partir del comportamiento temporal de $G_{0.15}^{m,j}$ mostrado en la Fig. 1 y las relaciones de $G_{0.15}^{peak}$ y $AG_{0.15}$ con *Rs* señaladas en las Fig. 2 y Fig. 3 se encontró que una función sinusoidal representa adecuadamente el comportamiento de $G_{0.15}^{m,j}$ entre las 17 horas del día actual y las 9 horas del día siguiente, y puede ser modelado por:

$$G_{0.15}^{m,j} = G_{0.15}^{peak} + AG_{0.15}\sin\left(\frac{\pi\left(115200+t_j\right)}{115200}\right), \quad 0\le t_j \le 57600s \tag{II.1}$$

En esta expresión, se asume $t_j = 0\,s$ para las 17:00 del día y $t_j = 57600s$ para las 09:00 horas del día siguiente. La expresión anterior se ajustó al periodo de tiempo en que se desarrolla una helada, es decir:

$$G_{0.15}^{m,j} = G_{0.15}^{peak} + AG_{0.15}\sin\left(\frac{\pi\left(115200+3600\left(ss-17\right)+t_j\right)}{115200}\right), \quad 0\le t_j \le 3600\left(24-ss+sr\right) \tag{II.2}$$

Donde $ss$ corresponde la hora en que se produce el atardecer, y $sr$ corresponde a la hora en que ocurre el amanecer, expresado en horas y números decimales (Ej: 19:45 = 19.75 ó 8:30 = 8.5), y 17 corresponde la hora (local time) en que se produce $G_{0.15}^{peak}$. Reordenando la Eq.(II.2) se obtiene:

$$G_{0.15}^{m,j} = G_{0.15}^{peak} + AG_{0.15}\sin\left(\frac{\pi\left(3600\left(15+ss\right)+t_j\right)}{115200}\right), \quad 0\le t_j \le 3600\left(24-ss+sr\right) \tag{II.3}$$

Por otra parte, con el propósito de obtener una expresión para $G_{0.15}^{m,j} - G_{0.15}^{m,j-1}$ se realiza el siguiente desarrollo:

$$\frac{\partial G_{0.15}^{m}}{\partial t}(t_j) \approx \frac{G_{0.15}^{m,j} - G_{0.15}^{m,j-1}}{\Delta t} \approx \frac{AG_{0.15}\,\pi}{115200}\cos\left(\frac{\pi\left(3600\ \left(15+ss\right)+t_j\right)}{115200}\right) \tag{II.4}$$

Por lo tanto:

$$G_{0.15}^{m,j} - G_{0.15}^{m,j-1} \approx \Delta t\,\frac{AG_{0.15}\,\pi}{115200}\cos\left(\frac{\pi\left(3600\ \left(15+ss\right)+t_j\right)}{115200}\right) \tag{II.5}$$

Entonces, $G_{0.15}^{m,j} - G_{0.15}^{m,j-1}$ equivale a:

$$G_{0.15}^{m,j-1} - G_{0.15}^{m,j} = -\frac{\Delta t\ AG_{0.15}\pi}{115200}\cos\left(\frac{\pi\left(3600\left(15+ss\right)+t_j\right)}{115200}\right) \tag{II.6}$$

Reemplazando Eq.(II.6) en la Eq.(22) se obtiene:

$$Ts_0^j = Ts_0^{j-1} + \frac{2\Delta t\left(Rn - G_{0.15}^{peak} - AG_{0.15}\sin\left(\frac{\pi\left(3600\left(15+ss\right)+t_{j-1}\right)}{115200}\right)\right)}{0.15\,Cv_{0.025}} - \frac{0.05}{k_s}\frac{\Delta t\,AG_{0.15}\pi}{115200}\cos\left(\frac{\pi\left(3600\left(15+ss\right)+t_j\right)}{115200}\right) \tag{II.7}$$

## V. CONCLUSIONES GENERALES

El modelo desarrollado por Santanello y Friendl (2003) estimó adecuadamente el comportamiento de la densidad de flujo superficial de calor en el suelo ($G_0$) durante horas luz.

El modelo Force restore realiza estimaciones de densidad de flujo superficial de calor del suelo ($G_0$) para las veinticuatro horas del día sin embargo, no presenta un buen comportamiento en la estimación de $G_0$.

El modelo numérico desarrollado para estimar el comportamiento nocturno de la temperatura superficial del suelo, en condiciones de heladas radiativas y de suelo desnudo, presentó un buen comportamiento; sin embargo, para efectos prácticos no es fácil implementarlo dado que requiere información que no siempre está disponible en una estación agro meteorológica.

El modelo mecanístico desarrollado presenta un buen comportamiento en la estimación de la temperatura superficial del suelo sin cubierta vegetal, y es de fácil implementación en condiciones donde el contenido de humedad del suelo está sobre capacidad de campo, periodo que se asocia a inicios de primavera y presencia de heladas radiativas

De los modelos desarrollados por otros autores, los que presentan un mejor comportamiento son los desarrollados por Allen (1957), para estimar la temperatura en la superficie del suelo, en condición de suelo desnudo, y por Gandia *et al.*, (1985) para estimar el comportamiento de la temperatura del aire a 2 m sobre el suelo.